



**University of
Nottingham**

UK | CHINA | MALAYSIA

Master of Research Thesis

2021-2022

A DROPLET PRODUCTION PRINTHEAD FOR A NOVEL METAL 3D.

DEPARTMENT OF MMME

UNIVERSITY OF NOTTINGHAM NINGBO CHINA

Name : Ricardo David Castro Bossano

Student ID : 20416145

Lead Supervisor : Dr. Adam Rushworth

Second Supervisor : Dr. Hao Chen

Abstract

In the last decade, Drop-on-Demand (DoD) metal 3D printing has been slowly becoming a popular research topic, due to its potential for becoming a new cheap and high-quality metal additive manufacturing method. Whilst DoD techniques have proven to work and even have produced a couple of commercial 3D printers, most of these printers are very limited in terms of what materials can they use and what temperatures can they operate.

This research aims to achieve consistent droplet production on an existing prototype that uses a new DoD technique able to use any metal wire as raw material and can operate at temperatures over 1000°C. To achieve this, extensive research on other DoD techniques has been carried out to find how to improve the prototype, and together with multiple droplet production experiments be able to find the best input parameters to achieve a consistent droplet production. To verify the consistency of the droplet production and statistical analysis of the resulting droplet production was then carried out.

An analysis of how each input parameter affects droplet production was produced, together with a set of parameters that allowed the prototype to have consistent droplet production. A droplet sample of 200 droplets of aluminum 6061 was produced, with an average diameter of 1.61mm and a standard deviation of 0.087mm. This proved that the current prototype can achieve constant droplet production, and the research for producing droplets of other materials can start.

Table of Contents

Abstract	ii
Table of Contents	iii
Table of Figures	vi
Table of tables	x
Abbreviations	xi
Chapter 1 Introduction.....	1
1.1 Background.....	1
1.2 Project Background	2
1.3 Aims, and objectives.....	7
1.3.1 Aim.....	7
1.3.2 Objectives.....	7
1.3.3 Proposed Deliverables/Outcomes for the project.....	7
1.3.4 Validation for the completion of Aim and Objectives	7
1.4 Thesis structure.....	9
Chapter 2 Literature Review.....	10
2.1 Introduction	10
2.1.1 Commercial Metal 3D printers.....	17
2.2 Metal Droplet Deposition 3D printing.....	20
2.2.1 Pneumatic Drop-on-Demand printing.....	21
2.2.2 Electrohydrodynamic Drop-on-Demand printing.....	26
2.2.3 Magnetohydrodynamic Drop-on-Demand printing	29
2.2.4 Impact-driven Drop-on-Demand printing	35
2.2.5 Piezoelectric Drop-on-Demand printing	38

2.2.6	Laser-Induced DoD printing	45
2.2.7	Other Droplet Deposition techniques	49
2.2.8	Droplet techniques comparison	50
2.2.9	Drop-on-Demand physical properties	52
2.3	Numerical analysis of Droplet-on-Demand printing	53
2.3.1	Dimensionless numbers	54
2.3.2	Wettability	57
2.3.3	Other	58
2.4	Conclusion	59
Chapter 3	Methods	61
3.1	DoD Printhead evolution	61
3.1.1	Novel DoD technique working principle	61
3.1.2	Printhead overview and initial condition	62
3.1.3	Printhead changes and final condition	71
3.2	Experiments conducted	85
3.2.1	Experiments to produce droplets	85
3.2.2	Experiments to achieve the best droplet	85
3.2.3	Experiments to achieve the best droplet production	88
3.2.4	Experiment procedure	89
3.3	Droplet sample collection	91
Chapter 4	Results and Discussion	93
4.1	Experiments Results and discussion	93
4.1.1	Wire Diameter	93
4.1.2	Temperature	94

4.1.3	Nozzle aperture	95
4.1.4	Wire movement	95
4.2	Droplet sample collection results and discussion	96
4.3	Other materials results	105
Chapter 5	Conclusion	107
5.1	Conclusion of the Research	107
5.2	Future Work and Recommendations	108
References	110
Appendix	122
	Old control code.....	122
	Engineering Drawings	125
	Droplet production sample measurements.....	128

Table of Figures

Figure 1. Early metal 3D printer prototype (2019).	2
Figure 2. Metal 3D printer prototype (2020).	3
Figure 3. Metal 3D printer prototype (2021).	5
Figure 4. Control system (2021 prototype).....	5
Figure 5. Droplet produced by 2020 prototype.....	6
Figure 6. Droplet produced by 2021 prototype.....	6
Figure 7. Desired normal distribution of consistent droplet production.	8
Figure 8. First full dense commercial 3D printer (EOSINT M270).	10
Figure 9. Metal AM’s most common methods and techniques.	11
Figure 10. SLM operating principle. [31].....	12
Figure 11. LENS operating principle. [32].....	12
Figure 12. Binder jetting operating principle. [32].....	13
Figure 13. Liquid metal Jetting example showing a liquid metal jetting system. [34].....	14
Figure 14. metal Droplet Deposition, a) Continuous stream, and b) Drop on Demand. [54].....	20
Figure 15. DoD techniques.	21
Figure 16. Schematics of the Pneumatic DoD printer developed at the University of Toronto. [58].....	22
Figure 17. Schematic of a pneumatic droplet generator developed at the University of Toronto. [19].....	22
Figure 18. schematics of the Pneumatic DoD printer developed at Northwestern Polytechnical University. [60].....	24
Figure 19. Quartz glass nozzle used in the metal droplet generator, (a) bottom view and (b) the side view of the nozzle. [61].....	24
Figure 20. Pneumatic droplet generator. [62].....	26
Figure 21. Electrostatic effect on a liquid material (Polymer solution). [65].....	27
Figure 22. Usual waveform of the ac voltage pulse with the stages of droplet production. [66] ..	28
Figure 23. Schematic of EHD printing system. [67]	28

Figure 24. MagnetoJet printer a) system schematic b) simulation showing magnetic and electric field. [72].....	30
Figure 25. Electronic pattern created by MagnetoJet deposited on top of a polymer. [74].....	31
Figure 26. Electromagnetic DoD printer schematic. [75].....	32
Figure 27. Droplet creation under a 5ms pulse of applied current. [75].....	32
Figure 28. Schematic of an electromagnetic MHD printhead. [76].....	33
Figure 29. Ejecting chamber of a DoD MHD printer. [77]	34
Figure 30. Impact-driven DoD generator a) schematic of the system b) vibrating rod with spring c) vibrating rod with steel ring. [78].	35
Figure 31. Schematic of impact-driven DoD generator. [79].....	37
Figure 32. Schematic view of an impact-driven DoD generator. [80].....	37
Figure 33. Squeeze Mode piezoelectric droplet generator printhead schematic. [82].....	38
Figure 34. Schematic of DoD piezoelectric squeeze mode printhead. [83].....	39
Figure 35. Bending mode working principle. [84]	40
Figure 36. Schematic of a piezoelectric bending mode DoD printer. [84]	40
Figure 37. 3D assembly of a piezoelectric bending mode DoD generator. [85]	41
Figure 38. Schematic diagram of a piezoelectric push mode DoD printer. [86]	42
Figure 39. Schematic diagram of the PMPJT system. [87]	43
Figure 40. Schematic of a piezoelectric push mode DoD printer. [88]	44
Figure 41. Schematic of a piezoelectric push mode DoD generator. [89].....	45
Figure 42. LIFT system schematic. [90].....	46
Figure 43. LIFT system experimental setup. [91].....	46
Figure 44. LIFT schematic. [92].....	47
Figure 45. Laser-induced DoD printer. [93]	48
Figure 46. Laser droplet generator a) side view, b) front view. [95].....	48
Figure 47. Schematic of an ultra-high frequency induction heating DoD printer. [96].....	49
Figure 48. Schematic of a continuous stream droplet deposition generator. [97]	50
Figure 49. Microstructure bonding depending on surface temperature and droplet temperature: a) Diagram b) Over remelted microstructure c) remelted microstructure d) no remelted microstructure. [99].....	52

Figure 50. Weber number vs Ohnersorge number, showing the four regions of droplet behavior. [60].....	55
Figure 51. Dimensionless printability regimes:(a) We_j vs $Oh-1$, (b) We_j vs Re , (c) We_d vs $Oh-1$, (d) We_d vs Re . [101].....	56
Figure 52. Wetted regions and droplets generated under different contact angles. [62]	58
Figure 53. Droplet formation process. [104]	61
Figure 54. Initial printhead of the Novel DoD metal 3D printer. [104].....	62
Figure 55. (a)Industrial chiller, (b)fume extractor, (c)ZVS induction heater.	63
Figure 56. Schematic of the circuit of the ZVS induction heater.	63
Figure 57. Eddy currents heating effect.....	64
Figure 58. (a)57HSE3N stepper motor, (b) HBS57 stepper motor driver.	65
Figure 59. a) Gripping disk, b) Gear system, c) wire feeder assembly.....	66
Figure 60. MyRIO Board.....	66
Figure 61. MyRIO hardware diagram. [105]	67
Figure 62. Control System.	68
Figure 63. K-type thermocouple.....	68
Figure 64. Crucible system.	69
Figure 65.Ceramic crucible (a)bottom view (b)front view.....	70
Figure 66. Quartz (a) top view, (b) front view.....	70
Figure 67. Graphite nozzle.....	70
Figure 68. Infrared pyrometer.....	77
Figure 69.PID temperature control box.	78
Figure 70. User interface of the wire/filament movement control.....	79
Figure 71. VI executed in the real time processor.	80
Figure 72. VI executed in the FPGA processor.	81
Figure 73. Quartz insert, graphite disk and nozzle evolution.	82
Figure 74. Tungsten Carbide nozzle (a) top view (b) bottom view.....	83
Figure 75. Final schematic of the Novel DoD printer.	84
Figure 76. Final schematic of a printhead for a novel DoD printer. [104]	84
Figure 77. Droplet production experiment being carried out.	91

Figure 78. 100 droplets sample 1.....	98
Figure 79. Calculated droplet diameter of sample 1.....	99
Figure 80. Calculated droplet diameter distribution of sample 1.....	99
Figure 81. 100 droplets sample 2.....	100
Figure 82. Calculated droplet diameter of sample 2.....	101
Figure 83. Calculated droplet diameter distribution of sample 2.....	101
Figure 84. Calculated droplet diameter of the combined samples.....	102
Figure 85. Calculated droplet diameter distribution of the combined samples.....	102
Figure 86. Brass droplet produced.....	106
Figure 87. UI of the VI executed in real-time.....	122
Figure 88. Block diagram of the motor control section of the VI.....	123
Figure 89. Block diagram of the PID control section of the VI.....	123
Figure 90. Block diagram of the temperature reading section of the VI.....	124
Figure 91. Block diagram code of the VI execute in the FPGA processor.....	124

Table of tables

Table 1. 3D printer systems overview.	4
Table 2. Advantages and disadvantages of most common metal AM methods.	15
Table 3. Relevant commercially available metal 3D printers.	17
Table 4. Approximate droplet size and pressure needed for different diameter nozzles. [61]	25
Table 5. DoD techniques comparison.	51
Table 6. Characteristics of the four regions on the We vs Oh diagram. [52]	56
Table 7. Calculated steps needed to create a droplet from a 2.5mm wire.	75
Table 8. Calculated steps needed to create a droplet from a 2mm wire.	75
Table 9. Calculated steps needed to create a droplet from a 1.6mm wire.	75
Table 10. Calculated steps needed to create a droplet from a 1mm wire.	76
Table 11. Experimental matrix with the constant variables for the experiment.	86
Table 12. Possible options for the constant variables of the experiment.	87
Table 13. Parameters used for the droplet sample collection.	97
Table 14. Calculated steps needed to produce the obtained droplets.	103
Table 15. 100 droplets sample 1 measurements.	128
Table 16. 100 droplets sample 2 measurements.	130

Abbreviations

DOD	Drop-on-Demand
3D	Three Dimensional
AM	Additive Manufacturing
CAD	Computer Aided Design
SLM	Selective Laser Melting
SLS	Selective Laser Sintering
UAM	Ultrasonic Additive Manufacturing
DD	Droplet Deposition
UNNC	University of Nottingham Ningbo China
ZVS	Zero-voltage Switching
FPGA	Field Programmable Gate Array
SM	Subtractive Manufacturing
PBF	Powder Bed Fusion
DED	Direct Energy Deposition
EBM	Electron Beam Melting
LENS	Laser-engineering shaping
MJT	Material Jetting
CS	Continuous Stream
EHD	Electrohydrodynamic
MHD	Magnetohydrodynamic
LIFT	Lase-induced Forward Transfer
PID	Product, integration, derivation
VMOS	Vertical metal oxide semiconductor
MOS	Metal oxide semiconductor

Chapter 1 Introduction

1.1 Background

In the past two decades, Additive manufacturing (AM) and three-dimensional printing (3D printing) have shown outstanding growth and development, as is shown in the yearly Wohlers Reports, which shows a sector growth of 19.5 % in 2021, and an average growth of 27% in the last ten years [1] [2]. The Wohlers Report is the AM and 3D printing industry's leading source for relevant economical and scientific news [3], consisting of 27th consecutive yearly reports based on 26 years of data collection and worldwide contacts [1] [4]. AM and 3D printing have become one of the most versatile technologies, being used in multiple industries like aerospace [5], energy generation [6], telecommunications [7], and construction [8]; and being researched in fields like biotechnology [9], chemical sciences [10], electronics [11] and biomedical engineering [12].

Additive manufacturing (AM) is a technology that allows the creation of 3D parts originally generated by 3D Computer Aided Design (CAD). AM is based on adding material in succession by different techniques to create the desired 3D part [13]. 3D printing, sometimes considered a synonym of AM, can be considered a subcategory of AM which includes all the techniques in which the material is added layer by layer [14].

AM techniques can be used with a variety of materials like polymers, metals, ceramics, concrete, edible items, and biological material [15]. Other than polymer AM, metal AM has experienced the biggest growth in the industry, showing an increase of 75.8% in 2013, 54.7% in 2014, 46.9% in 2015, and 79.9% in 2017, as reported by the corresponding yearly Wohlers Report [16].

Metal AM and metal 3D printing consist of the creation of 3D parts in which the raw material is metal powder, metal wire, or metal sheets. Metal AM has a diversity of techniques that involve different raw materials, energy sources, and working principles [17]. The more relevant metal AM techniques are selective laser melting (SLM), selective laser sintering (SLS), ultrasonic AM (UAM), and Droplet deposition (DD).

Metal Droplet Deposition consists of producing small droplets of molten metal, which are ejected to a moving substrate to form a desired shape by the remelting of these droplets [18]. Even though this method was previously used in polymers, it has proven to be complex to achieve and develop for metals; this is due to the properties of the metallic materials, which have a higher value of surface tension, melting temperature and thermal conductivity, making hard for droplets to remelt and create the desired shape with a good surface finish [19]. In the last years, droplet depositing has been a point of interest in research in the metal AM field, generating multiple new and novel droplet deposition techniques.

1.2 Project Background

In 2017 at the University of Nottingham Ningbo China (UNNC), the development of a novel metal 3D printer started. The project has been in development for the last 5 years and at the time of writing this thesis, it still is being actively developed. The development of the metal 3D printer has been conducted by different undergraduate, master's, and Ph.D. students at UNNC, supervised by Dr. Adam Rushworth.

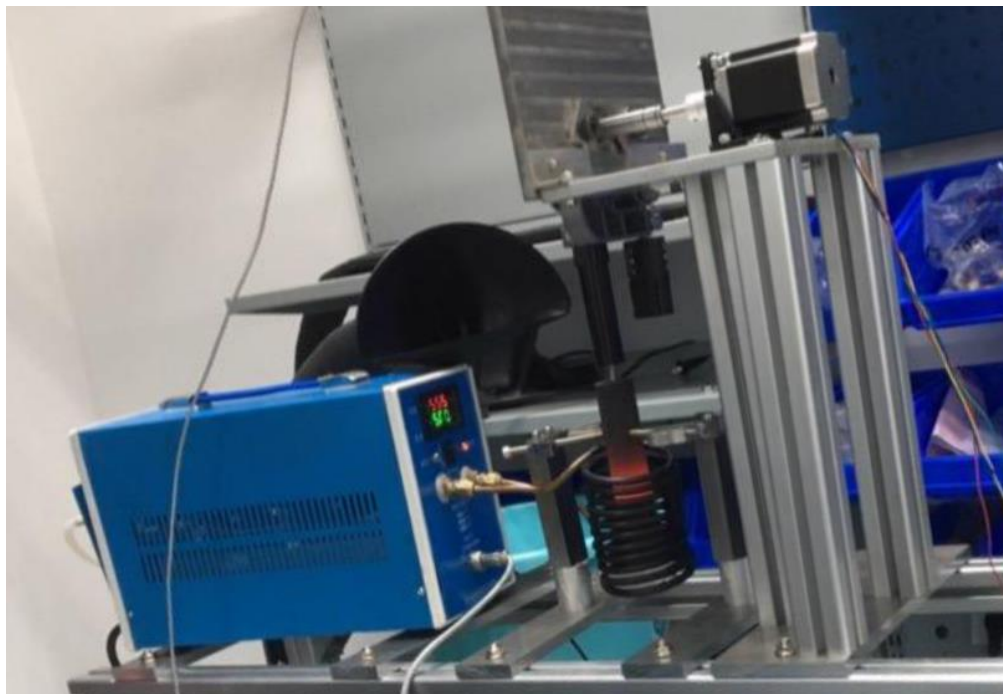


Figure 1. Early metal 3D printer prototype (2019).

The project at UNNC is focused on creating a metal 3D printer by using MJT (Material Jetting) as their metal AM method. MJT consists of depositing molten metal droplets to create 3D structures. MJT has shown being able to compete with modern metal 3D printers in resolution, precision, and smallest feature size, while at the same time being more affordable and compatible with more metallic materials compared to commercial metal 3D printers. For this, a new metal droplet deposition technique was developed based on drop-on-demand (DoD) droplet deposition.

This new DoD technique, provisionally given the name Metal Droplet Extrusion /Filament Droplet Extrusion, consists of a stepper motor that operates a wire feeder, which moves a metal wire downwards against the nozzle. The nozzle is heated by a zero-voltage switching (ZVS) induction heater. Part of the metal wire, while being in contact with the heated nozzle, melts and creates a melt pool at the nozzle, then when the downward force is produced by the stepper motor, the wire is pushed against the melt pool pushing the molten metal through the nozzle creating a droplet. This process is then repeated continuously to produce droplets while the substrate moves in XY directions and remelts the droplets in the desired position to create the desired metal part.

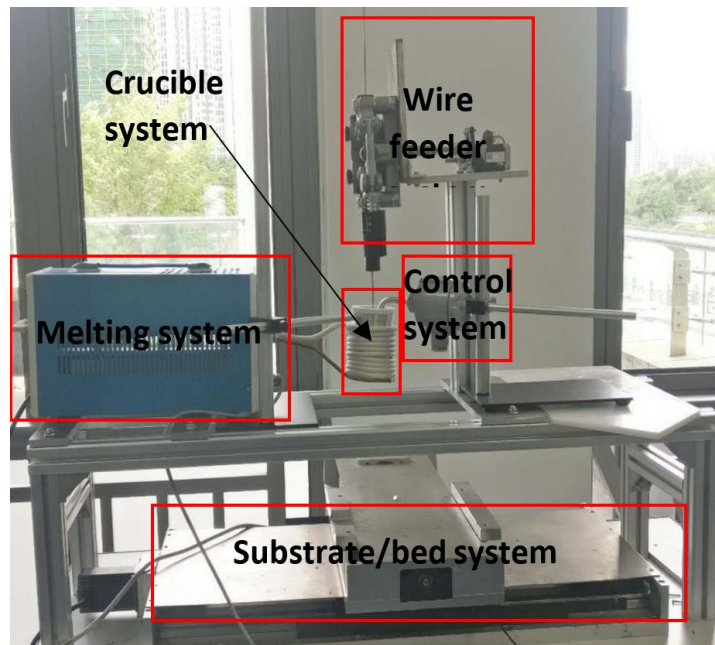


Figure 2. Metal 3D printer prototype (2020).

By 2020 the main systems of the 3D printer were defined, as shown in figure 1. There were five systems that the 3D printer would need to be able to operate: wire feeder system, crucible

system, control system, melting system, and substrate/bed system. Table 1 describes the five systems of the metal 3D printer, updated up to the 2021 prototype shown in Figure 3.

Table 1. 3D printer systems overview.

System	Description
Wire Feeder System	The wire feeder system function is to produce the downward force, achieved by pushing a metal wire of any metallic material downwards towards the crucible system. This movement supplies the crucible system with material and with the necessary downwards force to produce the droplets. This system is made up of a wire feeder attached to a stepper motor, and a support structure to support them and position them on top of the crucible system.
Crucible System	The crucible system function is to guide the wire, store the melt pool, and hold the nozzle that will aid in the formation of the droplets. The system is made up of a graphite nozzle, a quartz guide, and a ceramic crucible and its support. The wire goes through the quartz that guides it towards the nozzle, in a melt pool is formed, then the downwards motion of the wire towards the nozzle produces pressure in the melt pool thus allowing some of the molten material to escape through the nozzle, generating the droplet.
Melting System	The melting system function is to generate heat at the graphite nozzle inside the crucible system, to accomplish this a high alternating current at high-frequency is applied through a coil, which will induce current into the graphite nozzle, thus generating the heat. To generate the high frequency alternating current a ZVS (zero-voltage switching) induction heater is used. The system is made up of a 20 KW ZVS induction heater, a fume extractor (to absorb any fumes produced by the melting of the metals), and an industrial chiller (to cold down the ZVS induction heater components).
Substrate/Bed System	The substrate/Bed system function is to control the formation of the 3D part, achieved by controlling the movement of the substrate in the XY directions and controlling the temperature of the substrate to allow the proper remelting of the droplets. The system is made up of a 2-axis linear stage, a resistive heating element, and a graphite substrate.
Control System	<p>The control system function is to control and coordinate the wire feeder system, melting system, and substrate/bed system to allow the manufacture of 3D parts. This involves:</p> <ol style="list-style-type: none"> 1. Controlling the temperature of the nozzle, which is achieved by a closed loop control that regulates the on/off times of the ZVS induction heater, depending on the temperature reading of the thermocouple. 2. Controlling the production of droplets, which is achieved by controlling the movement of the wire, by controlling the movements of the stepper motor connected to the wire feeder. 3. Controlling the deposition of the droplets and formation of the 3D parts, which is achieved by controlling the movement and temperature of the substrate assembly. <p>The system is made up of a thermocouple (used to measure the temperature of the nozzle), an Arduino MEGA (used to read the signal of the thermocouple), motor drivers (used to control the stepper motors in the wire feeder and the substrate/bed system), and a myRIO board (microcontroller with a field programable gate array (FPGA), that is used to receive the readings form the Arduino MEGA and to send the corresponding signals to the ZVS induction heater and the motor drivers), shown in figure 4. LabView is used to create the code that is applied to the myRIO board.</p>

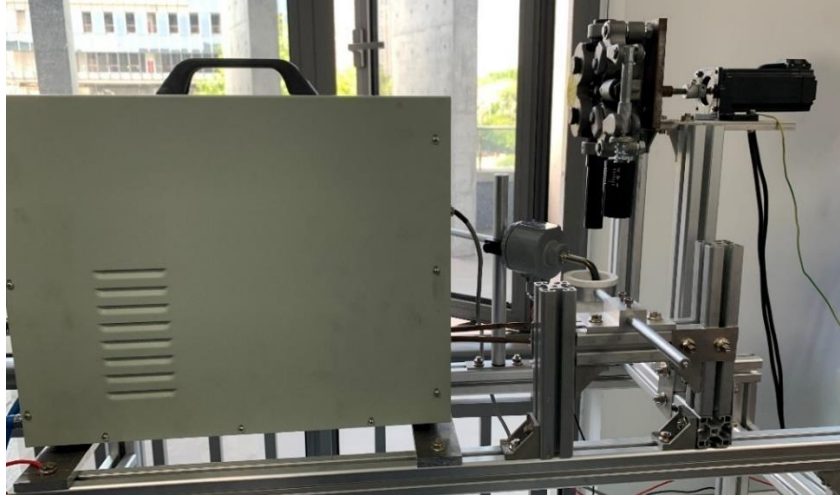


Figure 3. Metal 3D printer prototype (2021).

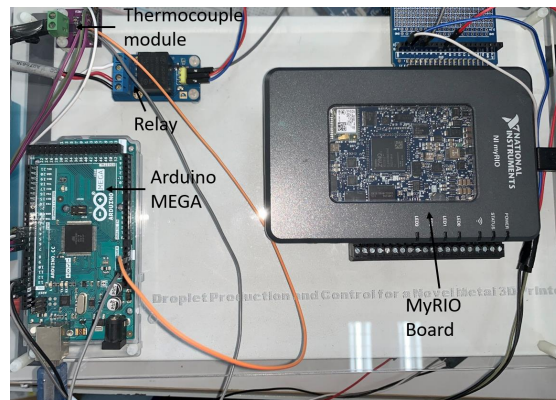


Figure 4. Control system (2021 prototype).

Despite the project being ongoing for a couple of years, having the main systems defined and the prototype assembled, it has not been able to work or validate that this new DoD technique is feasible for metal 3D printing. The project's main obstacle has been droplet production, the droplets resulting from the 2020 and 2021 prototypes can be observed in Figures 5 and 6, respectively. The 2020 prototype results show no consistency in shape or size, there are only two depositions that resemble droplets with a size of around 5mm, but the rest only show excessive molten material deposited each time. The 2021 prototype was able to produce three droplets of a decent size, two with a diameter of 550 μm and the last one with a diameter of 800 μm , in terms of shape, the droplet in Figure 6a shows an ideal droplet that solidified before reaching the substrate, the droplet in Figure 6b shows a droplet with an irregular and not ideal shape, and the last droplet in Figure 6c shows a droplet that impacted into the substrate and then solidified, showing a flat side and material surrounding the edge.

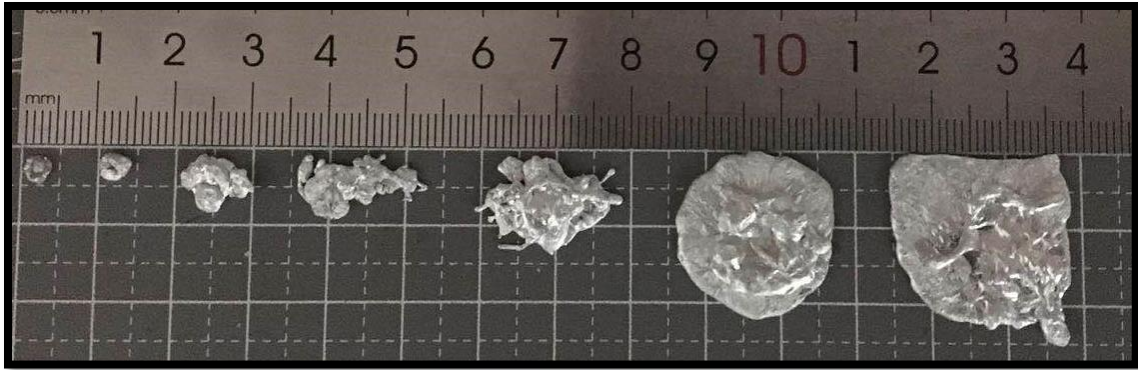


Figure 5. Droplet produced by 2020 prototype.

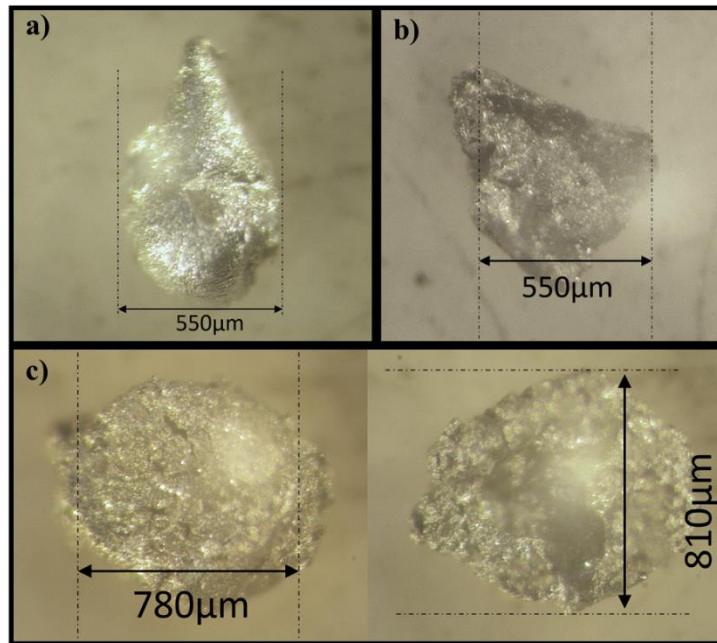


Figure 6. Droplet produced by 2021 prototype.

Droplet production is the first step needed for the metal 3D printer to verify that this new DoD technique is able to compete with existing techniques. With the previous results in mind, the main focus of the master research was decided, was to achieve a consistent droplet production, both in size and shape. To achieve consistent droplet production, the main efforts will principally involve the crucible system, control system, and wire feeder system, with some minimal involvement in the melting system, and no involvement in the substrate/bed system.

1.3 Aims, and objectives.

1.3.1 Aim

To achieve a consistent droplet production for a Novel metal 3D printer.

1.3.2 Objectives

1. Research other droplet deposition techniques to understand droplet formation.
2. Replace/optimize and modify existing systems of the printhead of a metal 3D printer to improve droplet production.
3. Test droplet deposition consistency.

1.3.3 Proposed Deliverables/Outcomes for the project

1. A better understanding of droplet formation.
2. Optimized and tested metal 3D printer systems of the printhead for droplet production.
3. Statistical analysis of the droplet production consistency.

1.3.4 Validation for the completion of Aim and Objectives

To validate the completion of objectives the following guidelines will be used:

Objective 1: A literature review of other droplet deposition techniques has to be written as part of the master's thesis, in which a good understanding of how droplets are formed in different techniques is shown. The understanding of droplet formation is applied to an existing 3D printer to improve droplet production.

Objective 2: A detailed record of the changes made to improve the printhead systems of the metal 3D printer has to be shown. Analysis and measurement of the improvements in the droplet production after the optimization/modifications to the printhead systems of the metal 3D printer are to be shown.

Objective 3: A statistical analysis of the droplet production of the system is to be produced, this will include the production of a considerable number of droplets and their measurement. The statistical analysis of the droplets is to be included in the master's thesis.

The desired droplet size is between 0.6mm and 2mm, the material decided to be used is aluminum alloy 6061. 0.6mm was chosen to be the minimum value since the nozzle diameter is 0.6mm, and 2mm was chosen to be the maximum value since most DoD techniques produce droplets with a diameter close to twice or thrice their nozzle diameter. For droplet production to be regarded as consistent, a distribution as shown in Figure 7 or better must be achieved (assuming the droplet production to have a normal distribution and the average droplet size is 0.6mm), with a standard deviation of 0.167mm or better. A standard deviation of 0.167mm was chosen since 99.8% of the produced droplets will be within the average droplet diameter ± 0.5 mm, and 68.2% of the droplets will have a diameter within the average droplet diameter ± 0.167 mm, thus the droplet size can be considered consistent and the variance within the droplet diameter should not affect the quality of the final produced part.

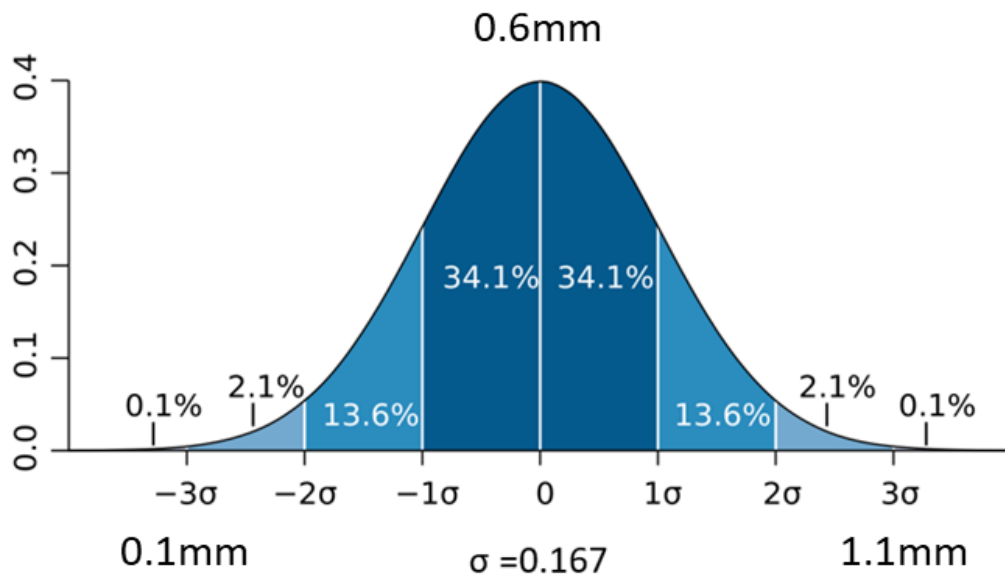


Figure 7. Desired normal distribution of consistent droplet production.

1.4 Thesis structure

In chapter 2, the literature review is presented. First, an introduction to metal 3D printers reviewing the most common methods is shown, then the more relevant commercial metal 3D printers will be mentioned. Then Droplet Deposition and Droplet-on-Demand are going to be introduced, then the most relevant Droplet-on-Demand techniques are reviewed and compared. Finally, different numerical analyses of droplet production are mentioned.

In chapter 3, the methods are shown. The evolution of the printhead is shown, first the prototype used at the start of the research is explained, then the evolution and changes made to the systems are detailed. Then the different types of experiments carried out during the research are mentioned together with the experiment's normal procedure. Finally, the droplet sample collection is explained.

In chapter 4, the results are shown. First, an analysis of the impact that some parameters have been observed to have in droplet production is discussed, then the results of the droplet sample collection are shown and statistically analyzed to prove if it is a consistent droplet production or not. Finally, some results obtained with other materials are detailed.

In chapter 5, the conclusion is shown, in which the aim and objectives are analyzed to see if they have been achieved, also, recommendations for future research of the project are made.

Chapter 2 Literature Review

2.1 Introduction

Almost all known metal elements are used in different daily applications like electronics, medical equipment, energy applications, and aerospace [20]. With the expansion of applications of metal parts/structures, traditional manufacture (casting, forging, and machining) has been proven to have a limited capability to satisfy all requirements for the new metal parts/structures. Because of this need metal 3D printing, which allows a higher part complexity and design freedom, has been having more attention and development [21]. Metal 3D printing was mainly developed to overcome the downsides of subtractive manufacture (SM), those downsides are the part simplicity, high material waste, and limited possible geometries [22]. In contrast to traditional manufacturing methods like SM, metal 3D printing facilitates the production of metal parts with complicated geometry, making it feasible to reduce component count and optimize the weight of metal parts in an assembly. A wide variety of metallic materials, including ones that traditional manufacturing is unable to employ due to the material's physical properties, can be used in metal 3D printing, making it more flexible [17].

AM involving metals started evolving over half a century ago from fusion welding, which used to do repairs of damaged or worn components [23]. But it was not until the last two decades that AM involving metals, now commonly known as metal 3D printing, completely changed the manufacture of metal parts. In 1990, Bourell was the first one to produce a 3D-printed metal part using laser sintering techniques in a copper-solder mixture [24]. It will be in 2004, with the commercial release of the EOSINT M270(the first commercial full dense metal 3D printer), that manufacturers started using metal 3D printers for the manufacture of metal parts.



Figure 8. First full dense commercial 3D printer (EOSINT M270).

Metal AM includes different manufacturing methods, the four most common being powder bed fusion (PBF), directed energy deposition (DED), material binder/jetting, and metal material extrusion. Each of these methods contains different techniques, the most famous of these are selective laser melting (SLM), selective laser sintering (SLS), electron beam melting (EBM) [25], and laser-engineered net shaping (LENS) [26] [27].

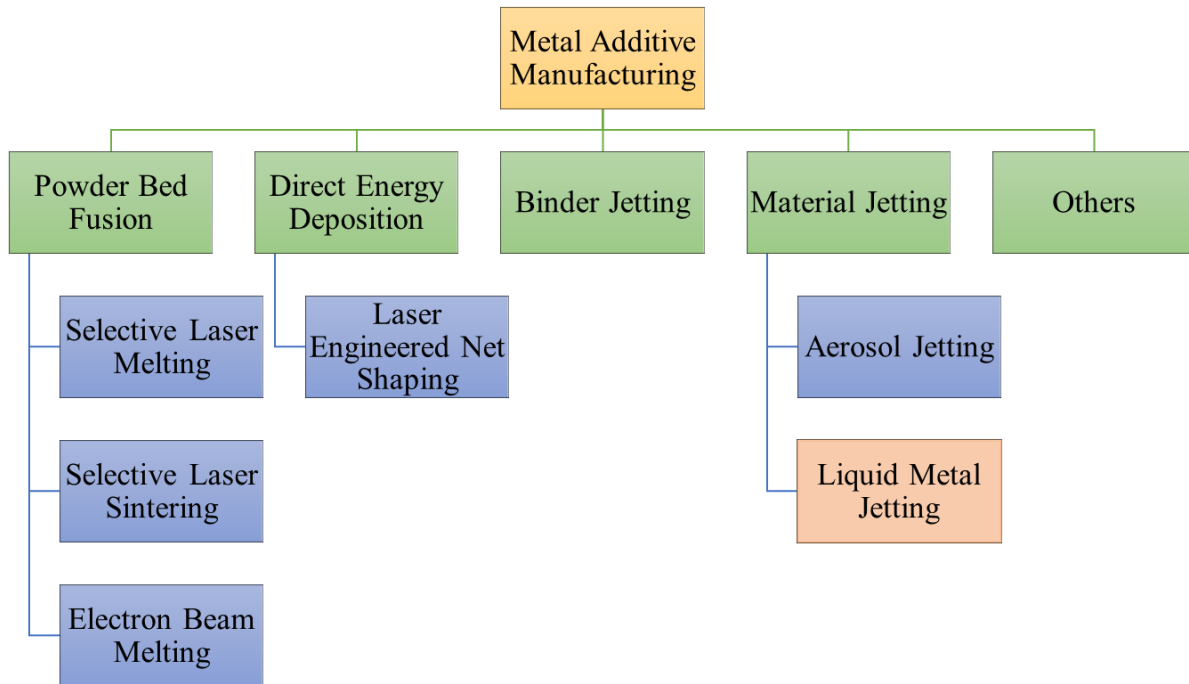


Figure 9. Metal AM’s most common methods and techniques.

Powder bed fusion is the most used method for metal 3D printers in the world, having more than 50% of the market share. Direct energy deposition and material binder/ jetting are the other 3D printing methods with a high market share with a combined of more than 35% of the market share [28].

Powder bed fusion (PBF) consists of the use of focused thermal energy (mostly laser beams or electron beams) to bond, fuse, or melt material together in a specific pattern [29]. A fine layer of metal powder is distributed into the base plate, then parts of this powder layer are fused together in the desired path, then another fine layer of powder is distributed on top of the previous layer, and then this process is repeated multiple times [30]. Selective laser melting (SLM) is the most popular among PBF, it creates parts using a focused laser beam (using scanning mirrors) into a specific path, to melt and fuse the powder metal layer into the desired shape [31].

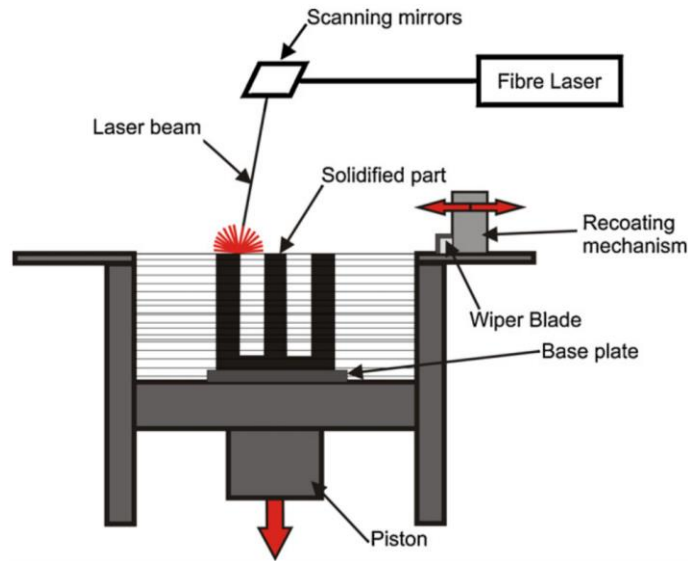


Figure 10. SLM operating principle. [31]

Direct Energy Deposition (DED) consists of the use of an energy source (mostly laser beams or electron beams) to melt the material on top of a substrate. DED uses metal wire or metal powder flow as its raw material. DED was first developed from welding, in which a metal wire is fed at a constant rate, and at the same time a laser is used to melt this wire on top of a substrate in a specified pattern to create the desired shape, but in 1996 a technique using metal powder flow was developed by Sandia National Laboratory. This new technique called laser-engineered net shaping (LENS) as now is one of the most common DED techniques. As shown in figure 10, LENS ejects metal powder into the substrate and simultaneously uses a laser to melt this powder in the desired position [32].

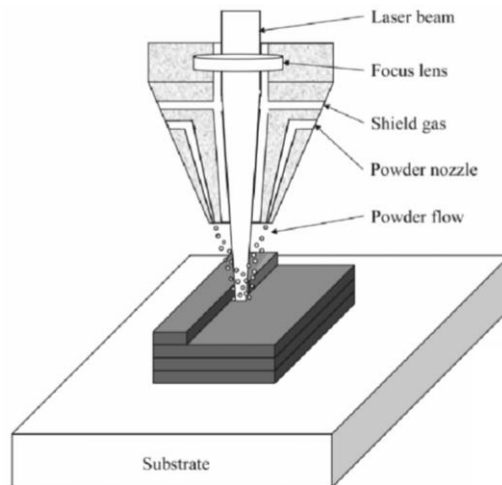


Figure 11. LENS operating principle. [32]

Material binding, also known as binder jetting, consists of one or multiple nozzles that eject liquid binder on top of the material to fuse it together. The raw material consists of a metal powder that is placed in thin layers, after a layer of metal powder is placed, the nozzle/nozzles move above the powder bed in the desired shape while ejecting the binder liquid, then another layer of metal powder is placed, and the process is repeated until the desired 3D shape is finished. The part resulting from this process is called the “green body” and it requires post-processing to become a fully dense metal part. The “green body” needs to cure for around 12 hours and then needs to be heat-treated for sintering, consolidation, and to burn away the binder [32].

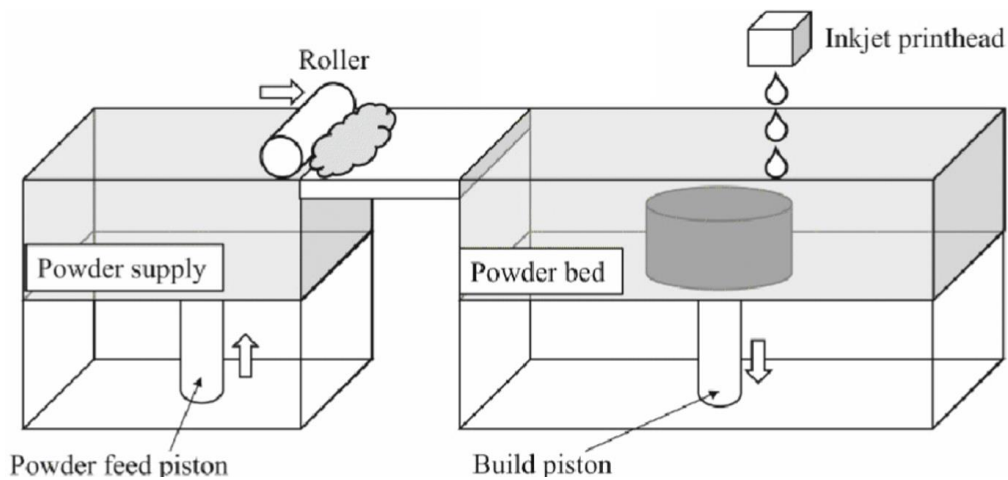


Figure 12. Binder jetting operating principle. [32]

Material jetting (MJT) consists of depositing small droplets of the desired material by using different inkjet methods [33]. These small droplets consist of liquid or molten metal, which are deposited into a moving substrate in a specified path that allows the creation of a 3D part [34]. MJT can be divided into aerosol jetting, in which an aerosol of droplets is deposited into a substrate, and liquid metal jetting, also referred to as droplet deposition (DD), in which a liquid/molten metal is deposited into a substrate in a single droplet by droplet manner [34]. MJT allows the use of multiple forms of raw material since what they finally require is just a liquid/molten state of those, any raw material that can be melted down into the nozzle can be used. Since the material used only needs to be at the nozzle, multiple nozzles would allow the printing of multiple materials at the same time which is a big advantage compared to other metal AM methods.

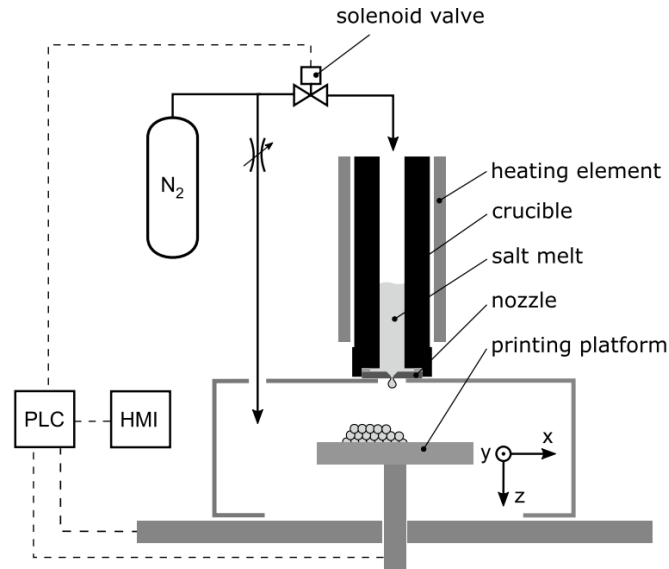


Figure 13. Liquid metal Jetting example showing a liquid metal jetting system. [34]

Beam metal AM methods (PBF and DED) lead the metal 3D printing field with a wide variety of commercial machines, but they are not made for consumer use, due to their price, size, complexity, and safety concerns. On the other hand, MJT techniques only require a molten metal supply of the desired material, thus the raw material can come in any shape or form, reducing the price and safety concerns that exist while using metal powders, making metal MJT a possible candidate for becoming a consumer metal 3D printing method, that will allow metal 3D printing to become widely available.

Even though Beam metal AM methods have been widely adopted for metal 3D printing, they still have some limitations and defects in the produced parts. Most common defects are related to the high cooling rates and high temperature gradients that are produced when using a beam or laser on the metal powders, which causes the produced part to have some residual stresses that produce distortion or cracking inside the printed part [35]. Another issue related to the high cooling rate of beam metal AM methods is “hot cracking” (solidification cracking, liquation cracking, ductility-dip cracking, and strain-age cracking) that occurs when the raw material is a non-weldable alloy [36] which include most Ni-based superalloys and some Al-based alloys like Aluminum 6061, 7075 and stainless-steel alloys [37] [38]. MJT techniques can solve these issues since the cooling rate of the material is far slower than beam metal AM methods, due to the material being completely melted first and then deposited on a heated substrate in which is kept at a high temperature to allow droplet remelting to form a solid part.

Table 2. Advantages and disadvantages of most common metal AM methods.

	Advantages	Disadvantages
<p>Powder Bed Fusion</p> <p>[23] [30] [31]</p>	<p>1.-Is the most famous and commercially available method for metal 3D printing, making it very reliable, and is often used as the main comparison for new metal 3D printing techniques.</p> <p>2.-Due to the very thin layers of powder and the high precision of the focused thermal energy (mostly lasers), it is able to create high-resolution parts with complex geometries.</p> <p>3.-The resulting parts do not need extensive post-processing other than cleaning and surface finishings if needed.</p> <p>4.-The resulting parts achieve a density higher than 99%, giving them the same or sometimes even better mechanical properties than the bulk materials.</p> <p>5.-This method does not have the need to include supports for the overhangs and other structures, because the powder layers act as a support for anything printed on top of them.</p>	<p>1.-The machine makes use of metal powders as raw material. Metal powders are expensive, hard to produce, and hard to handle.</p> <p>2.-Due to the way the material is added, fully enclosed cavities are impossible to create, making weight reduction limited for this method.</p> <p>3.-Even though not having supports is an advantage, for some materials it may cause some warping due to the heat of the part in creating affecting the powder bed that is offering support to it.</p> <p>4.-The surface quality is low, showing a layered finish, most times post-processing is needed to improve the surface finish.</p> <p>5.-Due to the need of preheating the powder bed, and cool it off after the finished part is produced, the print time is longer than other methods.</p>
<p>Direct Energy Deposition</p> <p>[32]</p>	<p>1.-The resulting part can achieve a density higher than 99%, creating strong parts with mechanical properties as good as bulk material.</p> <p>2.-It can not only be used to produce parts but also to repair and fix other parts.</p> <p>3.-Is the method that can print the largest parts compared to other metal AM methods, with a theoretically unlimited part size.</p> <p>4.The build of the parts produced is the highest among all the other metal AM methods.</p>	<p>1.-It has a very bad resolution of printing, making post-processing machining required in most parts.</p> <p>2.-The layers created are very thick, making most surfaces require post-processing.</p> <p>3.-Because of the bad resolution and thick layers, fine features are impossible to achieve.</p> <p>4.-Because it lacks the capabilities of creating support structures, it cannot manufacture structures like overhangs.</p>

<p>Binder Jetting</p> <p>[32]</p>	<p>1.-It has a remarkably high resolution and printing time.</p> <p>2.-Does not need supports for overhang structures, because the powder material acts as a support for the layer on top of it.</p> <p>3.-There is no part deformation or warping during the printing process, due to not having a heat source during the process.</p> <p>4.- It is able to produce parts in batches, making it highly productive.</p>	<p>1.-It requires extensive post-processing, which includes cleaning, de-binding, and sintering, this increases the overall part-production time and cost.</p> <p>2.-The parts shrink during the sintering process. This may cause warping and is hard to predict the final dimensions of the piece.</p>
<p>Material Jetting</p> <p>[33] [34]</p>	<p>1.-It has a remarkably high resolution with very thin layers.</p> <p>2.-It uses liquid/molten metal, which is considerably easier to handle than powders, cheaper to produce, and allows for a bigger variety of materials.</p> <p>3.-Is able to produce a good surface finish and very small features with high precision.</p>	<p>1.-Because of the thin layers produced, it takes more time to produce the parts compared to other metal AM methods.</p> <p>2.-The parts that can be manufactured by this method are small, due to the printing speed and part heating needed for remelting.</p> <p>3.-Is one of the newest methods, with very few commercial machines, which tend to be expensive and unreliable.</p>




In conclusion, there is a vast variety of metal AM methods, each with their advantages and disadvantages. The most used around the world at the moment is SLM, a technique that uses the PBF method, due to its reliability and long history. As a result of recent advances and research being done in other techniques and methods, SLM is no longer the only good metal AM option, having methods and techniques that surpass SLM in some respects like price and printing time. Making it a period in which each industry application may have a different preferred method and technique that allows them to manufacture their metal parts more efficiently with a higher quality and lower costs. With the growing interest in metal AM and the increasing demand for 3D-printed metal parts, it is the perfect time to research and develop new metal AM methods and techniques that may overcome the current disadvantages of metal AM or specific metal AM methods.

2.1.1 Commercial Metal 3D printers

Table 3. Relevant commercially available metal 3D printers.

Commercial metal 3D printer	Description
<p data-bbox="293 392 461 420">DMP Flex 100</p> 	<p data-bbox="578 436 1417 695">Developed by 3D systems SLM and released in 2018, the DMP Flex 100 is an SLM printer focused on the manufacturing of small complex parts. The materials available for this 3D printer are mostly stainless-steel powders and cobalt-chrome powder aimed for dental applications. It uses a 100 watts laser and is able to create parts with a maximum size of 100x100x80 mm with an accuracy of +/- 50 µm. The price for this machine starts at \$245,000. [39]</p>
<p data-bbox="315 749 440 777">EOS M100</p> 	<p data-bbox="578 793 1417 1052">Developed by EOS and released in 2015, the EOS M100 is an SLM printer focused on the manufacturing of metal parts for medical applications. The materials available for this 3D printer are cobalt-chrome, stainless steel, titanium, and tungsten, all in powder form. It uses a 200 watts fiber laser to create parts with a maximum size of 100x100x95 mm with layers 0.1mm thick. The price for this machine starts at \$350,000. [40]</p>
<p data-bbox="245 1106 509 1134">Arcam EBM Spectra L</p> 	<p data-bbox="578 1150 1417 1367">Developed by General Electric additive and released in 2019, the Arcam EBM Spectra L is an EBM (electron beam melting) printer. This metal 3D printer only has titanium powders as its available material. It uses an electron beam with a power of 4.5 kilowatts to create parts of a size of up to ø350x430mm. [41]</p>
<p data-bbox="225 1442 527 1470">Concept Laser M2 Series 5</p> 	<p data-bbox="578 1528 1417 1745">Developed by General Electric Additive and released in 2019, the Concept Laser M2 Series 5 is an SLM printer. It has a wide variety of metal powders that can be used, like stainless steel, maraging steel, aluminum, nickel, titanium, and cobalt. It uses either two lasers of 400 watts each or two lasers of 1 kilowatt each and is able to create parts of a size of up to 245x350x350 mm. [42]</p>

<p style="text-align: center;">SLM 125</p> 	<p>Developed by SLM solutions, the SLM 125 as its name indicates is an SLM printer. It uses a 400 watts fiber laser to create parts with layers of a minimum size of 20µm and a minimum feature size of 140µm. [43]</p>
<p style="text-align: center;">L-Series</p> 	<p>Developed by Formalloy and released in 2017, the L-Series is a DED printer. It uses a co-axial 4-stream nozzle with a blue laser of 450 nm with a power of 8 kilowatts that allows more efficient processing of copper alloys. It comes in different sizes and is able to create parts of a size up to 200x200x200 mm, 500x500x500 mm, or 1000x1000x1000 mm depending on the model. It is able to produce layers as small as 0.5 mm and with a resolution between 0.5 to 8 mm. [44]</p>
<p style="text-align: center;">Production System P-1</p> 	<p>Developed by Desktop metal and released in 2019, the Production System P-1 is a binder jetting metal 3D printer focused on high-volume batch production. It uses 2 piezo-electric printheads that have 4096 nozzles. It is able to print at a speed of 1,350 cc/hr, with layers of 30µm-200µm, and can create parts of a size of up to 200x100x40 mm. [45]</p>
<p style="text-align: center;">DM P2500</p> 	<p>Developed by Digital Metal and released in 2017, the DM P2500 is a binder jetting printer. It mostly uses stainless steel and titanium in powder form as its material. It is able to print 500cc/hr with layers 40µm thick and an accuracy of 10µm in the XY direction. The maximum part size that this printer is able to produce is 203x180x69 mm. [46]</p>
<p style="text-align: center;">LightSPEE3D</p> 	<p>Developed by SPEE3D and released in 2017, the lightSPEE3D is a material jetting printer (aerosol). It can produce aluminum and copper parts. Its print speed is extremely high at 100g/minute but has a poor resolution of 6mm. Due to the technique used the parts created by this method need post-processing machining and cannot create small details. It can create parts of a size of up to ø350x300mm. The price for this machine starts at \$650,000. [47]</p>

<p style="text-align: center;">Carmel 700M</p> 	<p>Developed by XJet and released in 2019, the Carmel 700M is a material jetting printer. It uses a technique called nanoparticle jetting, in which nanoparticles of the desired material are mixed in a liquid solution that evaporates, this mixed solution is sprayed by layers at 300 °C. It is able to create parts of a size of up to 501x140x200 mm. The price for this machine starts at \$599,000. [48]</p>
<p style="text-align: center;">MK1</p> 	<p>Developed by Vader Systems and released in 2016, the MK1 is a material jetting 3D printer that uses a droplet-on-demand technique called Magneto hydrodynamic (MHD). This 3D printer is no longer available, but it was sold for \$400,000. It was able to print parts of up to 305x305x305 mm with layers 0.1mm thick and an accuracy of 0.1 mm. [49]</p>
<p style="text-align: center;">Polaris</p> 	<p>Developed by Vader systems and released in 2017 as the follow-up to the MK1 3D printer. Using the same technique as MK1 (MHD) it is able to reach up to 1200°C, allowing it to work with materials like aluminum, bronze, and copper. This 3D printer has been discontinued but it was able to create parts of up to 305x305x305 mm. [50]</p>
<p style="text-align: center;">ElemX</p> 	<p>Developed by Xerox and released in 2020, the ElemX is the result of Xerox buying Vader systems and creating a printer using the same MHD technique. It is only able to use one aluminum alloy (4008) in wire form. It is able to produce parts of up to 300x300x 120 mm, with layers of a thickness of 0.24 and an accuracy of 0.5mm on the z-axis and 0.6mm on the x and y-axis. [51]</p>

2.2 Metal Droplet Deposition 3D printing

Droplet deposition (DD) is a common phenomenon, that exists in nature, agriculture, manufacturing, etc., in which a liquid that is ejected at high speed or is in free fall, divides into small droplets due to surface tension [52]. Metal Droplet Deposition is an additive manufacturing process that involves using this phenomenon to create metal parts without the need of using other tools or molds [53]. Metal DD uses a continuous production of metal droplets, deposited in layers to create the desired part, for this either the print head or the substrate move in XY or XYZ directions to allow droplets to be deposited next to each other, fusing them on a specific path, thus creating the desired metal 3D shape [54].

Depending on how the molten/liquid metal is ejected, metal DD can be divided into two categories: Continuous Stream (CS) and Drop on Demand (DoD). This will also influence how the droplet is formed [54]. DoD uses some sort of actuator to produce a pulsing downward force, which makes the molten/liquid metal be ejected through a nozzle, each time the force is applied a single metal droplet is ejected from the nozzle. CS uses an actuator to provide a continuous downward force, which makes the molten/liquid metal be ejected as a stream through the nozzle, after the stream has left the nozzle it will start grouping and forming droplets as it falls, this is due to the Plateau–Rayleigh instability [55].

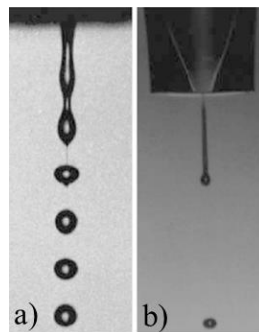


Figure 14. metal Droplet Deposition, a) Continuous stream, and b) Drop on Demand. [54]

As a result of how the droplet is formed, each category has its own advantages and disadvantages. DoD has high precision and repeatably, together with an ease of integration with a moving substrate to create 3D shapes, but it has a low print rate. On the other hand, CS has a high printing rate, but due to the difficulty of integration with the moving substrate to produce 3D shapes, it has a lower precision and repeatability.

Metal Droplet deposition has been researched for the past decades, allowing different techniques to be developed, the most relevant DoD techniques being shown in Figure 15. These DoD techniques differentiate from each other by how they produce the pulsed downward force.

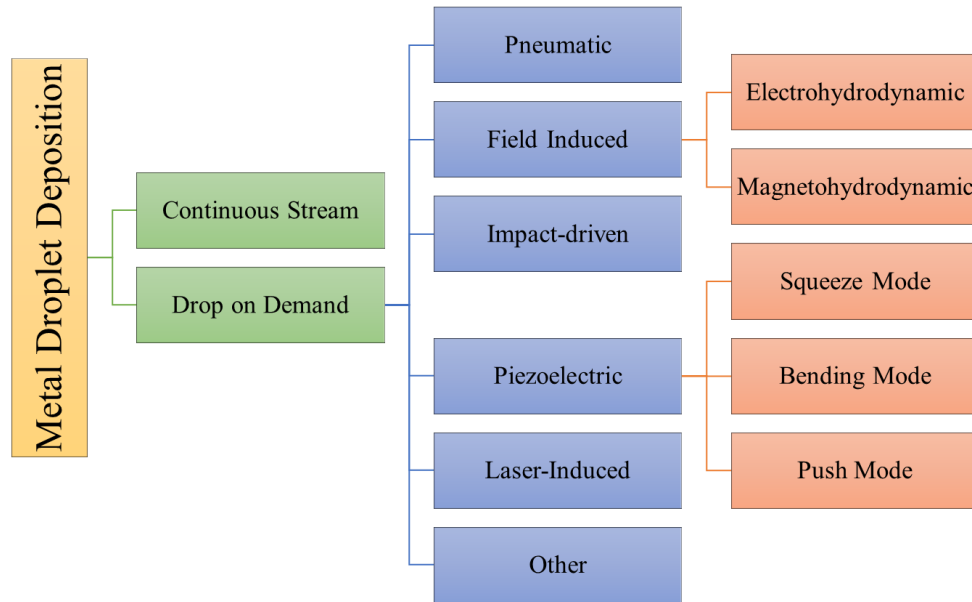


Figure 15. DoD techniques.

2.2.1 Pneumatic Drop-on-Demand printing

Pneumatic DoD printing consists of the use of compressed gas to produce metal droplets. This technique can be traced to different origins, from the study of water micro-droplet production [56] to studies of continuous streams of molten metal [57]. This technique has become one of the most used in DoD research only surpassed by piezoelectric DoD. Pneumatic DoD uses a compressed gas applied in pulses into a heated container with molten metal to force the metal through a nozzle, thus creating droplets [58]. The pressure released in pulses, together with the surface tension and gravity is the reason droplets can form when molten metal is ejected through the nozzle [59]. The droplet production is then synchronized with a moving XY stage, allowing the creation of any geometry by controlling the movement of these stages. Normally the pressure pulses are created by controlling a solenoid valve, this means there are no moving parts in the molten metal container, allowing the use of higher temperatures without the risk of damaging the actuators [58].

A research group at the University of Toronto developed a DoD printer based on a pneumatic metal droplet generator. This DoD system is formed by a droplet generator, an XY stage with a substrate, and a control system, as is shown in Figure 16 [19] [58]. The materials tested with this pneumatic DoD printer include indium, zinc, and bismuth, but tin was the main material used in testing [58].

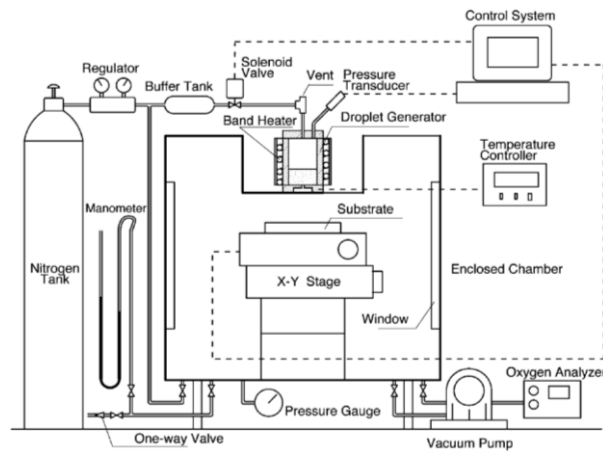


Figure 16. Schematics of the Pneumatic DoD printer developed at the University of Toronto. [58]

University of Toronto's droplet generator printhead, shown in Figure 17, consists of a steel cylinder container, filled with molten metal, with an interchangeable synthetic sapphire nozzle at the bottom, connected to a gas supply by a solenoid valve [19] [58]. The container is typically heated around 50°C above the melting point of the metallic material, by a 400W band heater that surrounds the container [19] [58].

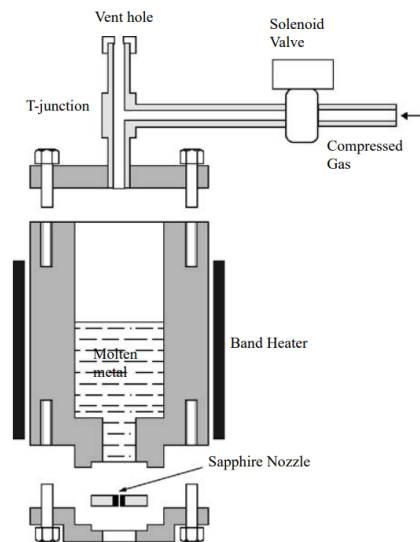


Figure 17. Schematic of a pneumatic droplet generator developed at the University of Toronto. [19]

This pneumatic droplet generator works by suddenly increasing the pressure of the container, which will push the molten metal through the nozzle, ejecting a droplet, and then rapidly dropping the pressure of the container to pull the molten metal back and prevent extra droplets to be ejected [58]. The pressure of the container was increased by opening the solenoid valve in pulses of 10 to 12 milliseconds (time that allows the ejection of a single droplet), which is connected to a nitrogen supply line with a gauge pressure between 70 to 400 kilopascals [58]. Due to the solenoid's maximum operating frequency (4 hertz), the high pressure was maintained for longer than desired, creating a long jet of molten metal that created multiple droplets. To solve this, a stainless-steel T-junction was installed in the output of the solenoid valve with one side connected to the container and the other side covered with a cap with a drilled hole, this hole helped the nitrogen be vented out, allowing a quick drop in pressure in the container [58].

This DoD printer is placed inside an aluminum chamber of a size of 305x 305 x 305 mm. This aluminum chamber helps to control the oxygen content that surrounds the printer, for this first the chamber is emptied with a vacuum pump, reducing the oxygen content to 35ppm, then the chamber is refilled with nitrogen to atmospheric pressure [58]. A low oxygen content (below 150pp) is needed because oxygen can cause metal oxidation that can block the nozzle [58].

This pneumatic droplet generator is able to produce droplets of a diameter between 170 μm and 600 μm , using nozzles with holes of a diameter of 76 μm to 254 μm [58]. A nozzle with a diameter of 177 μm was able to generate tin droplets of a size of 180 μm or 350 μm , a nozzle with a diameter of 254 μm was able to generate tin droplets of a size of 600 μm , and a nozzle with a diameter of 355 μm was able to generate tin droplets of a size of 750 μm [19].

Another DoD printer was developed at Northwestern Polytechnical University, this printer was developed with the purpose of creating complex and fully dense connections between microelectronic devices with solder, being able to solder copper cables to pins of a circuit using the deposited droplets and a remelting process [60]. This printer is made of a metal droplet generator, a pressure sensor, a CCD system, and a glove box [61]. Solder alloy Sn-40wt%Pb in molten form was used in this DoD printer. To prevent the solder to oxidize, the system was placed inside a glove box that was kept an oxygen level of less than 100 ppm [60] [61]. For the substrate, a copper substrate kept at 170°C to 220°C to allow a proper remelting of the solder droplets [60].

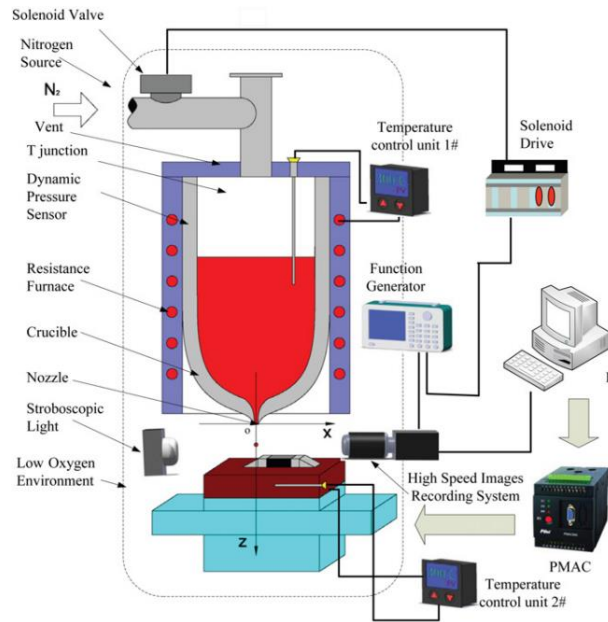


Figure 18. schematics of the Pneumatic DoD printer developed at Northwestern Polytechnical University. [60]

Northwestern Polytechnical University printhead, shown in Figure 18, consists of a quartz glass crucible with a small droplet at the bottom and connected to a T junction at the top. A resistance furnace is surrounding the crucible, which can be heated up to 265°C, and it is controlled by a commercial temperature controller unit [61]. The T junction connected at the top of the crucible is connected at one end to a solenoid valve, in which nitrogen is supplied in pulses, and the other end to the environment through a small vent [61]. The solenoid valve, positioned between the nitrogen supply and the T junction is able to increase the pressure, by pulses, of the crucible by opening and closing repeatedly, creating a single solder droplet at each high-pressure pulse in the crucible [61].

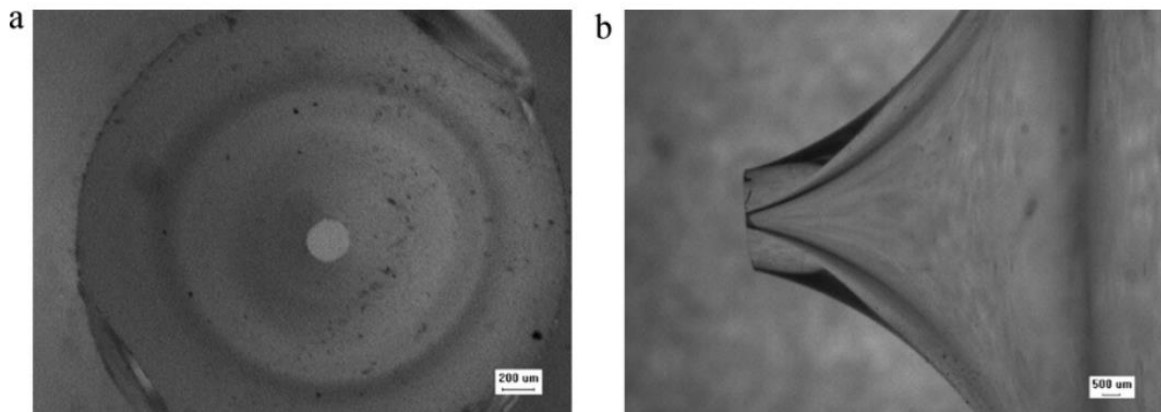


Figure 19. Quartz glass nozzle used in the metal droplet generator, (a) bottom view and (b) the side view of the nozzle. [61]

The droplet generator was tested with nozzles of different diameters than produced different droplet sizes and required different pressures to be able to produce a single droplet, shown in Table 4 [61]. It was shown that as the droplet diameter decreased the pressure needed to produce a single droplet is increased, and as the nozzle diameter decreases the proportion between the droplet size and the nozzle diameter increased [61]. A nozzle with a diameter of 120 μm was able to eject a droplet at 0.323 m/s, at this nozzle size 370 droplets were produced with an average diameter of 350 μm and a standard deviation of 9.4 μm [60].

Table 4. Approximate droplet size and pressure needed for different diameter nozzles. [61]

Nozzle diameter (μm)	Droplet diameter (μm)	Pressure (KPa)
100 μm	370 μm	14 KPa
120 μm	350 μm	10 KPa
150 μm	400 μm	8.5 KPa
200 μm	530 μm	5.5 KPa
220 μm	550 μm	5 KPa
260 μm	600 μm	5 KPa
300 μm	800 μm	5 KPa

Another relevant pneumatic metal droplet generator was developed by Zuo et al. [62], shown in Figure 20. The droplet generator was used to study the effect of wetting between nozzles of different materials at different temperatures and molten metal, specifically the impact it has on droplet size and deposition trajectory [62]. The DoD pneumatic droplet generator printhead consists of a graphite crucible, a solenoid valve, a snuffle valve, and an induction heating furnace. In contrast to other pneumatic DoD droplet generators, argon was used as the pressurized gas instead of nitrogen. This droplet generator was designed to be used for high-purity aluminum (99.99% pure), the raw material was in the form of a 30g ingot, which was inserted into a graphite crucible, where it gets heated and melted before the droplet production started [62]. The whole droplet generator was fitted inside a glove box filled with inert gas argon.

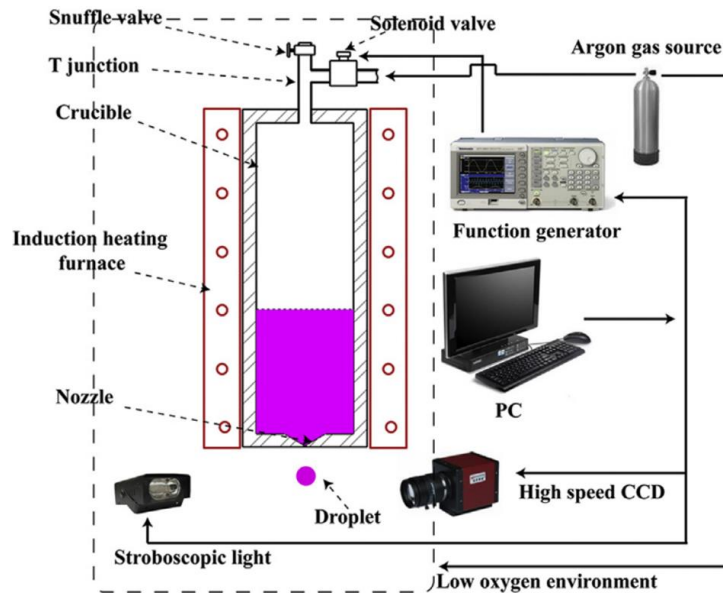


Figure 20. Pneumatic droplet generator. [62]

This pneumatic droplet generator functions in the same way as the past two, controlling the opening of the solenoid valve to generate pneumatic pressure pulses that push molten material through the nozzle at each pulse. The additional component that this droplet generator has, that the previous two do not, is a snuffle valve that is connected to a T junction connected also to the solenoid valve and to the graphite crucible. The nozzle is located at the bottom of the graphite crucible, it has a conical shape with an angle of 120° and a hole size of $500\mu\text{m}$ in diameter [62]. The main droplet production tested with this droplet generator was made with the graphite nozzle with a diameter of $518\mu\text{m}$, heated at 850°C and a pulsed pressure of argon at 50KPa , producing droplets of pure aluminum with an average diameter of $905.4\mu\text{m}$ [62].

2.2.2 Electrohydrodynamic Drop-on-Demand printing

Electrohydrodynamic (EHD) DoD printing consists of the use of pulsed electric fields to create droplets. EHD is mostly used in polymers or metal nanoparticles suspended in a solution and it does not always involve DoD, but also includes CS and filament-like extrusion [63]. EHD techniques make use of the influence of a strong electrostatic field, which induces charges into the liquid material, this charged liquid material is attracted toward the ground (grounded substrate). At a low electrostatic field, the liquid is prevented to exit the nozzle due to the surface tension of the liquid material [63]. As the electrostatic field increases, sheer stresses are produced on the surface of the liquid material due to the charges repelling each other. A repulsive force is produced

opposite to the surface tension, which causes the material to start leaving the nozzle [64]. After the critical electrostatic field is reached, the forces at the tip of the molten metal are disturbed, creating a cone, called Taylor cone, the length of this cone is increased until a jet/droplet is created [65]. Figure 21 shows this process used on a polymer solution.

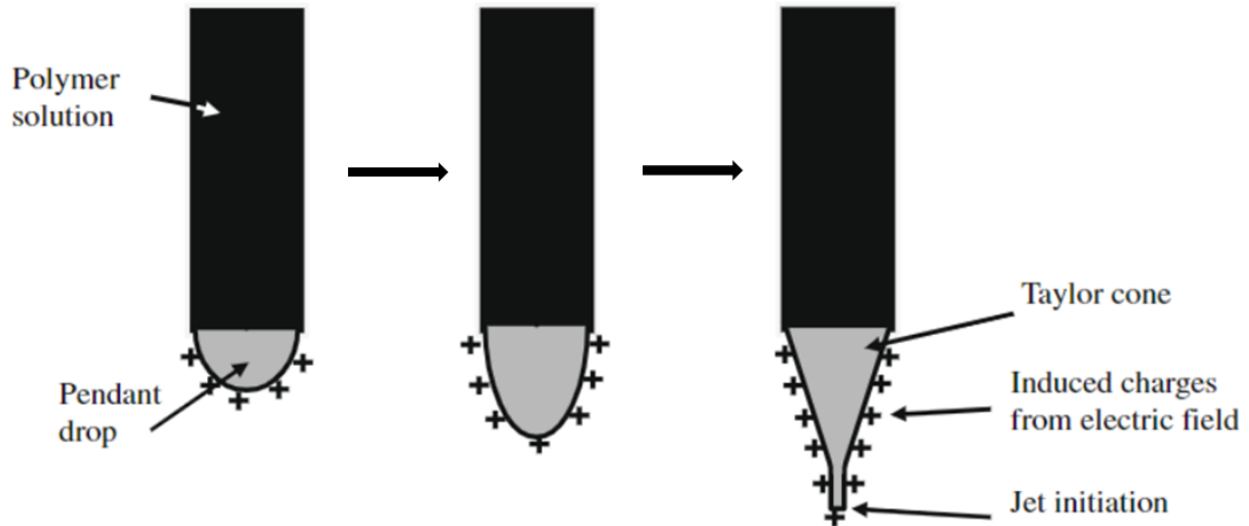


Figure 21. Electrostatic effect on a liquid material (Polymer solution). [65]

Wei et al. [66] developed an EHD DoD technique that makes use of modulated ac voltage pulses to generate droplets of silver NP ink. Figure 22 shows the common voltage waveform used in the production of droplets. There are three parameters that control the production of droplets for this EHD DoD printer, which are voltage maximum amplitudes, frequency of the sent pulses, and pulse duration [66]. The printing frequency is controlled by the ac pulse frequency. With the proper set of parameters for the maximum voltage and pulse duration, it is possible to create a single droplet for each positive and negative pulse [66]. The final printing frequency is two times the frequency of the pulse signal, this is due to the pulse signal being an ac signal, which in one period will have a positive and a negative pulse each producing a droplet [66]. The maximum voltage for the pulse will determine the amount of electric field if the voltage is not enough the Taylor cone will not form and the electrical stress will not be enough to eject the droplet [66]. The size of the droplet can be controlled with the duration of the voltage pulse, a longer pulse duration makes more surface charge to be accumulated, which produces a bigger droplet [66]. Also, because a positive and a negative charge are used in each pulse, they end up neutralizing each other at the substrate, which minimizes the residue charge in the printing process [66].

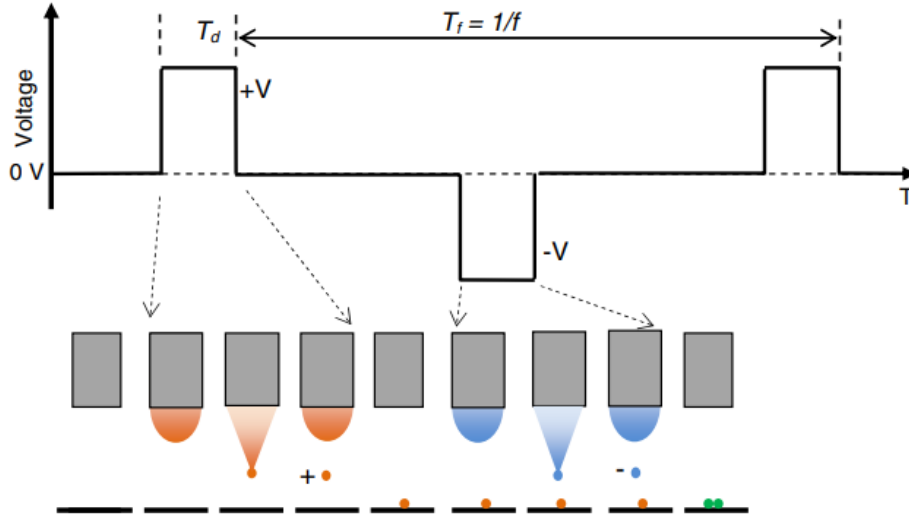


Figure 22. Usual waveform of the ac voltage pulse with the stages of droplet production. [66]

Han et al. [67] developed an EHD metal printing system, shown in Figure 23, the system is comprised of a high-voltage supply, a heating system, a three-axis machine, and a pneumatic dispensing system. A pneumatic dispensing syringe is used as the container for the liquid/molten metal, in this case, a field metal alloy made up of 51% Indium, 32.5% Bismuth, and 26.5% Tin [67]. The melting point of the material used is 60°C , and the syringe is kept at 193°C , by a heating rope, to achieve good flowability of the material. To provide the pulsed electric field to the material a high voltage supply is connected between the printing nozzle and the substrate, with the ground being connected to the substrate, and having a distance between the nozzle and substrate of $100\ \mu\text{m}$ [67].

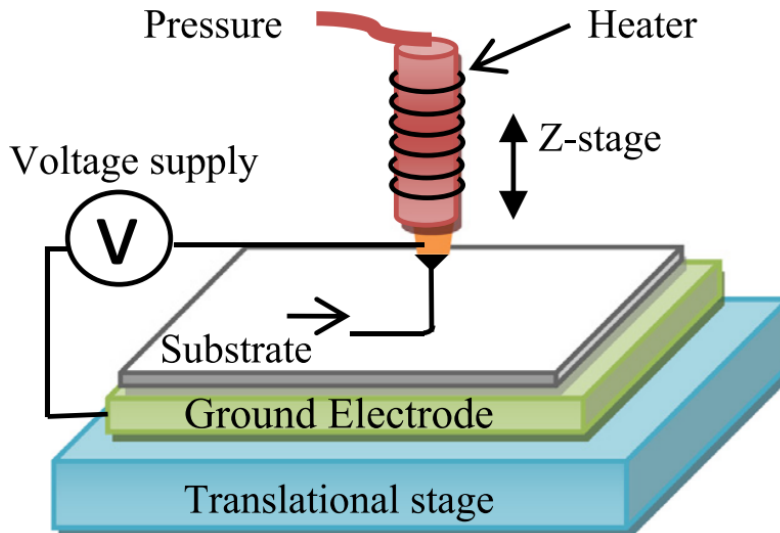


Figure 23. Schematic of EHD printing system. [67]

The printer initially tested only using the pneumatic syringe, proving that a large pressure(10psi) is required to produce a droplet, which had a size around 10 times bigger than the nozzle(160 μ m nozzle diameter) [67] [68]. After EHD is applied, the molten metal is able to produce a Taylor cone when a high voltage pulse is applied and able to produce droplet at a lower pressure(5psi), these droplets size was smaller than the nozzle and with a minimum size of 50 μ m [68]. At a higher voltage (>2000V), pressure from the pneumatic syringe is not needed, because the electrostatic force is big enough to overcome the surface tension of the material [68]. This machine also tested continuous filament printing which was able to create consistent uniform 50 μ m metal filaments when a constant high voltage is applied [68].

2.2.3 Magnetohydrodynamic Drop-on-Demand printing

Magnetohydrodynamic (MHD) DoD consists of using the effects that magnetic fields have when interacting with an electrically conductive fluid, to produce metal droplets. There are two main ways to use MHD to produce droplets, Magnetic MHD and electromagnetic MHD. Magnetic MHD makes exclusive use of a magnetic field applied to a liquid/molten material to produce droplets. On the other hand, electromagnetic MHD uses magnetic and electric fields applied to the liquid/molten metal to produce droplets.

2.2.3.1 Magnetic MHD DoD printing

Magnetic Magnetohydrodynamic (MHD) DoD consists of a pulsing magnetic field that induces a pulsing pressure inside a liquid/molten metal, which generates metal droplets. Even though MHD is not the most popular DoD technique in the research field, MHD is the technique that has achieved the most commercial success, being able to have 3 metal 3D printers commercially released (MK1, Polaris, and ElemX).

Vader Systems [69] developed an MHD DoD technique known as MagnetoJet. The MagnetoJet printhead consists of a ceramic heating chamber in which metal is continuously supplied, in form of a wire, by a wire feeder [70]. The wire is then melted by an induction heater and accumulated in the chamber. Around the chamber is a coil that when a pulse is supplied

through it, a magnetic field is generated. The generated magnetic field induces an electric field on the liquid metal. The magnetic and electric field in the liquid/molten metal produces a Lorentz force in the chamber. The Lorentz force generated is a radial force that points towards the center of the chamber, thus creating pressure that ejects material through the nozzle creating a droplet. Each time a pulse (positive or negative) is sent through the coil a single droplet is generated [71]. Figure 24 shows the schematic of the system and how the fields interact to generate the force needed to produce droplets.

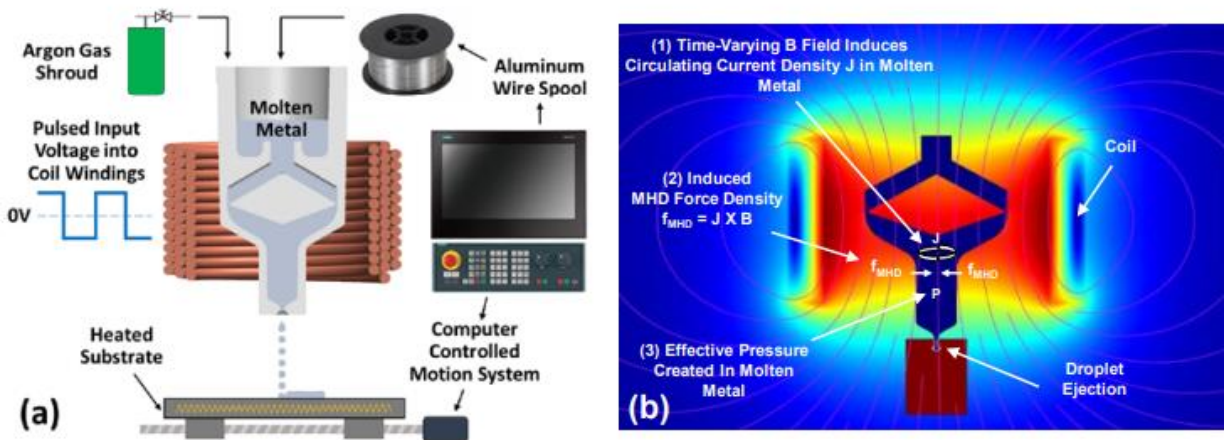


Figure 24. MagnetoJet printer a) system schematic b) simulation showing magnetic and electric field. [72]

Vader Systems has reported multiple advances with respect to the capabilities of this MagnetoJet technique, showing a clear advance in the last years [65-69]. In 2015, this technique showed it was able to create aluminum 6061 droplets of a diameter of $500\mu\text{m}$ to $1000\mu\text{m}$, at a printing rate of 0 to 300hz, these molten droplets were deposited successfully on a thermoplastic substrate, also the system was able to create structures made of gallium [69]. In 2016, this technique showed it was able to create aluminum 6061 droplets of a diameter of $250\mu\text{m}$ to $1000\mu\text{m}$, at a printing rate of 50 to 1000hz, these molten droplets were deposited successfully on a variety of substrates like thermoplastics, steel, and glass [70]. Finally, the last reported data in 2018 shows that this technique showed it was able to create droplets of a diameter of $50\mu\text{m}$ to $550\mu\text{m}$ using nozzles with a diameter of $100\mu\text{m}$ to $500\mu\text{m}$, at a printing rate of 40 to 1000hz, also the system was able to create solid metal structures made of a variety of aluminum alloys like aluminum 4041, 6061 and 7075 [73].

Meda et al. [74] did a study on the MagnetoJet technique developed by Vader System, by using their first commercial machine the MK1. Their study involves using aluminum 4043 to test the printing capabilities of the MK1 MagnetoJet printer applied to the fabrication of metal conductors on top of polymers [74]. By controlling the deposition frequency of the droplets, the impact on the printed features was shown, at high deposition frequency the droplets were ejected with different diameters, causing bulging, and overlapping structures, at low deposition frequencies the droplets, were ejected with small deviation in the droplet ejection, causing not straight features, and finally, an intermediate deposition printing was able to show a uniform droplet production, both in diameter and deposited direction [74]. With these findings, Meda et al. [74] were able to print electronic patterns with a uniform shape and high resolution, that was able to keep high electric conductivity, as shown in Figure 25.

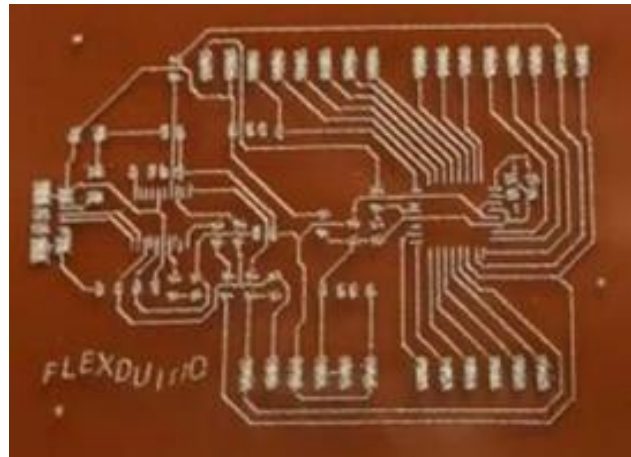


Figure 25. Electronic pattern created by MagnetoJet deposited on top of a polymer. [74]

2.2.3.2 Electromagnetic MHD DoD printing

Electromagnetic MHD DoD printing consists of the formation of droplets by an electromagnetic force applied into the liquid/molten metal, either a pulsed magnetic field applied into a constant electric field, or a pulsed electric field applied into a constant magnetic field.

An electromagnetic MHD printer was developed by Luo et al. [75], which involves an external magnetic field and an internal current, both applied simultaneously to liquid/molten metal, which is going to be driven by the resulting electromagnetic force. As shown in Figure 26, two electrodes are placed at opposite sides of the liquid metal container, and two permanent magnets

are placed at opposite sides and perpendicular to the electrodes. The electrodes generate an electric field and current in the liquid metal, and the permanent magnets generate a magnetic field perpendicular to the electric field. The electric and magnetic field generate Lorentz force on the charges moving through the liquid metal, which jointly produce a force perpendicular to both the electric and magnetic field on the liquid metal. This resulting downward force pushes the liquid metal through the nozzle, generating metal droplets [75].

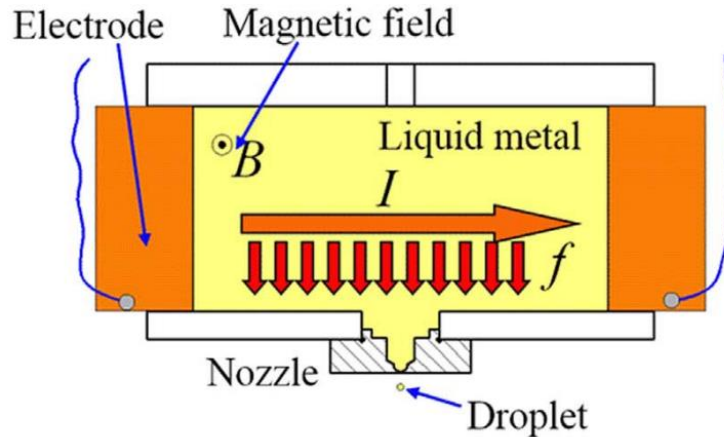


Figure 26. Electromagnetic DoD printer schematic. [75]

In this technique, the force produced in the liquid metal will depend on the current and the magnetic field applied. In the prototype developed by Luo et al. [75], a power source of 12 volts (40 Amperes maximum output) and a magnetic field with an intensity of 0.4T were used. A square wave was used for the current supplied, allowing it to control the production of the droplet. For each ON pulse of the square wave, a droplet is created, as shown in Figure 27.

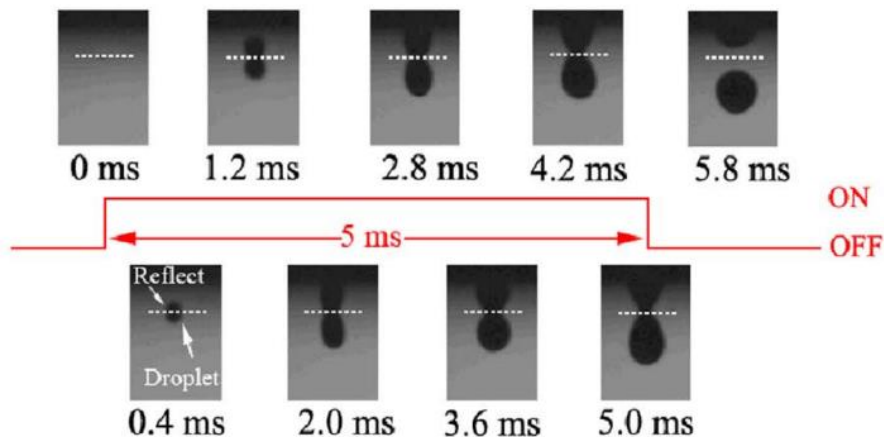


Figure 27. Droplet creation under a 5ms pulse of applied current. [75]

The materials evaluated in this prototype were mercury and an unspecified solder. For their main testing, they used a nozzle with a diameter of $300\mu\text{m}$ and a droplet production frequency of 100Hz . The droplets produced had an average diameter of $351\mu\text{m}$ with a standard deviation of $8\mu\text{m}$, measured from a sample of 100 droplets [75]. In conclusion, electromagnetic drop-on-demand printing presents an uncomplicated design for a stable and high-speed ejection DoD printer.

Suter et al. [76] developed an electromagnetic MHD DoD printhead, which uses micro-pumping MHD to generate droplets. The printhead consists of a rectangular container with two opposite walls insulators (microscope glass slides) and the other two electrodes (stainless steel electrodes), a ceramic nozzle at the bottom, and an open end at the top for material refill [76]. As shown in Figure 28 when a voltage is applied to the two electrodes, an electric field is created in the liquid/molten metal. When a magnetic field is applied perpendicular to the electric field, the Lorentz force acting on the moving electrons will push the material with a force perpendicular to both the electric and magnetic field [76].

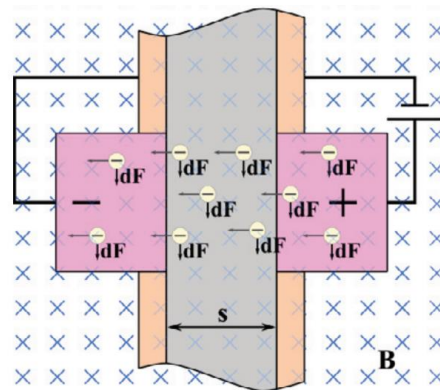


Figure 28. Schematic of an electromagnetic MHD printhead. [76]

Around the printhead, a coil is wound, and when a DC voltage is applied through the coil a magnetic field is created [76]. The magnetic field is also used to keep the temperature of the printhead by the resistive heat generated by the coil [76]. To create droplets using this printhead, first, a constant DC voltage is supplied to the coil to generate a constant magnetic field, then a pulsed DC voltage is applied to the electrodes to create a pulsing electric field on the liquid/molten metal. The pulsed voltage is a squared current that has a nominal value of 12V and a peak current of 1200A , each pulse has a period of 1 to 20ms [76]. The material tested in this printhead is tin, due to its low melting point, the printhead is heated to 300°C . The experimental chamber is flooded

with Nitrogen to avoid oxidation, with a nozzle of $500\mu\text{m}$ droplets of around $900\mu\text{m}$ were generated [76].

Simonelli et al. [77] developed another electromagnetic MHD DoD system, its printhead consists of an ejecting chamber surrounded by permanent magnets, which provide a constant magnetic field of intensity of 2T , and a pair of tungsten electrodes at the tip of the ejecting chamber, which create a pulsing electric field by running current through them, as shown in Figure 29. Due to the Lorentz force principle, when the electric field is created, a push force is applied to the molten/liquid metal that generates a metal droplet per pulse [77]. The materials used in this system are Sn and Ag, which are placed in the ejecting chamber, which is heated by an induction heater to allow the materials to melt. The system is placed inside an argon-filled environment to prevent oxidation [77].

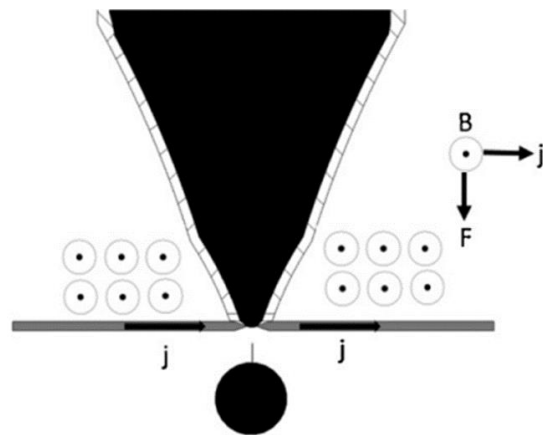


Figure 29. Ejecting chamber of a DoD MHD printer. [77]

The process of the droplet production of this printer starts with the Lorentz force being created by the pulsed current, which makes the molten metal be ejected through the nozzle forming a jet, then this jet breaks creating a droplet (due to surface tension), finally, the remaining jet is retracted into the nozzle (due to capillarity) and the process starts again [77]. The volume of the droplet can be controlled by adjusting the duration of the current pulse. The droplet's size and deposition speed are controlled by the shape of the nozzle, the intensity of the magnetic field, and the waveform of the pulsed electric current. The target printing resolution of this system is around $50\mu\text{m}$, but the system could achieve a bigger or smaller resolution depending on what is needed. With droplets produced at a frequency of 500 Hz , the droplet diameter deviation was within 10% of the average droplet diameter [77].

2.2.4 Impact-driven Drop-on-Demand printing

Impact-driven DoD printing consists of using the movement of a rod caused by the impact of an actuator to generate droplets. Luo et al. [78] developed an impact-driven DoD droplet generator, shown in Figure 30. The impact-driven droplet generator printhead consists of a crucible, with a nozzle at the bottom, and a solenoid-derived impacting system. The crucible is made of stainless steel and is heated to 400°C using an induce heater, this allows it to melt the metal and keep it liquid. The solenoid-derived impacting system consists of a solenoid that is able to generate an electromagnetic field by controlling the pulsed voltage going through it, this electromagnetic field moves an impacting rod; The impacting rod hits the top of the vibration transferring rod, which transfers this movement to the liquid/molten metal, which is forced through the nozzle, generating a droplet [78]. The vibration-transferring rod has either a spring or a solid metal ring between it and the crucible, these allow the creation of a harmonic vibration system or a compressional wave system respectively. The amount the piston head moves and the distance to the nozzle can be customized to allow different droplet characteristics [78]. The system is placed inside a low oxygen environment (less than 5pmm) that is filled with argon to protect the molten metal from oxidizing and clogging the nozzle.

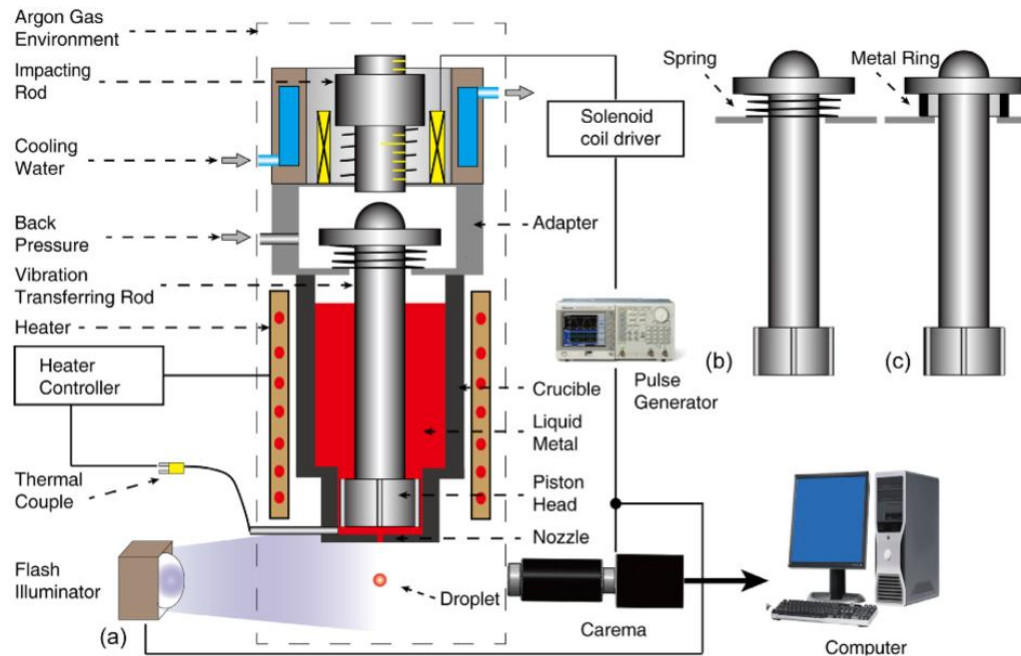


Figure 30. Impact-driven DoD generator a) schematic of the system b) vibrating rod with spring c) vibrating rod with steel ring. [78].

A pulse generator controls an electrical pulse that goes through the solenoid, the electric pulse going through the solenoid produces a magnetic field that moves the impacting rod downwards, where it hits the transferring rod, which is submerged in molten metal. Then depending on if the system has the spring or the metal ring two scenarios may happen. If the spring is installed, when the vibrating rod is hit, it pushes the molten metal through the nozzle creating the droplet, then the spring puts the vibration rod back at starting position, then another electric pulse is sent to the solenoid, and the process is repeated. If the metal ring is installed, when the vibrating rod is hit, it barely moves, but it transfers vibrations to the molten metal in form of stress generated in the rod, allowing for droplets to be formed, then another electric pulse is sent to the solenoid and the process starts again [78].

The material tested in the impact-driven DoD droplet generator was solder (Sn-40 wt% Pb) and a nozzle with a diameter of $100\mu\text{m}$ was used. Droplets of an average diameter of $145 \pm 76\mu\text{m}$ were produced using the vibrating rod with spring with an ejection rate of 25 Hz, limited by the reseating time of the impact system (spring). The ejection speed of the nozzle was considerably faster than other methods like pneumatic, which could allow for an increase in printing quality [78].

Another impact-driven DoD generator printhead was developed by Sohn et al. [79], shown in Figure 31. Consists of a solenoid vibrator connected to a rod that is partially submerged in a molten/liquid metal container made of stainless steel, which has a nozzle at the bottom [79]. At the top of the rod, there are restoration springs that help the rod return to its initial position [79]. Surrounding the system is a tubular heating element that keeps the temperature constant, so the metal stays in the liquid phase [79]. When a pulsed signal is applied to the solenoid vibrator, it exerts a downward force that pushes the rod towards the nozzle, the rod then pushes some of the material through the nozzle, thus creating the droplets, then the restorations spring return the rod to the original position to be able to start the process again [79]. The material used was solder (Sn-37Pb wt%), with this material and a nozzle with a diameter of $130\mu\text{m}$, droplets of diameter around $300 \pm 12 \mu\text{m}$ were generated [79].

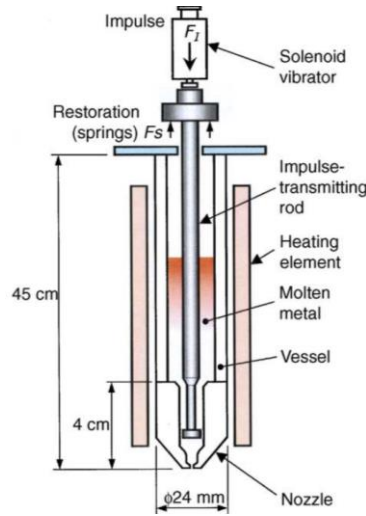


Figure 31. Schematic of impact-driven DoD generator. [79]

Korkut et al. [80] developed another impact-driven DoD generator printhead, shown in Figure 32. It consists of a solenoid actuator that is connected to a rod with a stroke restrictor, a molten/liquid metal container with a nozzle at the bottom which is surrounded by an induction heater that keeps a constant temperature of 220°C in the container [80]. When a pulsed signal is sent to the solenoid actuator, it pushes the rod, which transmits the displacement to the melt area, where the material is forced out through the nozzle, thus creating a droplet [80]. The material used was solder (Sn60Pb40) with a melting point of 193°C, and the droplets produce by this material were of a diameter ranging from 350µm up to 1420µm.

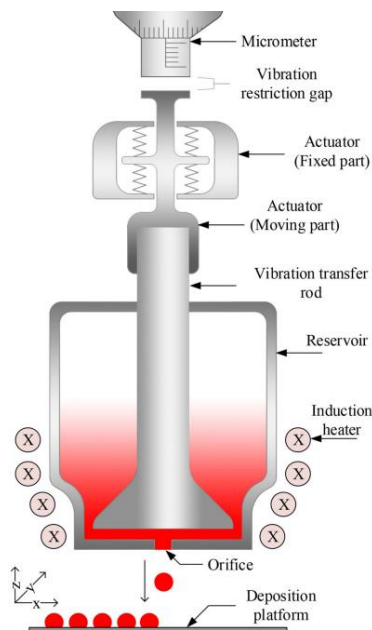


Figure 32. Schematic view of an impact-driven DoD generator. [80]

2.2.5 Piezoelectric Drop-on-Demand printing

Piezoelectric DoD printing consists of using piezoelectric actuators to generate metal droplets. Piezoelectric actuators use the reverse piezoelectric effect, piezoelectric effect refers to the phenomenon in which piezoelectric crystals generate a voltage when deformed, so the inverse of the piezoelectric involves sending a voltage to a piezoelectric crystal to generate deformation in the crystal, this deformation is easily controlled and very precise [81]. Depending on how the piezoelectric actuators are used to generate droplets, piezoelectric DoD printing can be divided into squeeze mode, bending mode, and push mode.

2.2.5.1 Squeeze mode piezoelectric DoD printing

Squeeze mode DoD printing consists of using the deformation of the piezoelectric crystal to exert a force on the external part of the container of the molten/liquid metal to produce droplets. The most commonly used method is to have the piezoelectric crystals surrounding the container, so when a voltage is applied, the piezoelectric crystal deforms, creating a displacement that pushes (squeezes) the container inside [82].

A squeeze mode piezoelectric DoD generator was developed by Marusak et al. [82], which uses early ink-jet heads as inspiration. The droplet generator printhead, as shown in Figure 33, consists of a glass tube of a diameter of 0.75mm that converges into a nozzle on one side, and the other side is connected to the molten/liquid metal supply and a tube-shaped piezoelectric crystal that is attached to the outer wall of the glass tube [82]. The print head is then placed in a protective shell which provides the print head with a contaminant and oxide-free environment (achieved by having a nitrogen-filled environment) together with a controlled temperature environment [82].

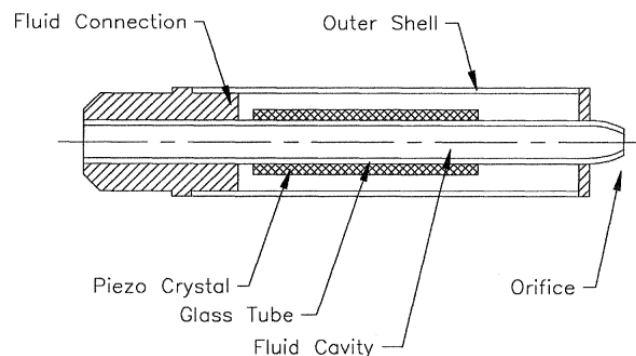


Figure 33. Squeeze Mode piezoelectric droplet generator printhead schematic. [82]

The process of producing droplets using this piezoelectric squeeze mode DoD printhead consists of first filling the glass tube with the desired liquid material (surface tension will prevent it to escape through the nozzle), then a pulsed voltage is applied to the piezoelectric crystal, this will squeeze the glass tube, which creates transient pressure waves with a direction towards the nozzle, this pressure wave pushes a small amount of liquid material through the nozzle, generating a droplet [82]. The material used by Marusak et al. was Indalloy-58, a solder made up of 50% Bi, 26.7% Pb, 13.3% Sn, and 10% Cd, and a low melting point temperature of 70°C. The droplets, created with a nozzle with a diameter of 50µm, had a diameter as small as 60µm, with a typical volume of 100 picolitres, and were ejected at a velocity of 1-5 m/s and a deposition rate of 500 droplets per second [82].

Another DoD printhead using piezoelectric squeeze mode was developed by Rumschoettel et al. [83], shown in Figure 34, the printhead consists of a glass tube with a nozzle at the bottom, a piezoelectric actuator connected to the top of the glass container, and a base place in which the piezoelectric actuator is secured. To produce droplets, first, a pulsed voltage is applied to the piezoelectric actuator, which deforms in the longitudinal direction, then this displacement is transmitted to the glass tube in which a compression wave is created, this compression wave travels in the glass tube towards the nozzle and when it reaches the section where the liquid/molten metal is located most of this pressure is transferred to the liquid/molten metal, which ejects a small amount of material, creating the droplet [83]. The material tested in this printhead is solder Sn63Pb37, and the temperature the printhead is maintain is around 550°C. The nozzle diameter is 100µm which is able to generate droplets of a size of 110µm at a deposition rate of 500 droplets per second [83].

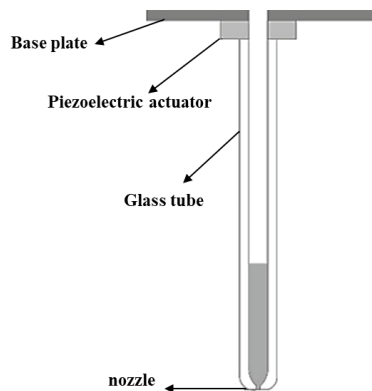


Figure 34. Schematic of DoD piezoelectric squeeze mode printhead. [83]

2.2.5.2 Bending mode piezoelectric DoD printing

Bending mode DoD printing consists of using the deformation of a piezoelectric crystal to drive a diaphragm (a flexible material designed to bend in one direction) that is in contact with the liquid/molten metal, thus when this diaphragm is moved by the piezoelectric crystal it bends and pushes the liquid/molten metal towards a nozzle, generating a droplet [84].

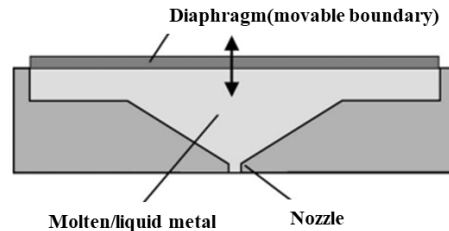


Figure 35. Bending mode working principle. [84]

A bending mode DoD printer was developed by Yokoyama et al. [84], shown in Figure 36, the printer consists of a printhead made of a piezoelectric actuator that drives a diaphragm that is in contact with a molten/liquid metal container that has a nozzle at the bottom, this is surrounded by a heater to keep the temperature constant and the material in a liquid state [84]. At the top of the printhead, a molten/liquid metal reservoir is located, which provides material through a small channel to the printhead container [84]. The whole system is under a constant flow of nitrogen to prevent the molten/liquid metal to oxidize [84].

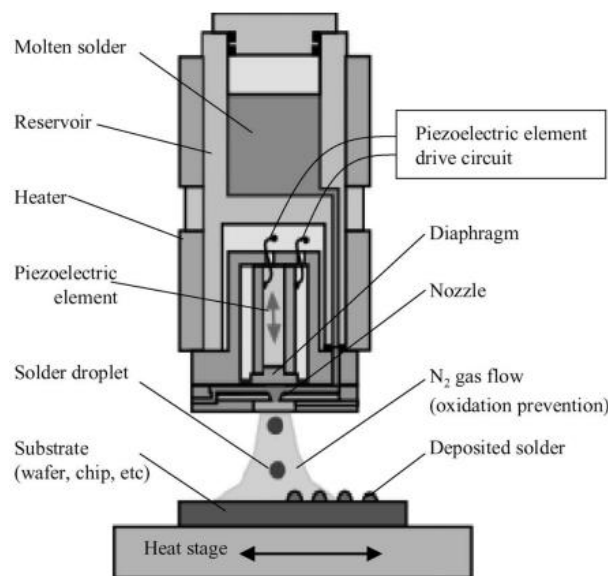


Figure 36. Schematic of a piezoelectric bending mode DoD printer. [84]

A pulsed voltage is sent to the piezoelectric actuator, which drives the diaphragm, causing it to bend towards the nozzle, pushing material through the nozzle, thus creating droplets. The material used in this DoD printer was a solder with a composition of Sn–3Ag–0.5Cu with a melting point of around 180°C. The printhead with a nozzle of a diameter of 14µm was able to produce droplets of a diameter of 13µm with a standard deviation of 0.81µm, with other nozzle sizes the printer was able to create droplets ranging from 13µm to 450µm [84].

Another piezoelectric bending mode DoD generator was developed by Li et al. [85], shown in Figure 37. It consists of a piezoelectric actuator connected to a displacement amplifier, a pushing rod, a copper film used as a diaphragm, and a cavity with a nozzle [85]. Molten/liquid metal is supplied at the top from a feed port which leads to the cavity with the nozzle. When a pulsed voltage is applied to the piezoelectric actuator a displacement is created which is amplified to then push the pushing rod, the pushing rod then deforms the copper film used as a diaphragm which bends into the cavity with the material, and this produces a positive pressure pushes some material through the nozzle, thus creating a droplet [85]. The material used was an unspecified tin alloy, which was heated up to 120°C, with this material and a nozzle of a diameter of 200µm, this DoD generator was able to create droplets of a diameter of 340µm [85].

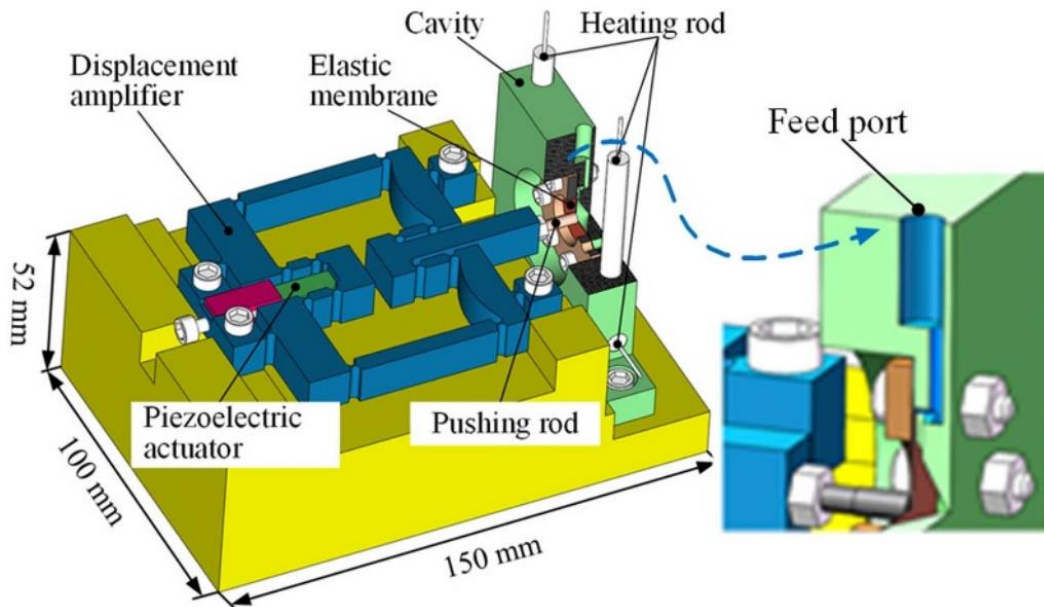


Figure 37. 3D assembly of a piezoelectric bending mode DoD generator. [85]

2.2.5.3 Push mode piezoelectric DoD printing

Push mode DoD consists of using the deformation of the piezoelectric crystal to drive a vibration bar or pushing rod, which is placed on top of a nozzle under molten/liquid metal, thus when it moves it pushes the material through the nozzle creating droplets [86].

Zhang et al. [86] studied and developed a piezoelectric push mode DoD printer, shown in Figure 38. The printhead consists of a crucible that stores molten/liquid metal and has a nozzle at the bottom, a heater that is around the crucible that helps maintain a constant temperature, a vibration bar that is partially submerged in the molten/liquid metal, and a piezoelectric actuator situated on top of the vibration bar [86]. When a pulsed voltage is sent to the piezoelectric actuator, it creates a stress wave that travels through the vibration bar, this vibration is then transmitted to the molten/liquid metal, when the stress wave reaches its peak, a small amount of material is ejected through the nozzle creating a droplet [86]. The material used in this printer was a solder with a composition of 63% Sn and 37% Pb which has a melting point of 183°C [86].

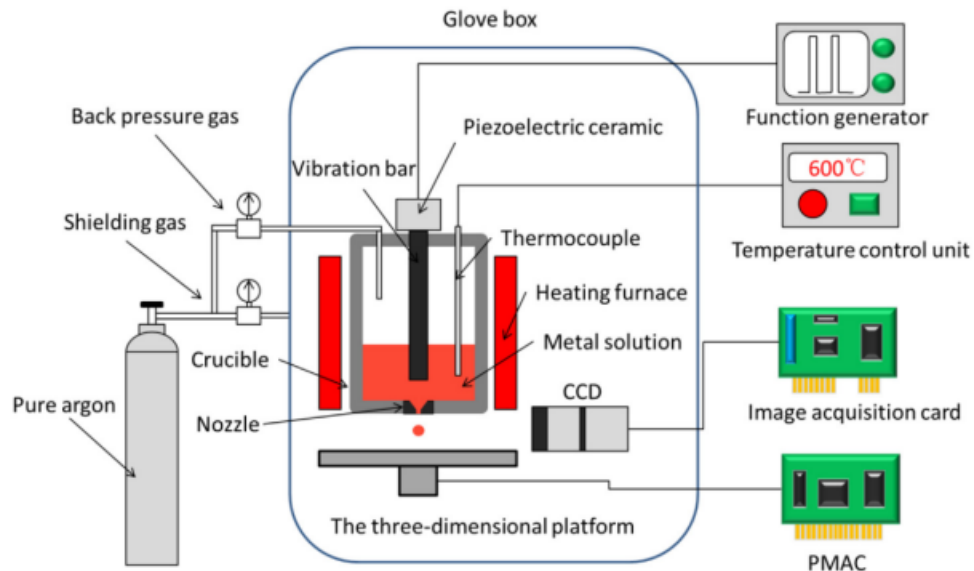


Figure 38. Schematic diagram of a piezoelectric push mode DoD printer. [86]

Ma et al. [87] developed another push mode piezoelectric DoD generator, given the name of piezoelectric membrane-piston-based jetting technology (PMPJT), shown in Figure 39. The DoD generator consists of a piezoelectric actuator connected to a vibration bar, a cooling chamber, a molten/liquid metal container with a nozzle at the bottom, a molten/liquid metal reservoir, and a heating system to keep the machine at a constant temperature [87]. The vibration bar has two

membranes and between them is the cooling chamber, the membranes allow water to flow in the chamber created between them to cool the vibration bar so it doesn't damage the piezoelectric actuator, the membranes also help hold the vibration bar in place and limit its movement in any other direction that is not vertically [87].

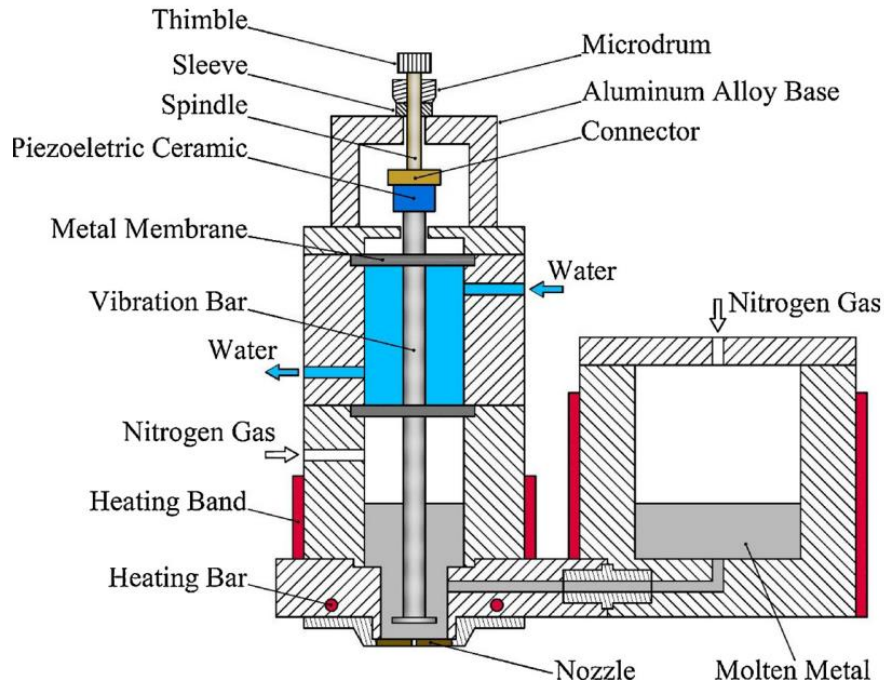


Figure 39. Schematic diagram of the PMPJT system. [87]

When a pulsed voltage is sent to the piezoelectric actuator, the vibration bar is pushed downwards that with the combined pressure created by a constant nitrogen gas flow, pushing some material through the nozzle, thus creating a droplet [87]. The material used was a tin-lead solder alloy with a composition of 63%Sn and 37% Pb and a melting point of 183°C [87]. With a nozzle of a diameter of 75 μ m droplets with a constant size of around 103.1 μ m were created, with other nozzle sizes and parameter droplets with a diameter as small as 85 μ m were created [87].

Another piezoelectric push mode DoD printer was developed by Lee et al. [88], shown in Figure 40. The printhead consists of an LZT (Lead Zirconate Titanates) piezoelectric actuator, an insulation block to protect the piezoelectric actuator from the heat, a molten/liquid metal chamber with an interchangeable nozzle at the bottom, a piston partially submerged into molten/liquid metal, a pressure control unit, and a furnace that keeps the chamber at a constant 400°C [88].

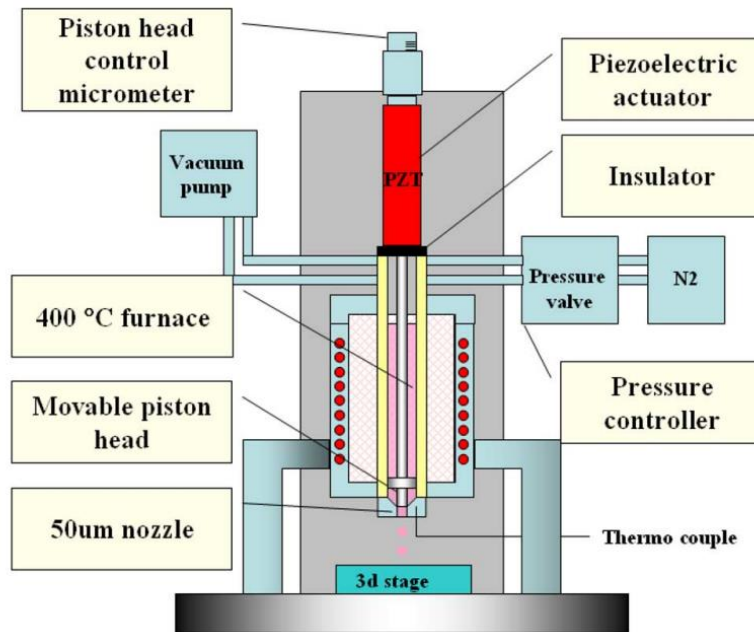


Figure 40. Schematic of a piezoelectric push mode DoD printer. [88]

To generate droplets a pulsed voltage is applied to the piezoelectric actuator, which oscillates the piston vertically, the downwards movement of the piston towards the nozzle, together with the constant pressure provided by the constant supply of nitrogen, pushes material through the nozzle, thus creating the droplet [88]. The material used was an unspecified solder, using this material and a nozzle of a diameter of 50 μm , droplets of a diameter of 65 μm were created, when a nozzle of a diameter of 100 μm was used, droplets of a diameter of 150 μm were created, by changing parameters like voltage supplied to the piezoelectric actuator and nozzle diameter, any droplet diameter size between 65 μm and 150 μm can be produced [88].

Another piezoelectric push mode DoD generator was developed by Yang et al. [89], shown in Figure 41. The droplet generators printhead consists of a piezoelectric stack, an amplifier system that uses a lever to amplify the displacement caused by the piezoelectric actuator, a needle, a heating system to keep the metal in a liquid phase, a cooling system to protect the piezoelectric stack, a molten/liquid metal reservoir and a nozzle [89]. When a pulsed voltage is applied to the piezoelectric stack, it displaces the lever, which amplifies this displacement and transmits it to the needle, which moves towards the nozzle, then the needle pushes the molten metal and makes some material escape through the nozzle, thus creating a droplet [89]. With a nozzle of a diameter of 50 μm , droplets of an average diameter of 275 μm with a variation within $\pm 3.8\%$ were created [89].

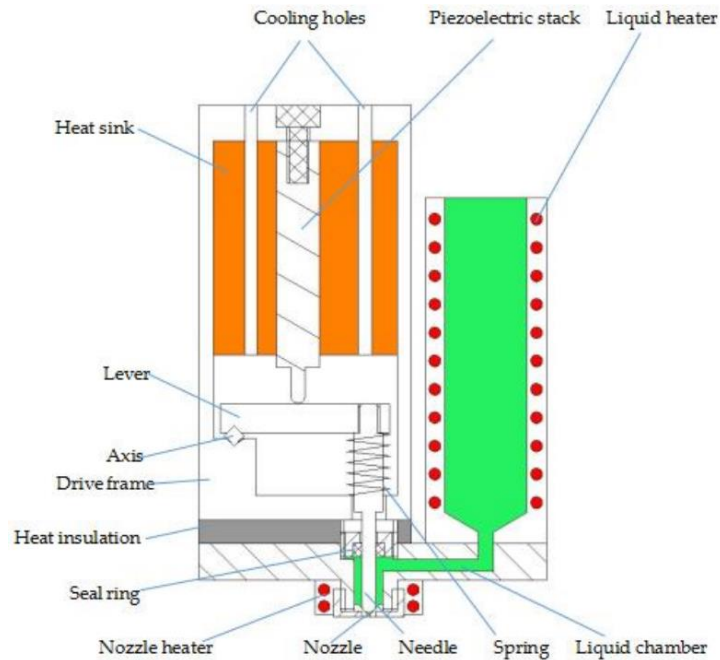


Figure 41. Schematic of a piezoelectric push mode DoD generator. [89]

2.2.6 Laser-Induced DoD printing

Laser-induced DoD printing consists of the use of a focused laser to melt metal material, thus creating metal droplets. In contrast with other techniques that need liquid/molten metal to start the production of droplets, laser-induced DoD printing needs a solid raw material in the form of metal wire/filament or thin metal sheets. There are two main techniques that make use of laser-induced methods to generate droplets, which are laser-induced forward transfer (LIFT) and an unnamed wire feeder-aided laser-induced droplet generation.

Willis et al. [90] developed a laser-induced forward transfer (LIFT) system as a method for additive micropatterning. The system consists of a Q-switched Nd: YAG laser $\lambda = 1.064 \mu\text{m}$, a focusing lens, a transparent donor substrate, an acceptor substrate, and a thin film of the desired printing material, as shown in Figure 42 [90]. The laser is focused on the top of the thin film of material, the laser spot diameter was around $25 \mu\text{m}$, then after the temperature of the molten film at the center of the laser spot reached above the melting point temperature of the film, it expands and reaches free fall, thus falling in droplet shape towards the acceptor substrate [90]. The material used was a $1 \mu\text{m}$ thick film of aluminum or nickel that was coated into a transparent donor substrate (glass microscope slide). Droplets of a diameter approximately of $3 \mu\text{m}$ were created with a relatively repeatable size only affected by energy fluctuations in each laser pulse [90].

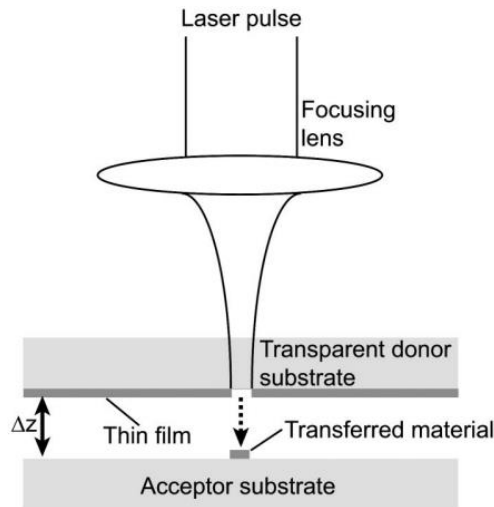


Figure 42. LIFT system schematic. [90]

Another LIFT system was developed by Yang et al. [91], as shown in Figure 43. The system consists of a femtosecond laser workstation that operates at a center wavelength of 775nm, a focusing lens, a quartz donor substrate, a thin layer of material, and an acceptor substrate [91]. When a laser with a pulse of 148fs is focused on the top of the thin layer of material through the quartz substrate (with a focus diameter of 16 μ m), the material will melt, and a droplet will form and fall to the acceptor substrate [91]. A droplet will form due to molten material being ejected from the acceptor substrate due to a compressive stress of the plasma at the moment of melting the free surface [91]. The material used was a thin copper film of 80nm of thickness deposited on a 3mm thick quartz acceptor substrate, with this film the system was able to create droplets of a diameter between 3 μ m and 15 μ m [91].

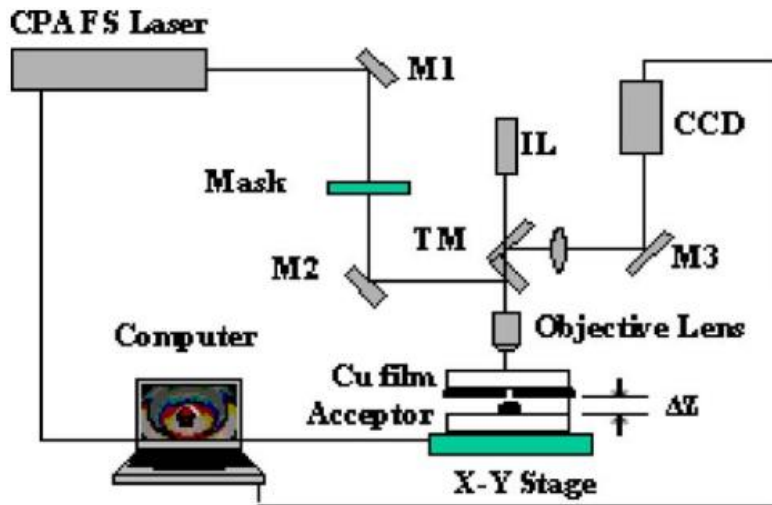


Figure 43. LIFT system experimental setup. [91]

Another LIFT system was developed by Serra et al. [92], shown in Figure 44. It consists of an Nd: YAG laser with a 355nm wavelength, a microscopic objective for focusing the laser, a transparent donor substrate (microscope slide), a thin layer of material, and a receptor substrate. When the laser is focused on the film of material through the donor substrate (with a pulse of 10ns and a frequency of 1Hz), a small part of the film melts and forms a droplet that falls onto the receptor substrate [92]. The material used was a thin layer of titanium of a thickness of 50nm coated into the donor substrate [92]. The droplets produced were small and consistent for use as a microscopic scale patterning system.

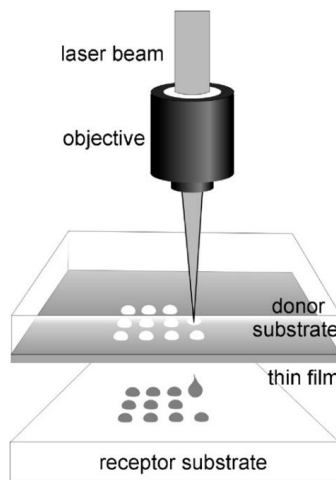


Figure 44. LIFT schematic. [92]

Other than LIFT there is another laser-induced DoD method, which uses a wire instead of a thin layer as the raw material. The method consists of using a laser-focused on the tip of a metal wire that moves using a wire feeder to produce a droplet. Govekar et al. [93] present a DoD generator using this method, as shown in Figure 45. The droplet generator consists of an industrial Nd: YAG, beam shaping optics, axicons, convergent lens, and a wire feeder system [93]. The process of creating droplets consists of two consecutive phases, in the first phase the laser is focused on the tip of the wire, which melts the material and creates a pendant droplet under the action of surface tension and gravity, then in the second phase the droplet falls after overcoming the surface tension force, the whole process occurs inside an argon shield atmosphere to prevent oxidation of the material [94]. The material used was a 0.6mm diameter wire of 99.6% Ni, which with the laser was heated up between 1650°C-1750°C which is around 200°C-300°C higher than its melting point [93]. With this system, droplets of a diameter of 850µm to 1250µm were generated, with a standard deviation of 15µm [93].

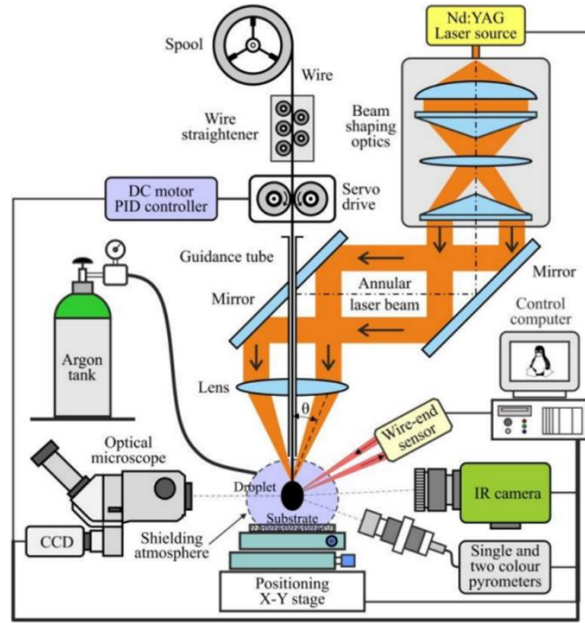


Figure 45. Laser-induced DoD printer. [93]

Another laser droplet generator was developed by Da Silva et al. [95], shown in Figure 46. The system consists of an Ytterbium fiber laser, a focusing lens, a beam splitter, and a wire feeder connected to a welding torch to guide the wire [95]. The laser is focused perpendicular to the wire and split into 4 beams, this is done to prevent the laser from just creating a hole in the wire instead of melting it and to help with the positioning of the deposition of the droplet, after the four beams reach the wire it melts and rolls into the wire forming a pendant droplet which falls after overcoming the surface tension force [95]. The material used was stainless steel 316L in form of a 1.2mm wire, stainless steel droplets of a diameter between 1.9mm and 3.1 μ m were created with this droplet generator [95].

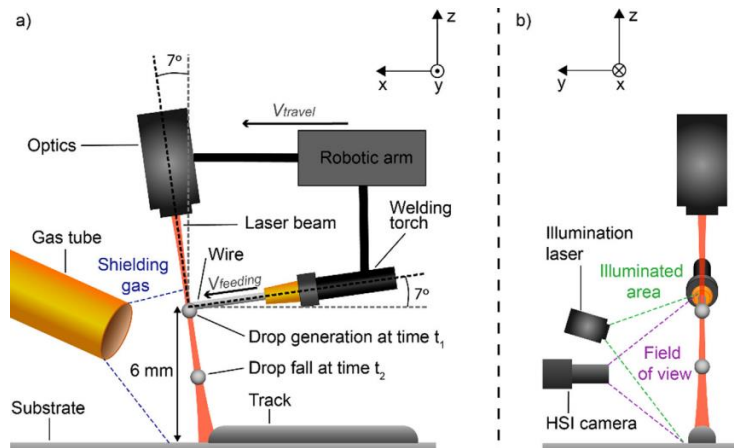


Figure 46. Laser droplet generator a) side view, b) front view. [95]

2.2.7 Other Droplet Deposition techniques

Droplet deposition metal 3D printing is a relatively recent technology that is actively being researched, thus new techniques are constantly being developed, like Metal Droplet Extrusion/Filament Droplet Extrusion the novel technique developed at UNNC that is investigated in this thesis.

Sun et al. [96] developed a new DoD droplet technique using ultra-high frequency induction heating technology, shown in Figure 47. The printhead consists of a high-frequency induction heater, with a working frequency ranging between 700kHz to 1150kHz, and a wire feeder, positioned on top of the coil of the induction heater in a manner that when the wire is feed is located in the middle of the coil [96]. To produce metal droplets, the wire is moved downwards at a speed of 0.012m/s until it reaches the coil, where it gets heated and melted, then a pendant droplet forms at the tip of the wire, and when the pendant droplet overcomes surface tension it detaches from the wire, thus creating a droplet [96]. The raw material used in this experiment is a 1.6mm diameter wire made of Inconel 625 alloy, and the droplets produced by this method had a diameter bigger than the wire. The printing section of the printer is enclosed in a protective box that is filled with argon to prevent the oxidation of the metal [96].

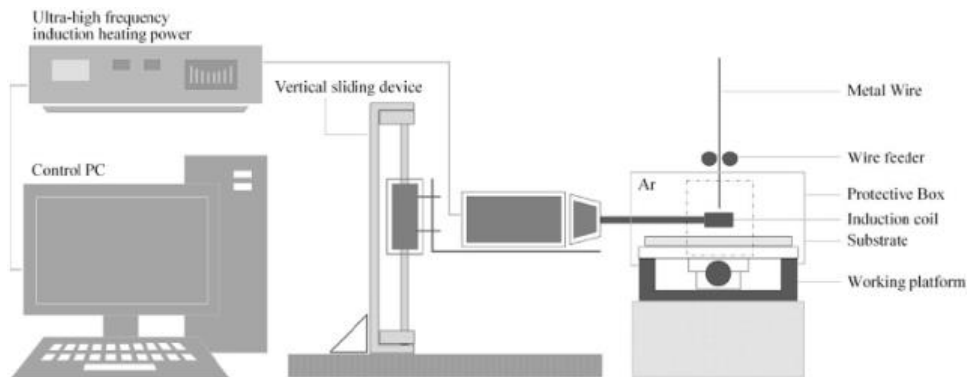


Figure 47. Schematic of an ultra-high frequency induction heating DoD printer. [96]

Until now only DoD techniques have been reviewed but there is a CS technique worth including for their similar components used and for the similar problems encountered by the printer investigated in this thesis, this is a droplet generator developed by Vega et al. [97]. The printhead consists of a crucible with a nozzle at the bottom, an induction heater, and a stepper motor driven wire feeder, as shown in Figure 48. The technique consists of lowering the wire until it reaches the

center of the coil, where it gets heated and melts, forming a pendant droplet that after overcoming surface tension falls towards a crucible with a nozzle, then together with pressure nitrogen injected into the crucible, a stream of molten metal is ejected through the nozzle, then due to Rayleigh instability the stream is divided into droplets [97]. The material used was a 1.5mm in diameter Sn95-Ag4-Cu1 wire (melting point of 217°C) and with a nozzle of 150µm droplets of 280µm were generated.

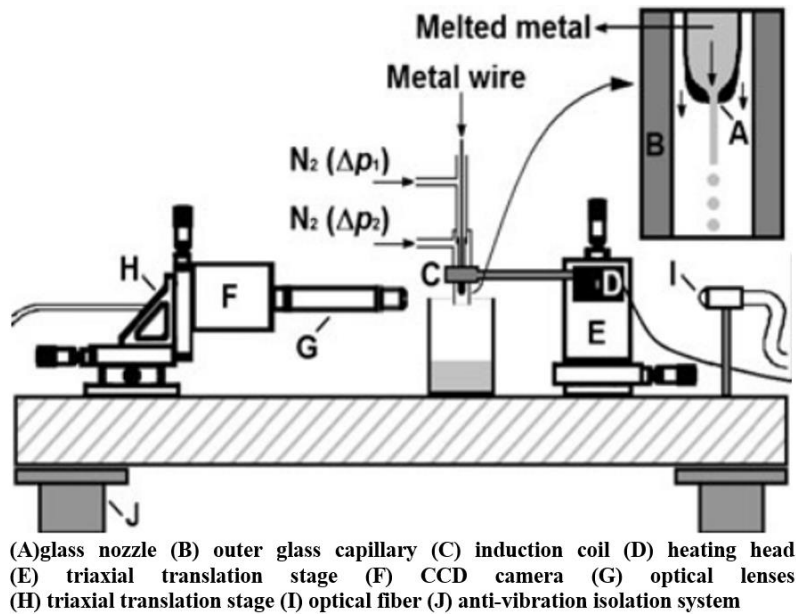


Figure 48. Schematic of a continuous stream droplet deposition generator. [97]

2.2.8 Droplet techniques comparison

From the DoD techniques that have been reviewed previously, the most useful parameters to compare, that allow us to observe the capabilities of each technique, are the diameter of the droplets produced with respect to the diameter of their nozzle and what material the droplets are made of since it will define the working temperature of the system. In Table 5, different systems are compared, only the studies that showed the material used and the diameter of both droplet and nozzle were included in the table.

Table 5. DoD techniques comparison.

Technique	Nozzle	droplet	Material	
Pneumatic droplet deposition	76µm-254 µm	170µm-600µm	Tin	[58]
	100 µm -300 µm	370µm-800µm	Solder alloy Sn-40wt%Pb	[60]
	518µm	905.4µm	Aluminum	[62]
EHD	160µm	1600µm	In51%-Bi32.5%-Sn26.5%	[67]
MHD	100µm-500µm	50µm-550µm	aluminum 4041, 6061 and 7075	[73]
	300µm	351µm	Mercury, Tin alloy	[75]
	500µm	900µm	Tin	[76]
Impact driven	100µm	145µm	Sn-40 wt% Pb	[78]
	130µm	300µm	Sn-37Pb wt%	[79]
	-	350µm-1420µm	Sn60Pb40	[76]
Piezoelectric Squeeze mode	50µm	60µm	Indalloy-58	[82]
	100µm	110µm	Sn63Pb37	[83]
Piezoelectric Bending mode	14µm	13µm	Sn-3Ag-0.5Cu	[84]
	200µm	340µm	Tin alloy	[85]
Piezoelectric Push mode	75µm	103.1µm	63%Sn and 37% Pb	[87]
	50µm	65µm	Tin alloy	[88]
	50µm	275µm	-	[89]

2.2.9 Drop-on-Demand physical properties

Due to Drop-on-Demand being an immature technique and lacking commercially available machines, properties of parts produced from this technique have not been widely studied. But there are individual studies of parts properties produced by their own DoD prototypes, which may not show replicable or relevant results for all DoD techniques but show what DoD printing is capable of producing.

Orme et al. [98] conducted a mechanical analysis on aluminum parts produced by a precise droplet deposition machine, in which it was shown that parts produced by droplet deposition were able to achieve an increased ultimate tensile strength of up to 30% compared to the stock ingot of the same material. Also, the produced parts density was not changed, thus showing no porosities within the part [98]. Thus, showing how the precise deposition of droplets can lead to a refinement of the microstructure that will enhance the mechanical properties of parts produced [98].

Zuo et al. [99] created parts of aluminum 7075 that achieve high tensile strength (373 Mpa) and an acceptable elongation of 9.95%, both values being very close to the raw material, an extruded bar of aluminum 7075. Also, a diagram of the microstructure of the produced part depending on the temperature of the droplet and substrate was calculated and tested, shown in Figure 49, which shows the behavior under different thermal conditions [99].

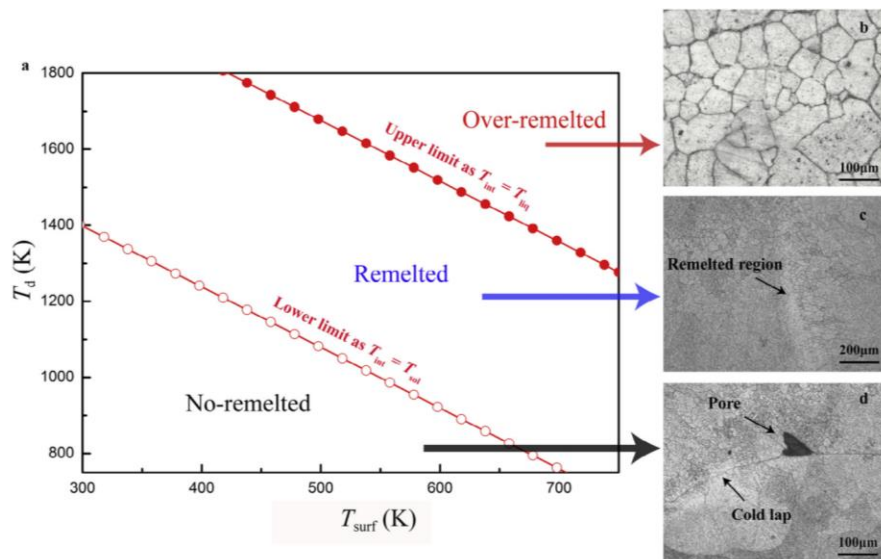


Figure 49. Microstructure bonding depending on surface temperature and droplet temperature: a) Diagram b) Over remelted microstructure c) remelted microstructure d) no remelted microstructure. [99]

Idell et al. [100] Was able to produce a tin part, using DoD techniques, which achieved mechanical properties similar to the raw material and by parts manufactured by traditional methods. The microstructure created by DoD gave enough heat input which allowed strain relief and recrystallization of the corners of the produced parts [100].

While there are not enough different studies to get a complete understanding of the properties of part manufacture by DoD, so far studies show that parts produce by DoD have similar of better properties than their raw material, and due to the low cooling rates and low temperature gradients allows the material to relief strain and reduce the failures that other metal AM method suffer, like hot cracking.

2.3 Numerical analysis of Droplet-on-Demand printing

The ejection of a single droplet is often used to do a numerical analysis of the droplet formation of a DoD system and to model the printability of a liquid/molten metal [101]. To test the printability, the consistency of the droplet production is the main evaluated factor, the ideal droplet production is a consistent production of droplets with the approximately same shape and size, and without any satellite droplet [101]. A satellite droplet is a droplet that is generated due to excess material being ejected from the nozzle or from the material being separated from the main droplet, satellite droplets are very small compared to the main droplet and are considered a defect. The main objective of conducting a numerical analysis is to determine the input parameters that will produce a consists and satellite-free production of a droplet.

Parameters that affect the droplet creation of DoD methods can be divided into four categories:

1. Material properties of the liquid/molten metal: density, surface, tension, and viscosity.
2. Dimensions of the printhead: nozzle diameter, nozzle length, nozzle angle, etc.
3. Actuator parameters: actuation duration, frequency, amplitude, etc.
4. Technique-specific parameters: parameters that affect specific techniques like pressure in pneumatic techniques.

2.3.1 Dimensionless numbers

Due to the nonlinear characteristic of the ejection dynamics of DoD generators, simulations and mathematical models are experimentally impractical and computationally demanding [101]. Instead, dimensionless quantities, which reduce multiple factors to a few relevant variables, have been widely used to describe these systems [102] [101] [52] [60]. The four main dimensionless quantities are the Reynolds number(Re), Capillary number(Ca), Weber number(We), and Ohnsorge number(Oh), which are defined in Equations 1-4 [102] [101] [52] [60].

$$Re = \frac{\rho D_1 v}{\eta}$$

Equation 1

$$Ca = \frac{\eta v}{\gamma}$$

Equation 2

$$We = \frac{\rho D_1 v^2}{\gamma} = Ca Re$$

Equation 3

$$Oh = \frac{\eta}{\sqrt{\rho \gamma D_1}} = \frac{\sqrt{We}}{Re}$$

Equation 4

Where:

ρ = density

D_1 = Initial droplet diameter

v = Droplet velocity

η = Dinamic viscosity

γ = Surface tention coefficient

Ohnsorge number expresses the relationship between the viscosity of the molten/liquid metal and the tension that occurs while generating a droplet [52]. Reynolds number expresses the ratio of the local inertial force that exists in the droplet to the viscous force of the molten/liquid metal [52]. Weber number expresses the ratio between the local inertia force to the surface tension

of the molten/liquid metal [52]. The Capillary number expresses the relation between the viscous drag force and the surface tension of the molten/liquid metal [52].

These dimensionless numbers are used in diagrams in which two of these numbers are plotted to find borders that limit the regions in which ideal droplet production exists. The most common diagram is the weber numbers vs the Ohnersorge number, shown in Figure 50. This diagram, first used and explained by Schiaffino et al. [103], contains four regions in which different behavior is observed.

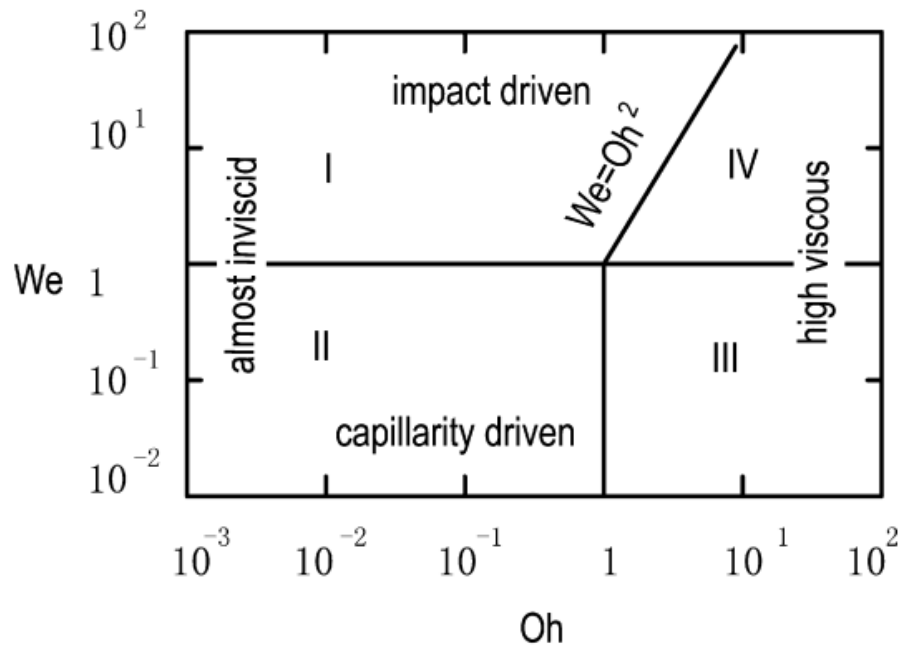


Figure 50. Weber number vs Ohnersorge number, showing the four regions of droplet behavior. [60]

In region I, the droplet generation process is driven by the impact and the pressure it generates [52]. In region II, the impact can be neglected and instead is driven by unbalanced capillary forces opposing fluid inertia forces, also there is some surface oscillation in this region [52]. In region III, the droplet generation process is driven by unbalanced capillary forces, mainly presided by viscous forces [52]. In region IV, the droplet generation process is driven by the impact forces, mainly presided by viscous forces [52]. The characteristic of these regions can be observed in Table 6.

Table 6. Characteristics of the four regions on the We vs Oh diagram. [52]

Region	Driving Force	Resistance	Characteristic spreading velocity	Characteristic spreading time	Re	-
I	Impact pressure	Inertia	v	D_1/v	$We^{1/2}Oh^{-1}$	$Oh \ll We^{1/2}$
II	Capillarity	Inertia	$(\gamma/\rho D_1)^{1/2}$	$(\rho D_1^3/\gamma)^{1/2}$	Oh^{-1}	$Oh \ll 1$
III	Capillarity	Viscosity	γ/η	$\eta D_1/\gamma$	Oh^{-2}	$Oh \gg 1$
IV	Impact pressure	Viscosity	$\rho v^2 D_1/\eta$	$\eta/\rho v^2$	$We Oh^{-1}$	$Oh \gg We^{1/2}$

Sukhotskiy et al. [101] produced different dimensionless numbers with different materials to define boundaries for the ideal droplet formation. For this they plotted We vs Oh^{-1} and We vs Re, shown in Figure 51, also two sets of We were used, one set (We_d) using droplet velocity (v) as the velocity in Equation 3, as is usual, and the other set (We_j) that replaces this value for the velocity of the liquid jet. Figure 51. Dimensionless printability regimes:(a) We_j vs Oh^{-1} , (b) We_j vs Re, (c) We_d vs Oh^{-1} , (d) We_d vs Re.

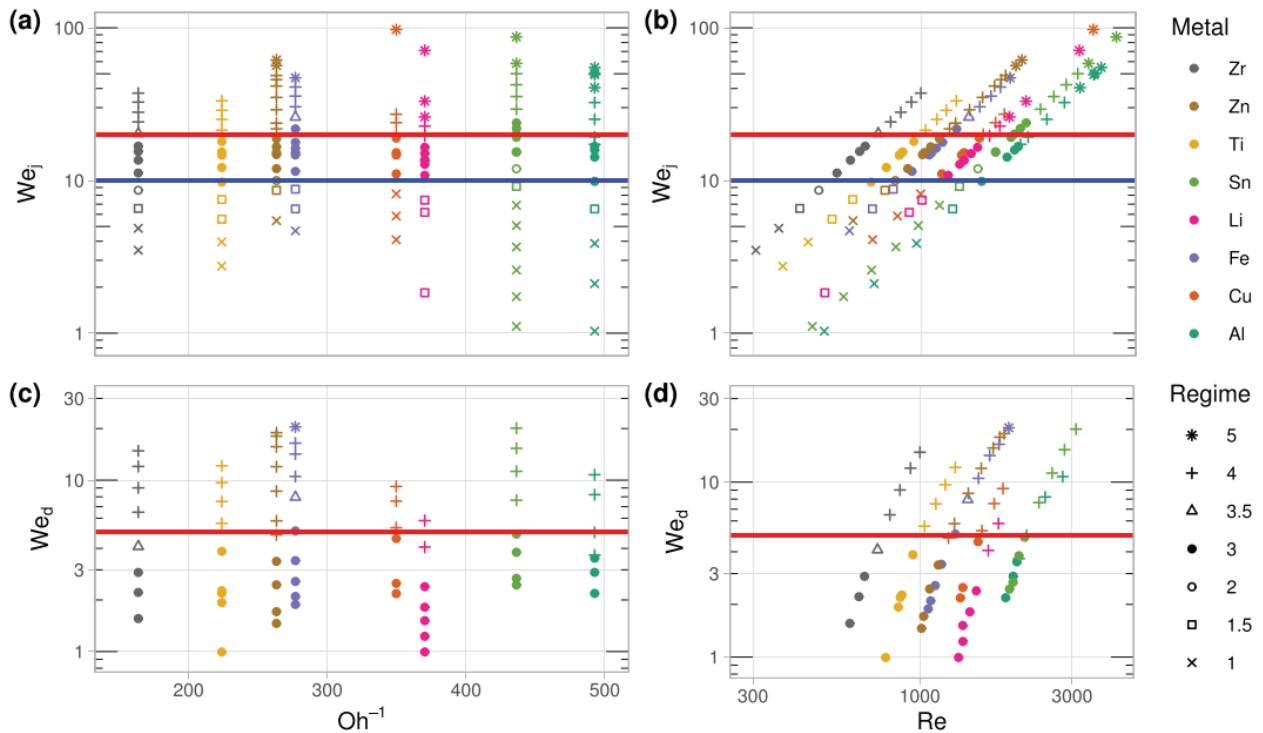


Figure 51. Dimensionless printability regimes:(a) We_j vs Oh^{-1} , (b) We_j vs Re, (c) We_d vs Oh^{-1} , (d) We_d vs Re.

[101]

In Figure 51 the regimes show the results of the droplet production result when the formation of a single was reported, where the regimes represent [101]:

- Regime 1: There was no material ejection due to the lack of energy needed to eject a droplet, instead a small amount of material bulges out of the nozzle but cannot overcome surface tension and returns.
- Regime 1.5: There was an ejection with a negative velocity which causes the droplet to return and recombine with the material.
- Regime 2: A slow droplet ejection in which a droplet is finally ejected but after a delay.
- Regime 3: An ejection of a single droplet with positive velocity, this is considered the ideal droplet deposition.
- Regime 3.5: An ejection of a single droplet in which a satellite was formed but shortly after recombined with the main droplet.
- Regime 4: An ejection of a single droplet with a single satellite.
- Regime 5: An ejection of multiple droplets or a spray of material.

2.3.2 Wettability

Since droplets are the building block of DoD printing, the smaller they are the better microstructure, appearance, and mechanical properties the final part can achieve. Droplet size is affected by different parameters like nozzle diameter, but one of the most impactful is the wetting behavior that exists between the molten/liquid metal and the surface of the nozzle. Zuo et al. [62] conducted a study of the wettability between aluminum and a graphite or BN nozzle. They found that during the droplet production, around the external part of the nozzle, the aluminum will create a wetted region that will first achieve its maximum diameter and then decrease due to the surface tension and gravity [62]. Depending on the materials and the temperature, the contact angle between the nozzle and the molten/liquid material varies due to the wetting behavior, and this contact angle affects the size of the droplet, as shown in Figure 52.

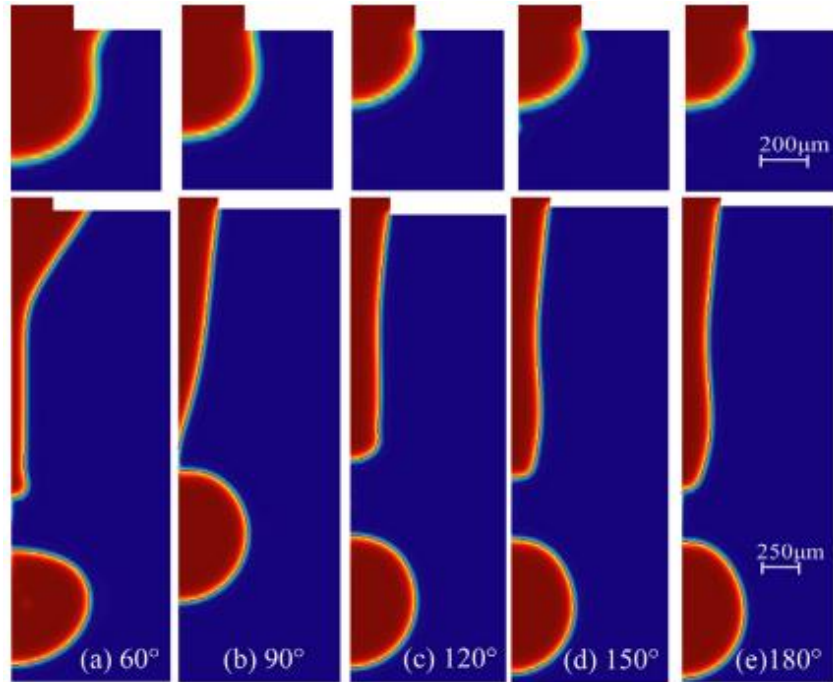


Figure 52. Wetted regions and droplets generated under different contact angles. [62]

2.3.3 Other

There are a variety of parameters that can affect droplet production in DoD systems, but there is not much research on the general parameters since most studies focus on their own techniques and methods. There are two phenomena caused by temperature changes that have been observed by Vega et al. [97] that resemble some of the problems encountered in this thesis. The first phenomenon is that above the melting point, the viscosity of the molten/liquid metal becomes very dependent on the temperature, which makes the molten/liquid metal very viscous when cooled; This can decrease the flow or even block the nozzle [97]. The second phenomenon describes how cooling occurs when the molten/liquid metals reach the nozzle, which can prevent the system to reach a steady state, which disrupts the whole DoD process [97].

2.4 Conclusion

There are multiple commercial metal 3D printers, but they are usually only able to work with metal powders as raw material which makes them hard to handle. A large number of commercial metal 3D printers and their raw materials are very expensive and limited.

MJT is one of the more recently developed metal AM methods, while is not a mature method compared to PBF or DED methods, shows a great potential of overcoming the existing challenges within metal 3D printing. Within MJT techniques, DD or more in particular, DoD techniques, are being developed to attempt to reduce the price of metal 3D printing and to make possible the use of other forms of raw material rather than powders. These new DoD techniques are able to generate droplets from a diameter of 50 μ m, which allows the final printed part to have properties like or better than other 3D printing methods; however, these new DoD techniques mostly work with low melting point metals, especially tin and its alloys.

There is, therefore, a gap in the existing metal 3D printing field for a technique that is able to work with high melting point materials, especially super alloys, like Aluminum 6061, at a reasonable cost, and able to use regular wire as raw material.

Based on the literature covering different DoD techniques, regardless of the type of actuation used, tight control of the actuation is needed to find the precise parameters to create the ideal droplet production. Also, a low-oxygen environment, like a nitrogen or argon-filled glovebox, is recommended to reduce the oxidation of the material.

To achieve the ideal droplet, a complete set of input parameters is needed, these parameters include the actuation parameters, nozzle geometry, and material properties, thus, each technique and each material used in the technique will have a completely different set of input parameters to achieve the ideal droplet.

As the literature shows, finding parameters to generate ideal droplets is a complex process in which the system parameters (mostly working temperature and nozzle geometry) end up being changed and set pretty tightly, thus limiting the capabilities of the system to only one material.

The review made to DoD techniques shows how regardless of the method used, the biggest challenge of metal DoD printing is to produce a droplet with the correct dimensions, consistency, and shape at the correct temperature for the specific material to be able to be deposited into a substrate and properly remelt to create a part with good properties. It also shows how the technique used to create the droplet is not as relevant, since different techniques that apply different technologies and ideas, are able to produce similar droplets, thus showing the potential for new different printheads to be developed.

Chapter 3 Methods

3.1 DoD Printhead evolution

3.1.1 Novel DoD technique working principle

Metal Droplet Extrusion /Filament Droplet Extrusion is a MJT metal 3D printer which uses a novel DoD printing technique that is being developed at UNNC, which is being used in the research conducted in this thesis. This technique consists of using a wire feeder, which is driven by a stepper motor, to move a metal wire/filament to produce droplets. The process, as shown in Figure 53, starts with the wire feeder moving the wire/filament downwards against a heated nozzle. As soon as the tip of the wire/filament has contact with the heated nozzle, it melts and creates a melt pool at the top of the nozzle in its conical section, as shown in Figure 53 (a). Then the wire is moved downwards, causing the melt pool to be pushed by the part of the wire/filament that is still solid, which makes some molten material go through the nozzle aperture creating a pendant droplet, as shown in Figure 53 (b). Next, the wire/filament is moved upwards to aid the pendant droplet to be detached from the rest of the molten material, as shown in Figure 53 (c). Finally, the rest of the molten metal returns to the melt pool, and a droplet is ejected, as shown in Figure 53 (d).

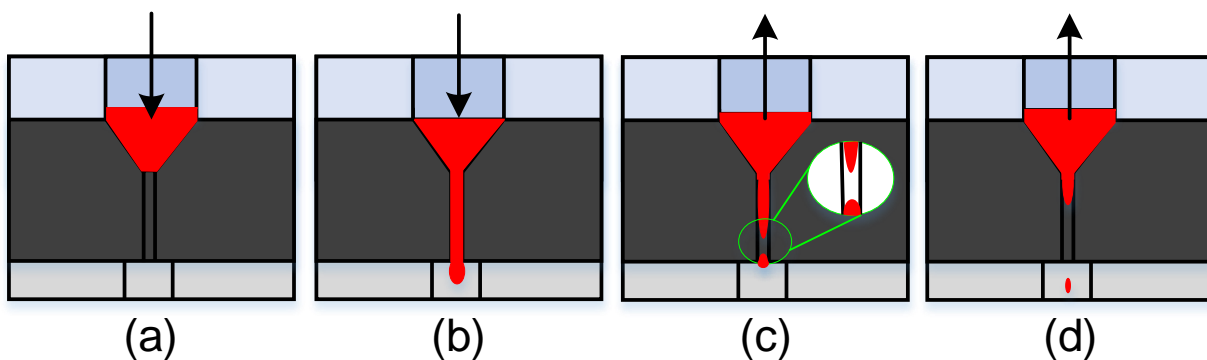


Figure 53. Droplet formation process. [104]

3.1.2 Printhead overview and initial condition

The prototype of the DoD metal 3D printer consists of 5 systems: wire feeder system, crucible system, control system, melting system and substrate/bed system. The printhead is made of 3 systems: the melting system, the wire feeder system, and the crucible system. The droplet production and temperature are controlled by the control system. Figure 54 shows the printhead, in which it can be observed the induction coil from the melting system, the wire feeder outlet from the wire feeder system, and the quartz components and graphite nozzle from the crucible system.

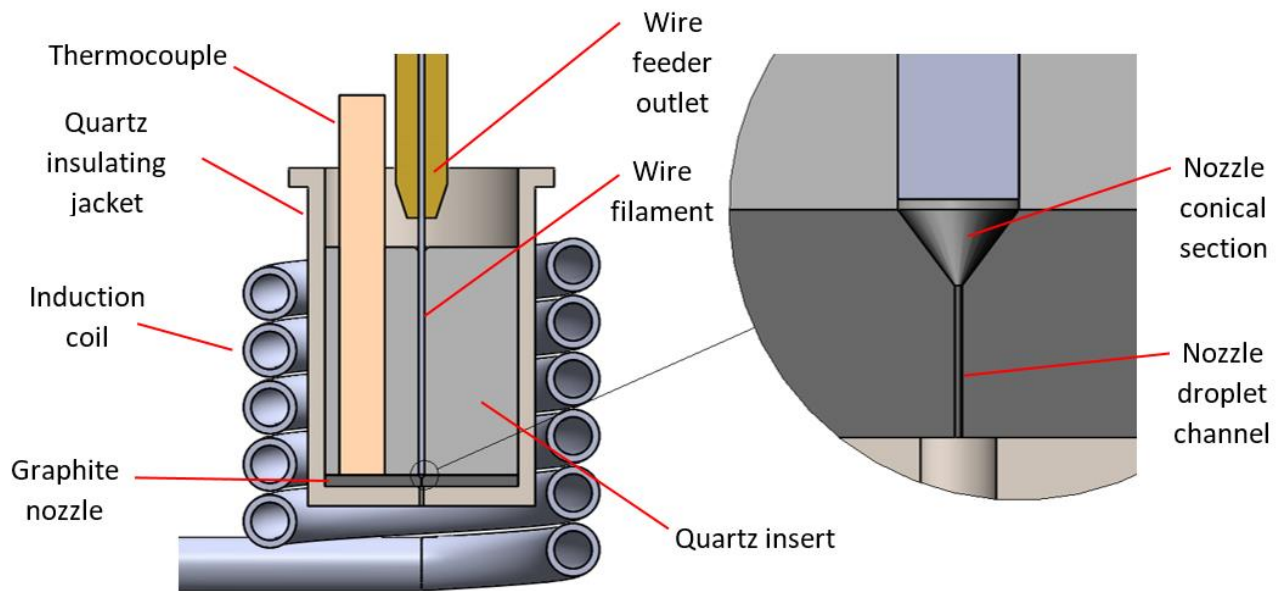


Figure 54. Initial printhead of the Novel DoD metal 3D printer. [104]

The following section is going to explain how each of these systems used to work, these systems are from the initial prototype used in the first months of the master research. During the research, this prototype has suffered various changes and updates that are going to be shown in the section after this one.

3.1.2.1 Melting system

The melting system has the function of heating up the nozzle up to the temperature required to melt the metal material, to achieve this a ZVS induction heater is used. The melting system is made up of an industrial chiller (S&A CW-5300), a fume extractor (Weller zero smog 2), and a ZVS induction heater (GP-20).



Figure 55. (a)Industrial chiller, (b)fume extractor, (c)ZVS induction heater.

While melting the metallic materials used in the printhead, fumes are emanated. The fumes are mostly impurities in the wire/filament, which can be hazardous. Because of this, a fume extractor is located at the top of the crucible system to inhale any emanated fumes.

When the ZVS induction heater is working, the coil and the electrical components inside get hot, thus they need a cooling system to keep them at a temperature under 40°C. Because of this, an industrial chiller is connected to the ZVS to allow the flow of water to cool it down.

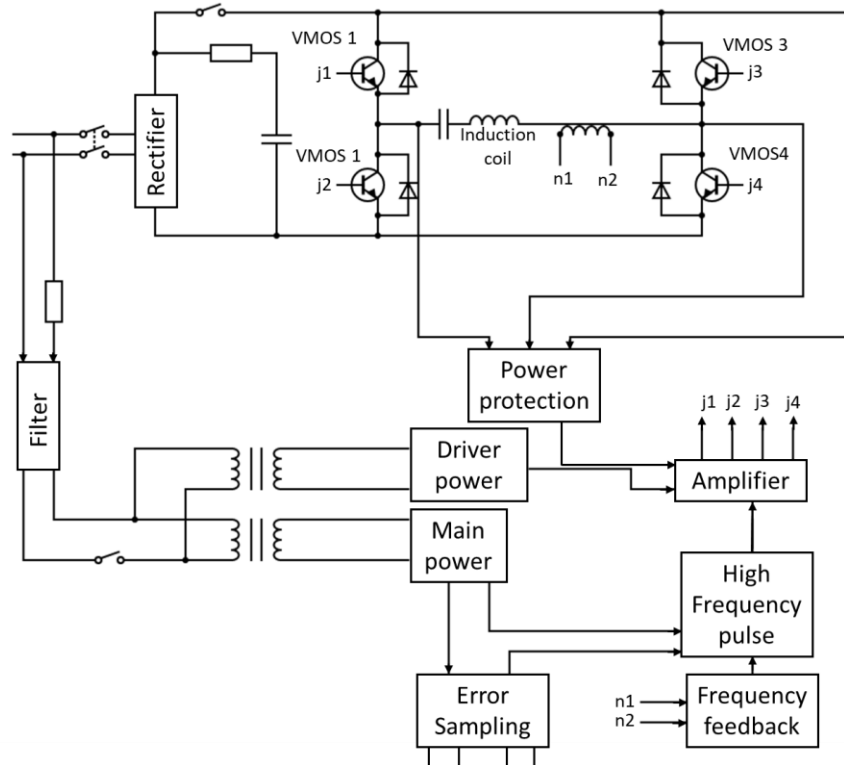


Figure 56. Schematic of the circuit of the ZVS induction heater.

The induction heater uses a ZVS (zero-voltage switching) circuit, shown in Figure 56, to produce an AC current with a high frequency between 50kHz and 300kHz that goes through a copper coil, the frequency will depend on the coil geometry. When the current flows through the copper coil, it generates an oscillating magnetic field, which will be responsible for the heating effect. When an item is placed in the middle of the coil, two heating effects will occur:

1. Hysteresis: Occurs when a magnetic object is in the middle of the coil, the alternating magnetic field creates friction with the object, thus creating heat.
2. Eddy-currents: The alternative magnetic field induces an alternating current in the object, which generates heat, this happens on conductive materials.

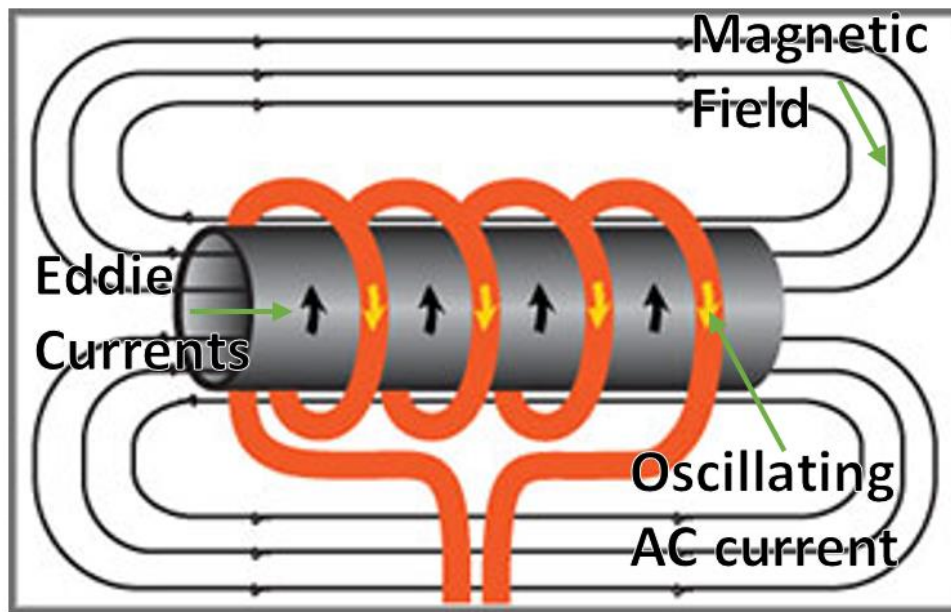


Figure 57. Eddy currents heating effect.

The induction heater can operate manually or automatically. When operated manually, the machine is turned on and off by a foot switch. When operated automatically, a timer allows to keep the machine for a predetermined amount of time. Regardless of the operation, the power output can be changed by adjusting the power nob.

3.1.2.2 Wire feeder system

The wire feeder system has the function of moving the wire upwards and downwards, it is made up of a wire feeder, a stepper motor, and a stepper motor driver. The stepper motor used in the system is an 57HSE3N, which is a two-phase hybrid stepper motor.

This stepper motor is able to produce 2,2Nm of torque at 200RPM, or when delivering 0.6Nm of torque is able to reach 2400RPM. Due to the 57HSE3N being a hybrid motor, it has smaller steps and is able to provide the required torque for the system. It has an encoder connected, which allows for a precise reading of the position and angular displacement. A HBS57 hybrid servo drive was used to drive the stepper motor, it has a closed-loop control that uses the encoder of the motor to achieve precise movement.



Figure 58. (a)57HSE3N stepper motor, (b) HBS57 stepper motor driver.

A wire feeder for welding adapted to be able to be driven by a stepper motor was used to transform the rotational motion of the stepper motor into the vertical movement of a wire/filament. With a wire feeder, the wire/filament can be moved downwards and upwards with high precision at high speeds. It uses a gear system with a gear ratio of 1:1, connected to gripping disks that attach to the wire/filament, thus when rotated the wire is pushed up or down depending on the direction of the rotation. The wire feeder used accepts wires/filaments of a diameter between 2mm and 2.8mm.

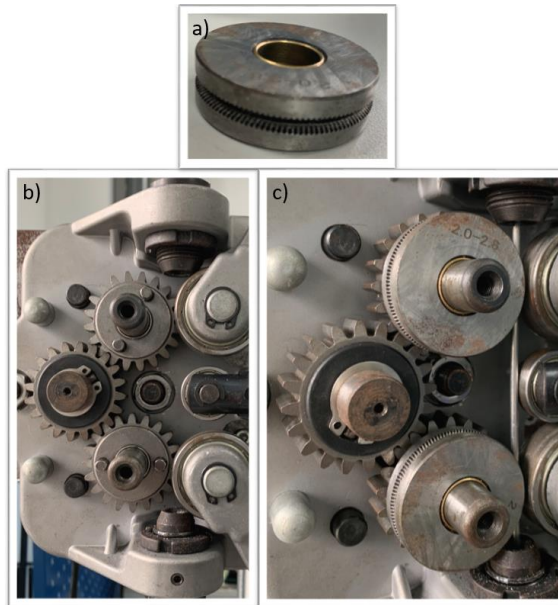


Figure 59. a) Gripping disk, b) Gear system, c) wire feeder assembly.

3.1.2.3 Control system

The control system has the function of controlling the temperature of the graphite nozzle, controlling the movement of the bed/substrate system, and controlling the movement of the wire/filament, thus controlling the droplet production. This system is made of two microcontrollers, a thermocouple, an amplifier, and a relay.

The main microcontroller used is a myRIO 1900, which uses LabVIEW (Laboratory Virtual Instrument Engineering Workbench) as its programming language. The myRIO has both real-time and FPGA (field programmable gate array) processors, with an abundant reconfigurable I/O.



Figure 60. MyRIO Board.

LabVIEW is based on a graphic interface that represents the code, having building blocks as their main instructions. LabVIEW makes the use of an FPGA simpler since it uses its same block structure for programming the FPGA.

The myRIO board was chosen as the main microcontroller due to its high processing speed and the FPGA processor that includes which allows it to do multiple parallel processes at high speeds with high precision. The myRIO board has an abundant number of digital and analog I/O which makes it flexible at the moment of controlling multiple systems.

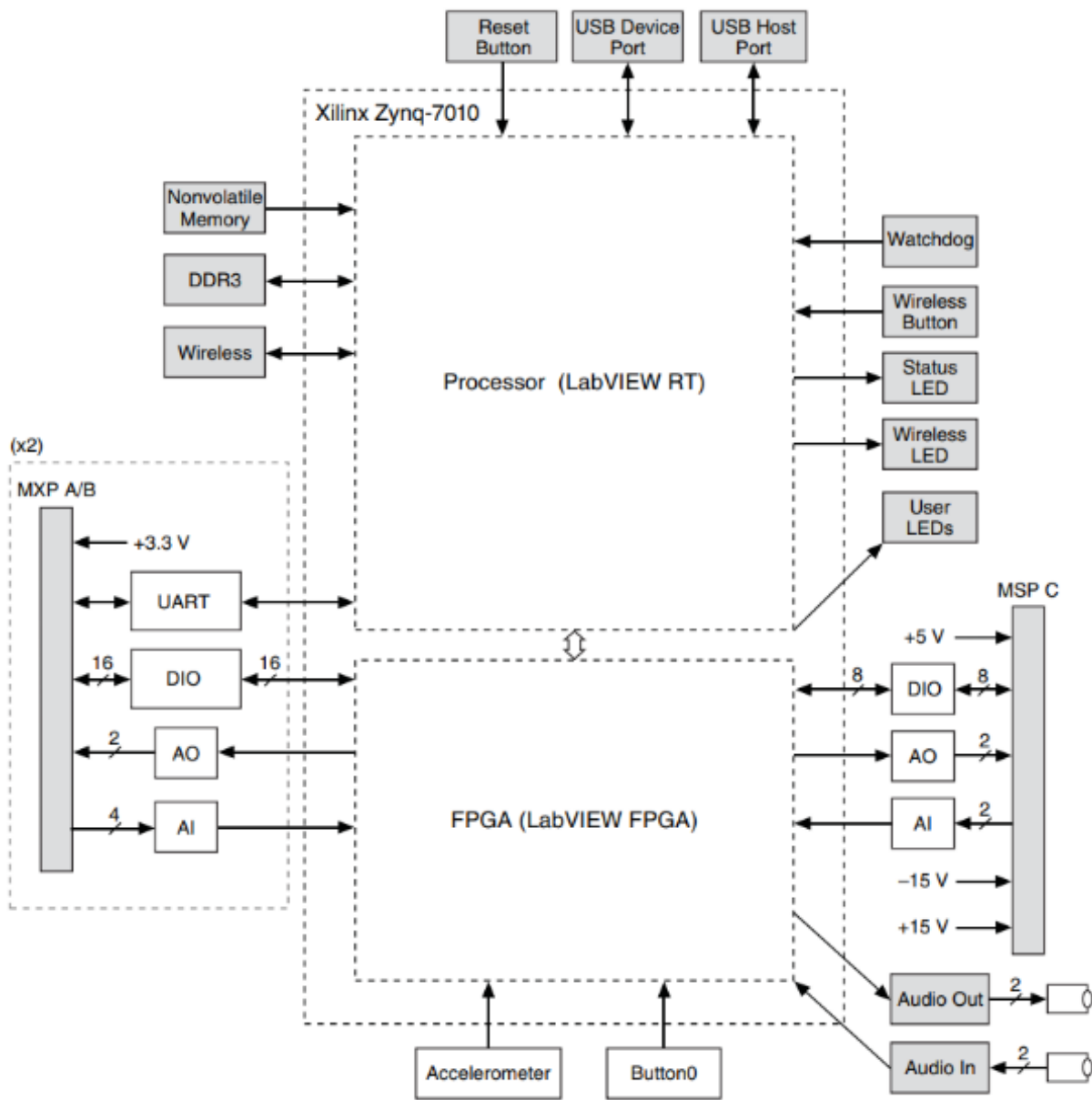


Figure 61. MyRIO hardware diagram. [105]

To control the temperature, the system uses a type K thermocouple (readings up to 1300°C) to read the temperature at the nozzle, which then is amplified by a thermocouple module which is read by an Arduino MEGA. Here the Arduino MEGA is only used to read the temperature from the amplifier and send this value to the myRIO. Then the myRIO uses a PID control to control the on and off timing of the ZVS induction heater, by using a relay connected to the manual mode switch of the ZVS induction heater.

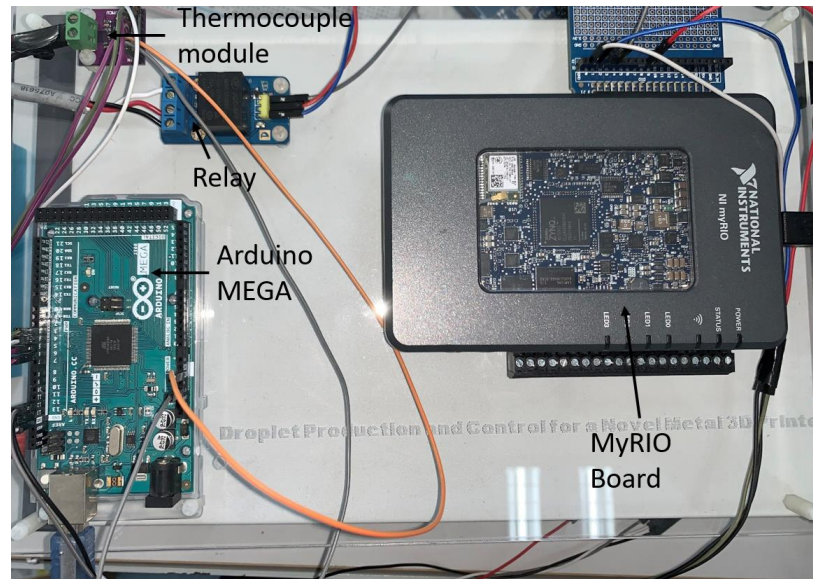


Figure 62. Control System.

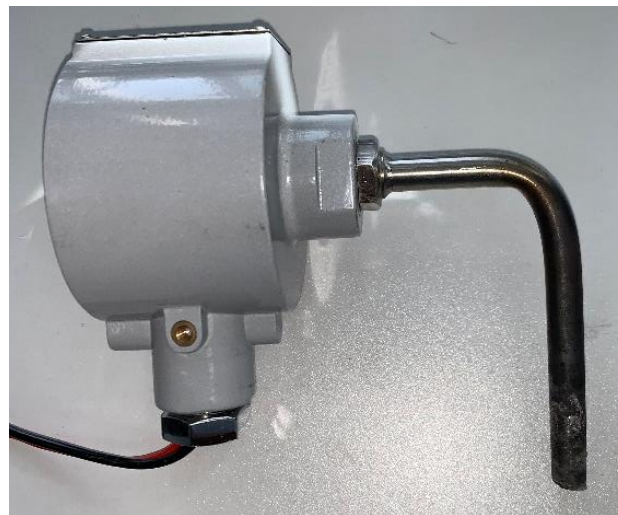


Figure 63. K-type thermocouple.

For the control of the movement of the wire/filament, the myRIO is connected to the motor drive, and with a simple code that sends square wave pulses, it is able to control the movement of the stepper motor. By controlling the number of pulses sent, it can control the amount the motor rotates, thus controlling the distance the wire/filament moves; and by controlling how often the pulses are sent the speed of the rotation of the motor, thus the speed of the movement of the wire/filament can be controlled.

The codes for the temperature control and the motor control for this initial prototype can be found in the appendix.

3.1.2.4 Crucible system

The crucible system has the function of containing the nozzle, aiding in the formation of droplets, and guiding the wire/filament toward the nozzle. The crucible system is made of 3 parts: a ceramic crucible, a quartz insert, and a graphite nozzle in the shape of a disk.

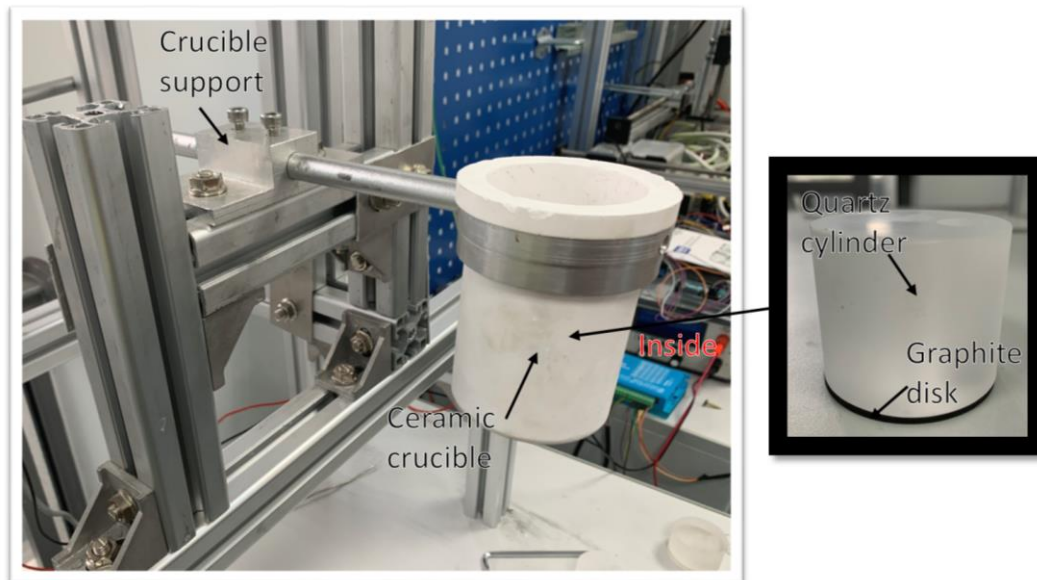


Figure 64. Crucible system.

The ceramic crucible is made of silicon dioxide (SiO_2), which is a quartz ceramic material. Due to its physical properties, it can withstand extremely high temperatures. A hole has been drilled at the bottom of the crucible to allow the droplets to fall through it. It has the function of holding the graphite nozzle and the quartz insert and acts as an insulator to help keep the temperature inside itself.

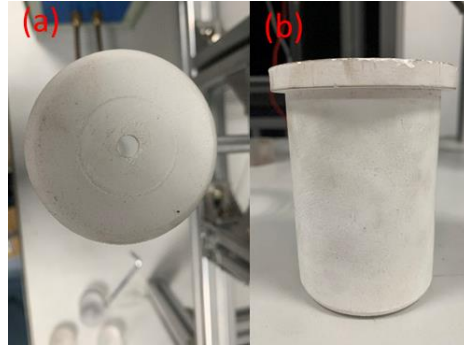


Figure 65. Ceramic crucible (a) bottom view (b) front view.

The quartz insert is a cylinder made out of fused silica, it has two holes, one allows the wire to be guided toward the nozzle and the other allows a thermocouple to reach the graphite nozzle. It also works as an isolator, keeping the higher parts of the wire/filament from melting.

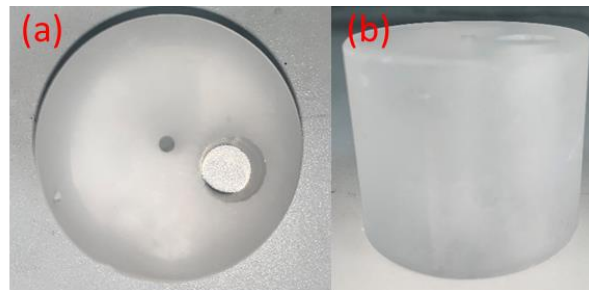


Figure 66. Quartz (a) top view, (b) front view.

The graphite nozzle is a nozzle made of graphite in the shape of a disk. It has the function of melting the metal and aiding in the formation of droplets. Since graphite is a high-resistance material, when it is placed in the middle of the induction coil it will rapidly generate heat, which is used to melt the wire/filament and create the melt pool. The nozzle has an aperture of 500 μm , and when molten material is pushed towards the nozzle, some material escapes this aperture creating droplets.



Figure 67. Graphite nozzle.

3.1.2.5 Systems interaction

To be able to produce droplets the four systems mentioned previously need to work together tightly. First, the crucible system needs to be placed inside the coil of the ZVS induction heater in a way that the graphite nozzle is positioned in the middle of the coil, to allow it to be heated more effectively. Then the thermocouple is inserted through the quartz insert until it reaches and touches the graphite nozzle to be able to have an accurate temperature reading. After that, the control system can start heating the graphite nozzle until the desired temperature is achieved. Then the control system can lower the wire/filament, which in this case is a wire of Aluminum of 2.5mm diameter, through the quartz insert until it reaches the nozzle. Finally, the control system can send the precise pulses needed to produce droplets to the stepper motor, which allows the wire to be moved downwards and upwards in a precise manner to displace the precise amount of material needed to generate a droplet.

3.1.3 Printhead changes and final condition

During the research, multiple improvements have been made to the DoD metal 3D printer prototype, which allowed for better production of droplets. The three systems that made up the printhead (Melting system, wire feeder system, and crucible system) and the control system, which control the production of droplets suffered changes in design and had some components replaced. Even though these systems suffer changes, the 4 systems still have the same functions they had before in regard to droplet production.

3.1.3.1 Melting system

The melting system consists of a fume extractor, an industrial chiller, and a ZVS induction heater. The only change made to the system was the replacement of the ZVS induction heater with another ZVS induction heater. The new heater is a 15kW ZVS induction heater instead of a 20kW, this does not affect the functionality of the printer, since the 15kW ZVS induction heater is still able to easily reach temperatures over 1000°C. The biggest difference is that the new ZVS induction heater has been modified to be able to control the power output of the heating system by a 5volts analog signal. The change was made since controlling the temperature by only turning the machine on and off had two major setbacks, the first one is that it took over 25 minutes to reach

steady state of the desired temperature, and the second one is that when the system reached a steady state the temperature keeps oscillating between the desired temperature $\pm 50^{\circ}\text{C}$, which causes problems and irregularities when attempting to create droplets because physical properties like wettability are temperature dependent. The new induction heater with a new control method was able to reach a steady state in less than 5 minutes and the temperature fluctuation at the steady state was $\pm 1^{\circ}\text{C}$, which allows for better droplet production.

3.1.3.2 Wire Feeder system

The wire feeder system consists of a wire feeder, a stepper motor, and a stepper motor drive. The only change to the system was the replacement of the wire feeder with a new wire feeder. The wire feeder was replaced due to two reasons:

1. The precision of the wire feeder was poor, due to the slipping of the gripping disk with the wire/filament, and misalignment in the gear system of the wire feeder.
2. The wires/filaments that can be used in this wire feeder need to be of a diameter between 2mm and 2.8mm. Wires/filaments of these diameters displace too much material when moving downwards, making it harder to achieve droplet production.

To verify if the diameter of the wire/filament affects the droplet production calculation of the angular displacement needed for the stepper motor to move the mass equivalent of a droplet from the wire/filament was carried out:

First, considering a droplet a perfect sphere, the volume of the ideal droplet can be calculated by:

$$V_{droplet} = \frac{4\pi r_{droplet}^3}{3}$$

Equation 5

Where:

$V_{droplet}$ = volume of the ideal spherical droplet

$r_{droplet}$ = radius of the ideal spherical droplet

A perfect droplet is considered a sphere since a liquid in free fall will eventually form a sphere, either directly by surface tension between the molten metal and the air to create a single sphere, or by Rayleigh instability in which the molten metal is separated into different spheres or the same (multiple droplets or jet) or different sizes (creation of satellite droplets).

After calculation the volume of the ideal droplet, its mass can be calculated by using the density of the material, since the droplet its produced when is molten, the density of molten aluminum 6061 should be used, the closest density value found was of aluminum at 571°C. (obtained from the properties analysis conducted of Aluminum 6061 by Seli et al. [106])

$$\rho_{571} = 0.002574g/mm^3 \quad [106]$$

$$m_{droplet} = V_{droplet} \times \rho_{571}$$

Equation 6

Where:

ρ_{571} = density of aluminum 6061 at 571°C

$m_{droplet}$ = mass of the ideal spherical droplet

Then, the volume of the wire/filament needed to move can be calculated by using the mass of the droplet and the density of the aluminum 6061 at 177°C, which is the closest to the approximate temperature the wire/filament would be in the system.

$$\rho_{177} = 0.002685g/mm^3 \quad [106]$$

$$V_{wire} = m_{droplet} / \rho_{177}$$

Equation 7

Where:

ρ_{177} = density of aluminum 6061 at 177°C

V_{wire} = volume of the wire needed to produce the droplet

Then, by using the formula of the volume of a cylinder like the wire/filament, the length of wire/filament that has the amount of mass needed to produce the droplet can be calculated.

$$V_{wire} = \pi r_{wire}^2 l$$

Equation 8

Where:

r_{wire} = radius of the wire

V_{wire} = volume of the wire needed to produce the droplet

l = length of wire needed to produce a droplet

Then, by using the radius of the gripping disk the angular displacement needed for the wire/filament feeder to move the amount of wire/filament needed to create a droplet can be calculated, and since the gear ratio to the stepper motor is 1:1, this displacement will also be the motor displacement.

$$l = 2\pi r_{gd} * \frac{\theta}{360}$$

Equation 9

Where:

r_{gd} = radius of the gripping disk

θ = angular displacement of the wire feeder and stepper motor needed to create a droplet

Using Eqn. 12-16, the following tables, Table 7-10, were created including different ideal diameters for the desired droplets to observe what size of wire/filament is adequate for droplet production, the gripping disk has a radius of 18mm and the motor needs 400 steps to complete a revolution.

Table 7. Calculated steps needed to create a droplet from a 2.5mm wire.

Desired droplet diameter	Droplet of desired Volume	Mass of desired droplet	Volume of wire needed	Length of wire needed	Angular displacement needed	Steps needed
0.5mm	$0.065417mm^3$	0.000168g	$0.062712mm^3$	0.012782mm	0.040707°	0.04523
0.6mm	$0.11304mm^3$	0.000291g	$0.108367mm^3$	0.022088mm	0.070342°	0.078158
1.0mm	$0.523333mm^3$	0.001347g	$0.501698mm^3$	0.257mm	0.325659°	0.361844
1.6mm	$2.143573mm^3$	0.005518g	$2.054956mm^3$	0.418845mm	1.3339°	1.482111
2.0mm	$4.186667mm^3$	0.010776g	$4.013587mm^3$	0.818056mm	2.605273°	2.894748

Table 8. Calculated steps needed to create a droplet from a 2mm wire.

Desired droplet diameter	Droplet of desired Volume	Mass of desired droplet	Volume of wire needed	Length of wire needed	Angular displacement needed	Steps needed
0.5mm	$0.065417mm^3$	0.000168g	$0.062712mm^3$	0.019972mm	0.063605°	0.070673
0.6mm	$0.11304mm^3$	0.000291g	$0.108367mm^3$	0.034512mm	0.10991°	0.122122
1.0mm	$0.523333mm^3$	0.001347g	$0.501698mm^3$	0.159777mm	0.508842°	0.565381
1.6mm	$2.143573mm^3$	0.005518g	$2.054956mm^3$	0.654445mm	2.084219°	2.315799
2.0mm	$4.186667mm^3$	0.010776g	$4.013587mm^3$	1.278212mm	4.07074°	4.523044

Table 9. Calculated steps needed to create a droplet from a 1.6mm wire.

Desired droplet diameter	Droplet of desired Volume	Mass of desired droplet	Volume of wire needed	Length of wire needed	Angular displacement needed	Steps needed
0.5mm	$0.065417mm^3$	0.000168g	$0.062712mm^3$	0.031206mm	0.099383°	0.110426
0.6mm	$0.11304mm^3$	0.000291g	$0.108367mm^3$	0.053925mm	0.171734°	0.190816
1.0mm	$0.523333mm^3$	0.001347g	$0.501698mm^3$	0.249651mm	0.795066°	0.883407
1.6mm	$2.143573mm^3$	0.005518g	$2.054956mm^3$	1.02257mm	3.256592°	3.618435
2.0mm	$4.186667mm^3$	0.010776g	$4.013587mm^3$	1.997207mm	6.360531°	7.067257

Table 10. Calculated steps needed to create a droplet from a 1mm wire.

Desired droplet diameter	Droplet of desired Volume	Mass of desired droplet	Volume of wire needed	Length of wire needed	Angular displacement needed	Steps needed
0.5mm	0.065417mm ³	0.000168g	0.062712mm ³	0.079888mm	0.254421°	0.28269
0.6mm	0.11304mm ³	0.000291g	0.108367mm ³	0.138047mm	0.43964°	0.488489
1.0mm	0.523333mm ³	0.001347g	0.501698mm ³	0.639106mm	2.03537°	2.261522
1.6mm	2.143573mm ³	0.005518g	2.054956mm ³	2.617779mm	8.336875°	9.263195
2.0mm	4.186667mm ³	0.010776g	4.013587mm ³	5.112849mm	16.28296°	18.09218

As shown in Table 7, the wire feeder that restricts the wire diameter to 2mm to 2.8mm is not adequate for droplet production, since the steps needed for any desirable droplet diameter are very small, and the stepper motor will not be able to achieve such movements, resulting in either displacing not enough material to produce droplets or too much material that will produce satellite droplets.

As shown in Tables 2-4, a wire diameter smaller than 2mm seems adequate for the stepper motor to be able to move the steps needed for the correct amount of material to be displaced to create a single droplet. For this reason, the wire feeder was replaced with a wire feeder with higher precision that is able to change the gripping disk to accommodate wires between the diameter of 0.6mm to 2mm.

3.1.3.3 Control system

The control system, which has the task of controlling the temperature of the nozzle and controlling the movement of the wire/filament suffered major changes. The temperature control part was totally replaced, and the control of the movement of the wire/filament was reprogrammed.

Since the ZVS induction heater was replaced with one that can be controlled by controlling the power output, the temperature control had to be redone. Since the past system was made of a thermocouple, an Arduino MEGA, a myRIO, and a relay, the new system was made trying to improve and simplify the system.

Due to the thermocouple taking too long to read the temperature of the nozzle, the temperature reading been not accurate, and the positioning of the thermocouple being restrictive, it was decided to replace it with another type of temperature sensor. An infrared pyrometer was chosen as a replacement since it can measure the temperature from a distance, the measuring of the temperature is instantaneous, and the reading is very accurate. The infrared pyrometer chosen was a 1 μ m wavelength sensor, able to measure temperature in the ranges of 700°C to 2600°C, shown in Figure 68.

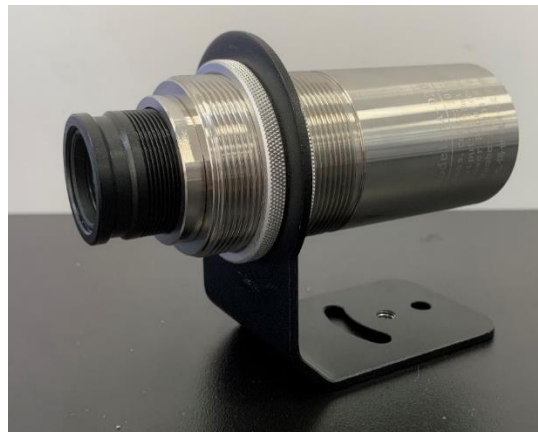


Figure 68. Infrared pyrometer.

The Arduino MEGA was taken out of the system since it was redundant to have two microprocessors, and the function it had was to read the thermocouple, which is no longer part of the system. The relay, which was responsible for turning the ZVS induction heater on and off, was also taken out of the system due to the new ZVS induction heater having a power output control instead of an on/off control.

Having the PID temperature control on the myRIO became time-consuming since the code written for it required manually setting the PID values. Since the temperature control was out of the scope of the project, a commercial PID temperature control box was added to the system. The PID temperature control box is an Anthone LU-920 SERIES, shown in Figure 69, it has autotuning PID values and was able to keep the desired temperature within $\pm 1^\circ$.



Figure 69. PID temperature control box.

The final temperature control system is a closed loop system made of an infrared pyrometer, which measures the temperature of the graphite, and a PID control box, which uses the temperature reading to control the power output of the ZVS induction machine. The system is able to reach a steady state of the desired temperature in less than 5 minutes and with a small ripple of $\pm 1^{\circ}\text{C}$.

The control for the movement of the wire/filament consists of only the myRIO board, which is connected to the motor driver. The code written in LabVIEW was redone from the start to simplify, optimize and correct the code, and also to add new functions needed for better control of the movement of the wire. The code is made of two VIs (virtual interface) executed on the myRIO, which are the main file type of LabVIEW, one VI is in the real-time processor and the other is in the FPGA processor, both executed at the same time.

The VI executed in real-time is the UI (user interface), which allows the user to input the parameters for the movement of the wire/filament and allows the user to start the movement. The UI is shown in Figure 70 and the code of the VI is shown in Figure 71.

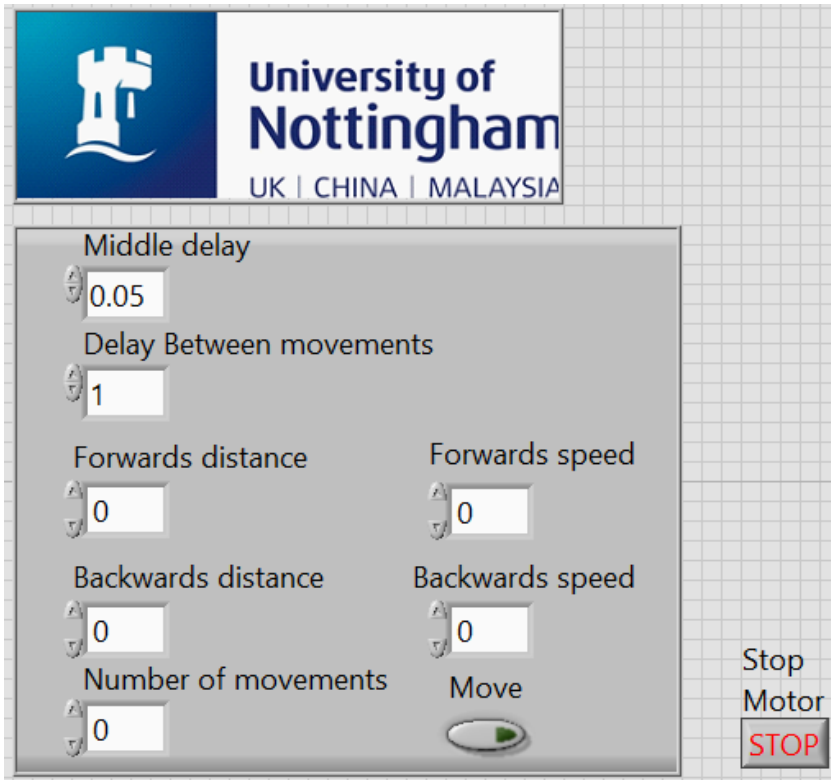


Figure 70. User interface of the wire/filament movement control.

The code allows the user to input different parameters to control all the aspects of the movement of the wire. The first parameter is the distance it moves either forwards or backward, forwards refer to the movement downwards toward the nozzle, and backward refers to the movement upwards, the value to input is the desired movement in steps, a revolution is 400 steps. The second value to input is the forward and backward speeds, which will control the velocity in which the wire moves in their respective directions, the value to input is the delay time between pulses, so the smaller it is, the faster the movement is going to be. Then the next parameter to input is the number of movements, which refers to how many times the movement to produce droplets is going to be repeated, the movement to produce droplets consists of a movement downwards and then a movement upwards. The final parameters to input are the delays, the middle delay refers to a delay between the movement downwards and upwards, while the delay between movements refers to a delay between the movement that will produce a droplet and the next one.

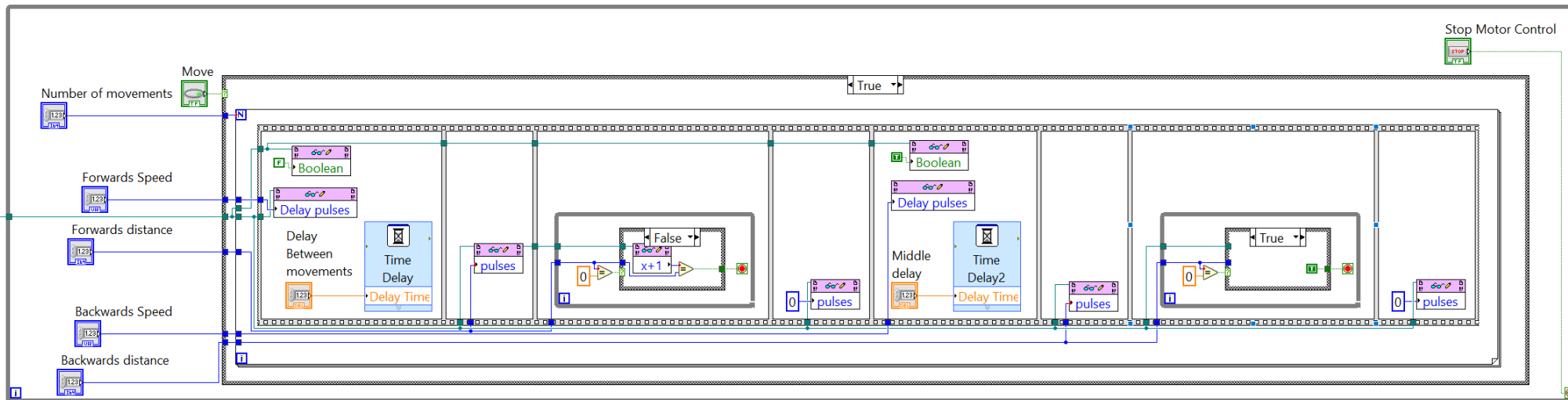


Figure 71. VI executed in the real time processor.

The code consists of starting an interaction with the VI executed in the FPGA processor, then the user input the parameters, and when the user pushes the button “move”, it sends these parameters, at the appropriate time, to the VI being executed in the FPGA.

The VI executed in FGGA is responsible for receiving the parameters from the VI executed in real-time, generating, and sending the pulsed signal to the motor driver which will achieve the desired motion of the wire/filament. The VI is shown in Figure 72.

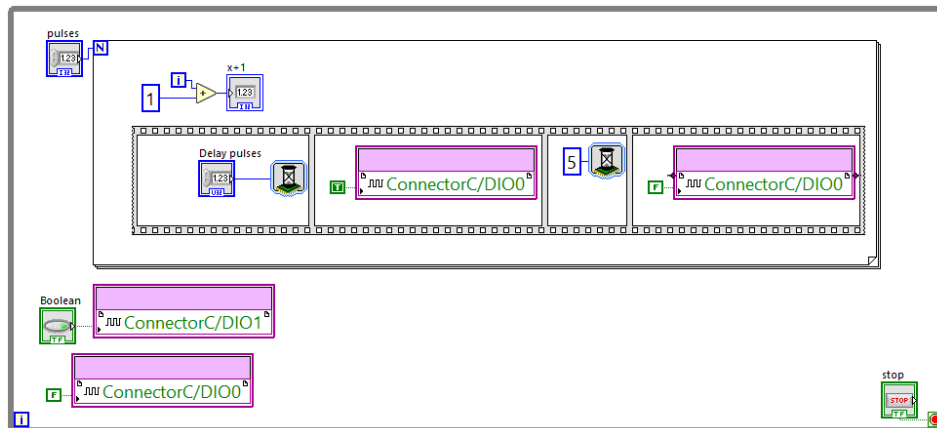


Figure 72. VI executed in the FPGA processor.

The code consists of a pulse generator in which parameters are received from the VI executed in real-time, and the pulses are sent to the motor driver. As per the datasheet of the stepper motor driver, a pulse of 5ms is needed, so the code sends a 5ms pulse each time. The code also controls the direction of the movement depending on the input received.

The final wire/filament movement control system consists of a myRIO board connected to the stepper motor driver. The code involve in the control of the movement of the wire/filament consists of getting the input parameters for the desired movement and then converting it to timed pulses and sending them to the motor driver, which will cause the desired movement in the wire/filament.

3.1.3.4 Crucible system

The crucible system consists of a ceramic crucible, a quartz insert, and a graphite nozzle. Other than the ceramic crucible that holds all the other components in place, all the components of the crucible system have had multiple changes and multiple versions.

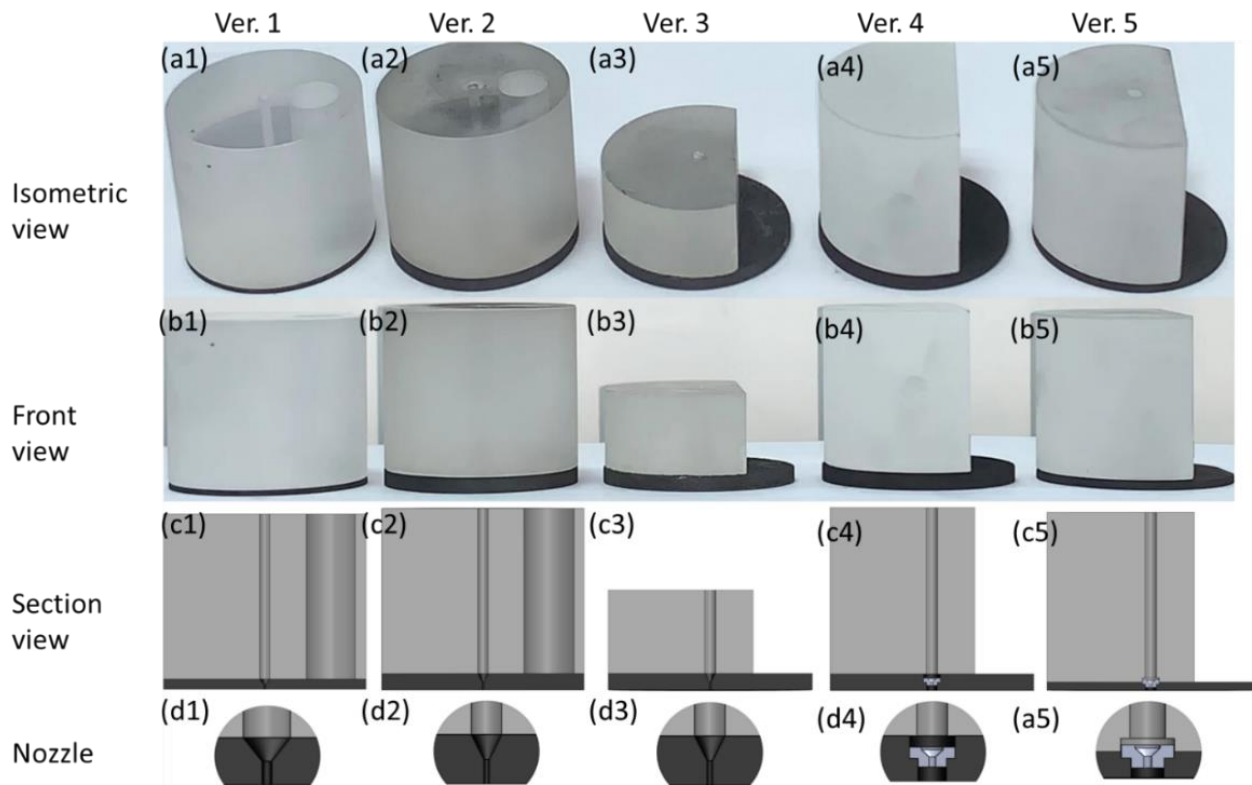


Figure 73. Quartz insert, graphite disk and nozzle evolution.

Figure 73 shows 5 versions of the quartz insert, graphite disk, and nozzle, each of which was made to solve a specific problem and to improve droplet production to attempt to reach a consistent droplet production. These 5 versions are the versions that improved the droplet production the most, other than these 5 versions there have been multiple others between them that either did not improve or that made it worse.

Version 1: This version was the one available at the start of the project, the quartz insert has two holes, the middle hole guides the wire towards the graphite nozzle, this hole was made for a 2.5mm wire, and the side hole guides the thermocouple to the graphite.

Version 2: This version changes the diameter of the middle of the hole to be able to be used with 2mm wire and 1.6m wire. It also changes the thickness of the graphite nozzle disk, which is increased to allow for a faster heating time.

Version 3: This version changes the quartz insert, the quartz insert has a cut on the side now. The cut allows the infrared pyrometer to have a clear path of visibility to the graphite nozzle. It also reduces the height of the quartz insert to try to reduce the size.

Version 4: This version changes the height of the quartz insert back to the original height due to the wire melting at the top of it, due to lack of insulation. It also makes the biggest

change, replacing the graphite nozzle disk with a graphite disk with a hole in which a tungsten carbide nozzle is placed.

Version 5: This version adds a cavity for the tungsten carbide nozzle at the bottom of the quartz insert, it also reduces the height of the quartz disk to allow parts of the tungsten carbide to be inserted in the quartz insert, this is to prevent the molten metal to flow between the quartz insert and the graphite disk.

The final crucible system consists of a quartz insert, a graphite disk and a tungsten carbide nozzle, engineering drawings of these three components can be found in the appendix.

The quartz insert guides the wire/filament to the nozzle and has a cut on the side, which leaves an open space for the infrared pyrometer to measure the temperature of the graphite disk. The graphite disk is the main component that gets heated, by the ZVS induction heater, to allow the material to melt at the nozzle. The graphite disk has a hole to accommodate the nozzle. The graphite disk used to also be the nozzle but due to the graphite degrading and changing shape, due to the high temperature needed, it was decided to get a nozzle of other material to be used. A tungsten carbide nozzle was chosen due to its high melting point (2870°C) and high-temperature resistance, and also for high enough resistance that will allow the ZVS induction heater to have a small effect on it, thus getting heated. The tungsten nozzle is a commercially available nozzle used for spraying high-temperature liquids and gases, shown in Figure 74. Three nozzles with different diameter apertures were purchased and tested, a 6mm, a 3mm, and a 1mm, but only the 6mm was thoroughly tested.

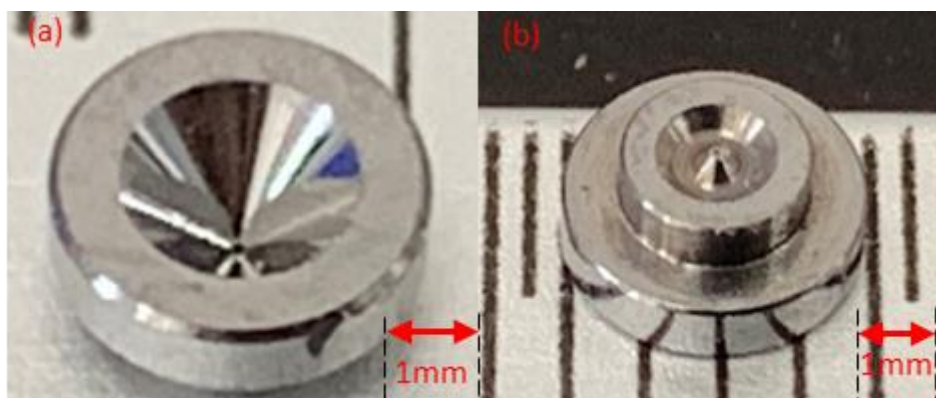


Figure 74. Tungsten Carbide nozzle (a) top view (b) bottom view.

3.1.3.5 Final printhead schematic

The final prototype of the novel DoD printer and the final printhead are shown in Figure 75 and Figure 76 respectively.

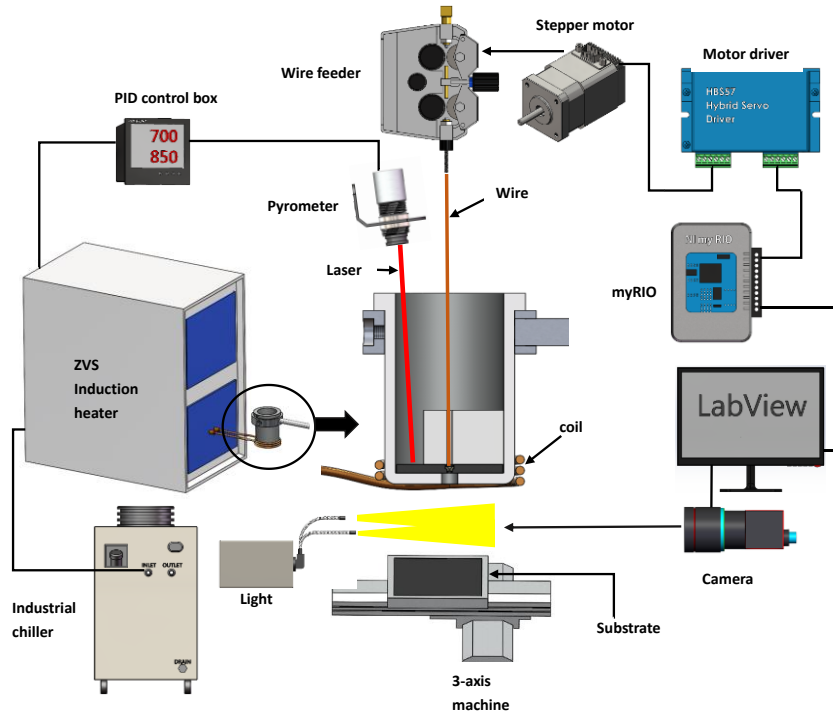


Figure 75. Final schematic of the Novel DoD printer.

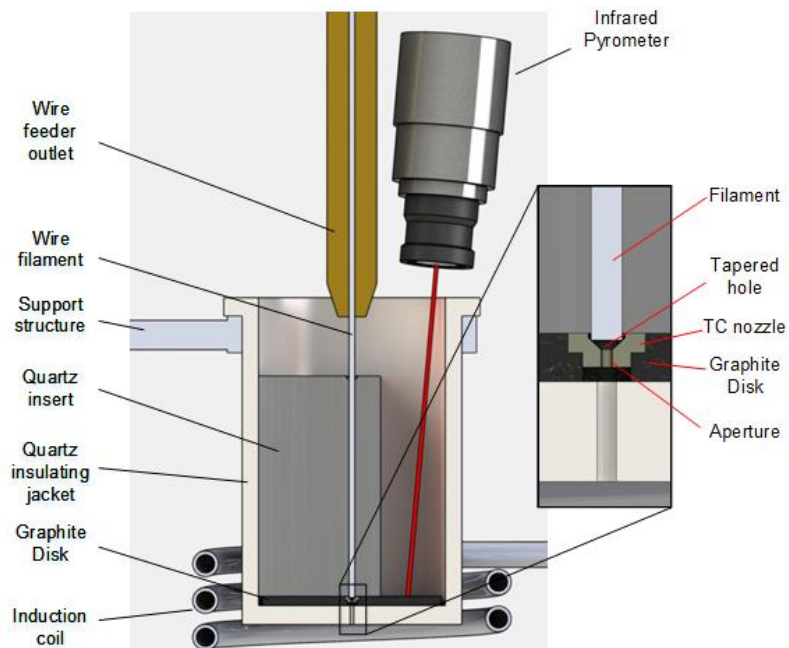


Figure 76. Final schematic of a printhead for a novel DoD printer. [104]

3.2 Experiments conducted

During the duration of this research, multiple experiments related to droplet production were carried out. All experiments were carried out using the DoD printer prototype at UNNC. There were three main types of experiments, experiments trying to produce droplets, experiments trying to produce the best droplets, and experiments trying to produce a consistent droplet production. The main material used was aluminum 6061, but rarely Inconel 718, stainless steel 304, and brass were part of these experiments, so unless specified otherwise assume the material used was aluminum 6061.

3.2.1 Experiments to produce droplets

These experiments had the objective of checking if the machine can produce droplets at all. These experiments were carried out mostly at the start of the research, when it was not proven that the machine was able to create droplets, or when a system suffered big changes, to verify if the changes did not prevent droplet production.

It consisted of testing multiple parameters in quick succession until a droplet was generated. To be considered that a droplet was truly generated, the droplet has to be formed as soon as the wire movement is finished and the droplet diameter needs to be of a reasonable size (between the nozzle diameter to up to four times its diameter), this is to confirm that a droplet was created due to the actuation of the wire instead of molten metal accumulating at the bottom of the nozzle and just falling due to gravity. Usually, these experiments had a duration between 3 hours and 5 hours.

These experiments were also used as a way to learn and understand the behavior of the machine and of droplet production since the limit values of the parameters and the usual effect of the parameters in the droplet production were found during these experiments.

3.2.2 Experiments to achieve the best droplet

These experiments had the objective of achieving the best droplet that the machine could achieve. These experiments were carried out after a particular version of the machine was proven to be able to produce droplets, and its capabilities need to be tested. These were the experiments that were carried out the most, since every iteration of the machine that was able to produce droplets needed deep testing.

It consisted of testing all the parameters of each version of the machine that was able to produce a droplet, testing each parameter in a different experiment. The parameters were temperature, wire diameter, forward and backward distance, the velocity of the forward and backward movement, and the delay between the downward and upwards movement. To try to achieve the best droplet, the shape and size of the droplet were considered. For this the droplet was deposited in a graphite substrate more than 30cm away, allowing the droplet to solidify before reaching the substrate, and then the droplet was analyzed before depositing the next droplet. Each test of the parameters had a duration of 4 hours to 6 hours.

These experiments helped find the best values for some of the parameters: temperature, wire diameter, downward, and upwards speed, and delay between the downward and upwards movement.

Table 11. Experimental matrix with the constant variables for the experiment.

Raw Material and diameter	
Temperature of the nozzle	
Wire guide and insulation component	
Nozzle holder component	
Nozzle	
Room Temperature	

Table 11 was used as the experimental matrices when experiments to achieve the best droplet were conducted. Table 11 contains variables that were chosen at the start of the experiment and that remain constant throughout the whole experiment due to them being hard or impossible to change while conducting the experiment without having to restart the experiment, this includes the raw material, the desired temperatures and the components that form the printhead.

Table 12. Possible options for the constant variables of the experiment.

Variable	Options
Raw Material and diameter	-Aluminum 6061: 1mm, 1.6mm, 2mm, 2.4mm, 2.5mm -Inconel 718: 2.4mm -Brass: 1.6mm -Stainless Steel 304: 2.4mm
Temperature of the nozzle	700°C, 750°C, 800°C, 820°C, 840°C, 860°C, 880°C, 900°C, 920°C, 940°C, 1000°C
Wire guide and insulation component	Quartz insert: version 1, version 2, version 3, version 4, version 5.
Nozzle holder component	Graphite disk thickness: 2mm, 3mm, 4mm, 5mm.
Nozzle	-Tungsten Carbide Nozzle Aperture: 0.1mm, 0.3mm, 0.6mm -Graphite Nozzle Aperture: 0.5mm
Room Temperature	18°C to 25°C

For the experiments first the constant variables for that experiment were chosen and recorded in Table 11, the choices for the variables are shown in Table 12. For the Raw material and diameter, the material was chosen from a variety of Al 6061, Inconel 718, Brass and Stainless Steel 304, with most of the experiments using Al 6061, then the diameter of the chosen material was selected, either 1mm, 1.6mm, 2mm, 2.4mm, or 2.5mm, with most of the experiments using 1.6mm. All the raw materials were a commercially available 1m long filament/wire, usually used in welding, purchased from 上海名牌焊材 online store (link: https://shop140642253.taobao.com/shop/view_shop.htm?spm=a1z0d.6639537). For the temperature of the nozzle a value between 700°C to 1000°C was chosen, with values between 800°C to 940°C with intervals of 20 degrees being the most used. The wire guide and insulation component consist of one of the quartz inserts shown in Figure 73. The Nozzle holder component refers to the graphite disk that holds the tungsten carbide, the different choices for this variable depend on the thickness of the graphite, having values ranging between 2mm to 5mm with 1mm increments. The nozzle choice is either a graphite nozzle or a tungsten carbide nozzle, for the tungsten carbide nozzle the diameter of the aperture can be 0.1mm, 0.3mm or 0.6mm. The quartz inserts and graphite disk were design by me but manufactured by the local manufacturing company PRO FAB^X, while the tungsten carbide nozzles with different

apertures were purchased from 苏州点易得点胶耗材配件店 online store (link: <https://shop308124567.taobao.com/?spm=2013.1.1000126>). The room temperature was also recorded to see if there was any effect on the droplets, usually within 18°C to 25°C.

Then the experiment starts, and a set of values for the variables is chosen. Each experiment will test one or two variables at a time. For the delay between forward and backwards values between 0.01 seconds to 1 seconds were tested, with interval of 0.1 seconds. For the delay between movements values between 0.5 seconds to 5 seconds with intervals of 0.5 were tested. For forwards and backwards distance values between 0 to 30 steps. For forwards and backwards speeds values between 40 steps/microsecond to 1000 steps/microseconds were tested in intervals of 100 steps/microseconds.

After a droplet with a single value was produced, it was measured, and its shape was recorded, the most common shapes or morphologies include, normal spherical droplet shape, splash, single satellite, multiple satellite, multiple droplets or spray, long tail, etc. Then the same set of values was tested with single droplets 2 to 5 more times to check consistency of the results. In case there was anything unexpected, like molten material going around the nozzle or wire bending, it was recorded, and the experiment was stopped.

3.2.3 Experiments to achieve the best droplet production

These experiments had the objective of finding the parameters that will allow the most consistent droplet production. These experiments were carried out in the iteration of the machine that had achieved the production of good droplet diameter and shape, and also was able to produce droplets with different sets of parameters, showing that the version of the system was good for droplet production.

It consisted of finding the forward and backward distance that will achieve a consistent production of droplets since in previous experiments of the tested version the other parameters should have been found. A consistent droplet production would be one that produces a droplet each time a movement command is sent, for testing this, 3 moving commands were sent at the same time to try to achieve 3 consecutive droplets. If three droplets were produced, then the parameters were slightly adjusted to try to reduce the droplet size while still keeping the production of 3 droplets. This process was repeated until the smaller diameter was achieved while keeping the production of 3 droplets per 3 moving commands. Since the deposition of

the 3 droplets was consecutive, a container filled with water was placed under the nozzle, to capture the droplets and solidify them instantly to avoid droplets fusing together.

Table 11 was used as the experimental matrix when experiments to achieve the best droplet production were conducted. When these experiments were conducted the variables of Table 11, were mostly decided or the most optimal options were already found. For the values of the other variables a set of values were tested and recorded each time only varying one of them, with the main focus being forward and backwards distance, with the values tested being between 0 and 30 with intervals of 1 and different combinations between forwards and backwards.

These experiments were the culmination of parametrization and will obtain the best parameters for the version of the machine being tested. Each test had a duration of 3 hours to 5 hours.

3.2.4 Experiment procedure

The following steps were carried out in most experiments:

1. Prepare the quartz insert, graphite disk, and nozzle and place them inside the crucible.
2. Secure the crucible in the middle of the coil of the ZVS induction heater.
3. Prepare the desired substrate to capture the droplets.
4. Turn on the industrial chiller, computer, infrared pyrometer, myRIO, and fume extractor.
5. Record room temperature and other parameters that will be used in the experiment.
6. Insert the wire through the wire feeder and through the quartz insert until it reaches the nozzle.
7. Position the infrared pyrometer, being sure that it has a clear view of the exposed surface of the graphite.

8. Turn on the stepper motor and the PID temperature control box.
9. Set the desired temperature on the PID temperature control box.
10. Turn on the ZVS induction heater.
11. Wait until the machine reaches a steady state at the desired temperature.
12. Initialize the motor control code on LabVIEW.
13. Input the parameter of the wire movement and record them.
14. Execute the motor code on LabVIEW.
15. Observe the results.
16. Record the results.
17. Go back to step 13 until all the parameters have been tested, the best parameters have been found or the expected outcome has been reached.
18. Turn off the ZVS induction heater.
19. Wait until the crucible colds down.
20. Remove the wire from the wire feeder.
21. Carefully with the appropriate tool remove the crucible and place it on the sand.
22. Turn off the rest of the components of the machine.

In case something went wrong or something unexpected happened the experiment would stop, and the process would jump to step 18. Figure 77 shows a picture of the system performing an experiment on droplet production.



Figure 77. Droplet production experiment being carried out.

3.3 Droplet sample collection

After the final version of the printhead was developed and tested, and the best parameters for it were found, a droplet sample collection was conducted to collect enough droplets to do a statistical analysis of the droplets to test the consistency of the machine in droplet production.

Two samples of 100 droplets each were created. Each sample was created on a different day, with the same parameters but starting the process from the beginning for each sample to assure that the droplet production is consistent any time that this machine with the same set of parameters is used.

The process of droplet collection was the same as a normal experiment with the following exceptions, before sending the executing code to produce the sample, some droplets were produced to clean the nozzle and to unclog it, then when executing the code to produce the sample it was selected to produce 100 droplets in one time so the 100 droplets will be created consecutively. A container filled with water 10cm away from the nozzle was used as a substrate to collect the droplets and prevent them to fuse together, similar to Figure 77.

After the samples were collected, the droplets were carefully taken out of the water, then the droplets were placed on top of an absorbent paper towel, leaving a distance of 1cm between droplets, then another absorbent paper towel was placed on top to prevent droplet oxidation. The droplets were left to dry for 2-3 days in the absorbent paper towel to assure no water was present, afterwards the droplets are placed inside a small container for storage and transport.

After the two samples were produced, dried, and stored, they were taken to be measured. First the weight of each droplet was measured using a scale with precision within ± 0.0001 g, then the 3 main dimensions of each droplet (height, width, and thickness) were measured.

Chapter 4 Results and Discussion

4.1 Experiments Results and discussion

While carrying out dozens of experiments using Aluminum 6061 the following results were obtained and were categorized depending on the effect that parameters had:

4.1.1 Wire Diameter

Wires of a diameter of 1mm, 1.6mm, 2mm, 2.4mm, and 2.5mm were tested multiple times with multiple in multiple conditions.

For the 2.5mm in diameter wire, it was very hard to produce droplets, regardless of what parameters were used, producing droplets only 1% of the time, the other times the wire minimum motion will displace too much molten metal, causing the metal to overflow and go to undesirable places like between the graphite and the quartz insert. The few droplets produced range from 0.5mm to 3mm in diameter.

For the 2.4mm in diameter wire, a droplet was produced 25% of the time (When talking about a percentage of droplets produce it refers to the relation between the droplets produced and the number of droplets that the movement of the wire intended to be created) and the droplet size ranged from 1mm to 3mm in diameter, but most droplets were in the range of 1.1mm to 1.3mm in diameter. But a big number of problems were encountered using 2.4mm, a big amount of material was still going to undesirable places due to the wire displacing an excessive amount of material when moving, the force of the wire broke the graphite nozzle multiple times, and overall, the droplet production was not reliable.

For the 2mm in diameter wire, a droplet was produced around 50% of the time, with droplets diameter ranging between 1mm and 1.3mm. The amount of material displaced still was too big and the excess material was still going to undesirable places.

For the 1.6mm diameter wire, a droplet was produced around 80% of the time for droplets of a diameter between 1.2mm to 1.5mm, or 100% of the time for a droplet diameter around 1.6mm. Since a droplet was produced 100% of the time this wire was chosen to be one used in the final experiment.

For the 1mm wire, the results were inconclusive since at a normal glance no droplets were produced, but a closer view of the substrate using a microscope revealed what appears to be droplets of a diameter of 60 μ m. Since it was not possible to accurately measure, analyze, transport, or capture these possible droplets, the testing with this wire stopped and has been delayed until the necessary equipment is obtained.

During the experiment with different wire diameters, it was confirmed that the calculations recorded in Tables 7-10 were accurate since the number of steps needed matched, is when the best droplet consistency was obtained, and also when the values of the required number of steps were exceeded it caused an over displacement of the molten aluminum, causing it to go to undesirable places.

4.1.2 Temperature

A variety of temperatures ranging from 700°C to 1000°C were tested since the melting point of aluminum 6061 is around 585°C to 650°C depending on the grade.

At 700°C the aluminum was not liquid enough to produce any droplets. At 800°C droplets of a diameter size between 1mm to 1.2mm can be produced, but only 25% of the time a droplet is produced. At 880°C droplets of a diameter size around 1.3mm can be produced, but only around 60% of the time. At 900°C droplets of a diameter around 1.6mm can be produced 100% of the time. At 1000°C only 20% of the time droplets can be produced, and the diameter is around 2mm.

It seems that the closer to the lowest limit in which the aluminum is just molten enough to produce droplets, around 800°C, is where the smallest droplets will be produced, but with a low percentage of droplets produced, then as the temperature goes up the droplet size increase but the consistency of the droplet production increases until it reaches 100% of droplets produced, at around 900°C, until it reaches a point in which the metal is too liquified that stars going to undesirable places instead of creating droplets, at around 1000°C.

4.1.3 Nozzle aperture

Three nozzle aperture diameters for the tungsten carbide nozzle were tested 0.1mm, 0.3mm and 0.6mm.

It was found that the 0.6mm diameter was the only one able to produce droplets with the current system. The 0.1mm and the 0.3mm orifice were too small compared to the existing gap between other components, like the gap between the quartz insert and the graphite or the gap between the tungsten carbide nozzle and the quartz insert, which makes the metal flow to undesirable places easier than to flow through the nozzle, thus, no droplets are produced.

4.1.4 Wire movement

The parameters that affect the droplet production and droplet size the most are the wire movement parameters, but since these parameters are related to the wire diameter and vary so widely is hard to find a pattern most of the time.

4.1.4.1 downwards and upwards distance and velocity

These parameters have two main components, the first one is the final displaced wire, which can be calculated by subtracting the upwards distance from the downwards distance, and the second one is the magnitude of the displacement in each motion. For example, a movement can consist of 5 steps downward and 3 steps upwards, in which the final displacement is 2 steps, and then another movement can consist of a 7 steps downwards and 5 steps upwards, with also will have a 2 steps final displacement, but the magnitude of each motion is bigger than in the first one.

For the final displaced wire, it was found that the calculated values of needed steps, Eqns. 12-16 and Tables 7-10, were accurate and when having the diameter of the wire and the expected droplet size, the needed steps to move the motor could be easily calculated. The closest the final displaced wire value is to the calculated needed step the more consistent the droplet production becomes.

For the magnitude of each motion is better to keep it as small as possible, but also to surpass a lower limit of 3 steps for the upwards movement, to start producing droplets, after

the limit of 3 steps, droplets can be produced but increasing these values causes the molten metal to go to undesirable places and reduces the consistency of the droplet production.

For the speeds, there was no noticeable change in droplet size or production unless the velocities are reduced to under 1250 steps/second.

4.1.4.2 Delay between forward and backward movement:

Delays between 0.01 seconds to 1 second were tested for the delay between forward and backward movements.

It was found that the minimum value for the delay is 0.05 seconds since anything smaller causes the stepper motor driver to miss steps and instead of changing the direction immediately it takes longer making the downwards movement longer than desired and the upwards movement shorter. It was also found that any value over 0.1 seconds results in a significant reduction of droplet consistency, reducing the droplets production around 50%, and if the value is over 0.2 seconds no droplets were produced. Thus, a delay of 0.05 seconds was chosen to be the best value for droplet production.

4.1.4.3 Delay between movements:

Delays between 0.5 seconds and 5 seconds were tested for the delay between movements.

It was found that a delay under 0.8 seconds caused the wire to bend at the top due to it moving faster than it melted. At 1 second there is no problem with the droplet production. At any value between 1 second and 2 seconds delay there is no change in droplet production. But anything longer than 2 seconds may cause the nozzle to get obstructed. Thus, a value of between 1 and 2 seconds for the delay between movements is used.

4.2 Droplet sample collection results and discussion

The creation of droplet samples to test the consistency of the droplet production is the culmination of all the experiments and research made. The parameters found to be the best for droplet production with good consistency are:

Table 13. Parameters used for the droplet sample collection.

Parameter	Value
Room Temperature	20°C
Graphite temperature	900°C±1°C
Aluminum 6061 wire diameter	1.6mm
Nozzle aperture	0.6mm
Downwards movement distance	7 steps
Upwards movement distance	3 steps
Downwards movement speed	2000 steps per second (0.57meters per second)
Upwards movement speed	25000 steps per second (7.07 meters per second)
Delay between downwards and upwards movement	0.5 second
Delay between movements	1 second
Number of movements	100 movements

With these parameters, two sets of 100 droplets each were produced, shown in Figure 78 and Figure 81. Each droplet was measured in its 3 dimensions (length, width, and thickness) and also was weighed on a scale with a precision of 0.0001g, then the ideal droplet diameter was calculated using the mass and assuming a perfect sphere shape, these were recorded in Table 15 and Table 16 found in the appendix.

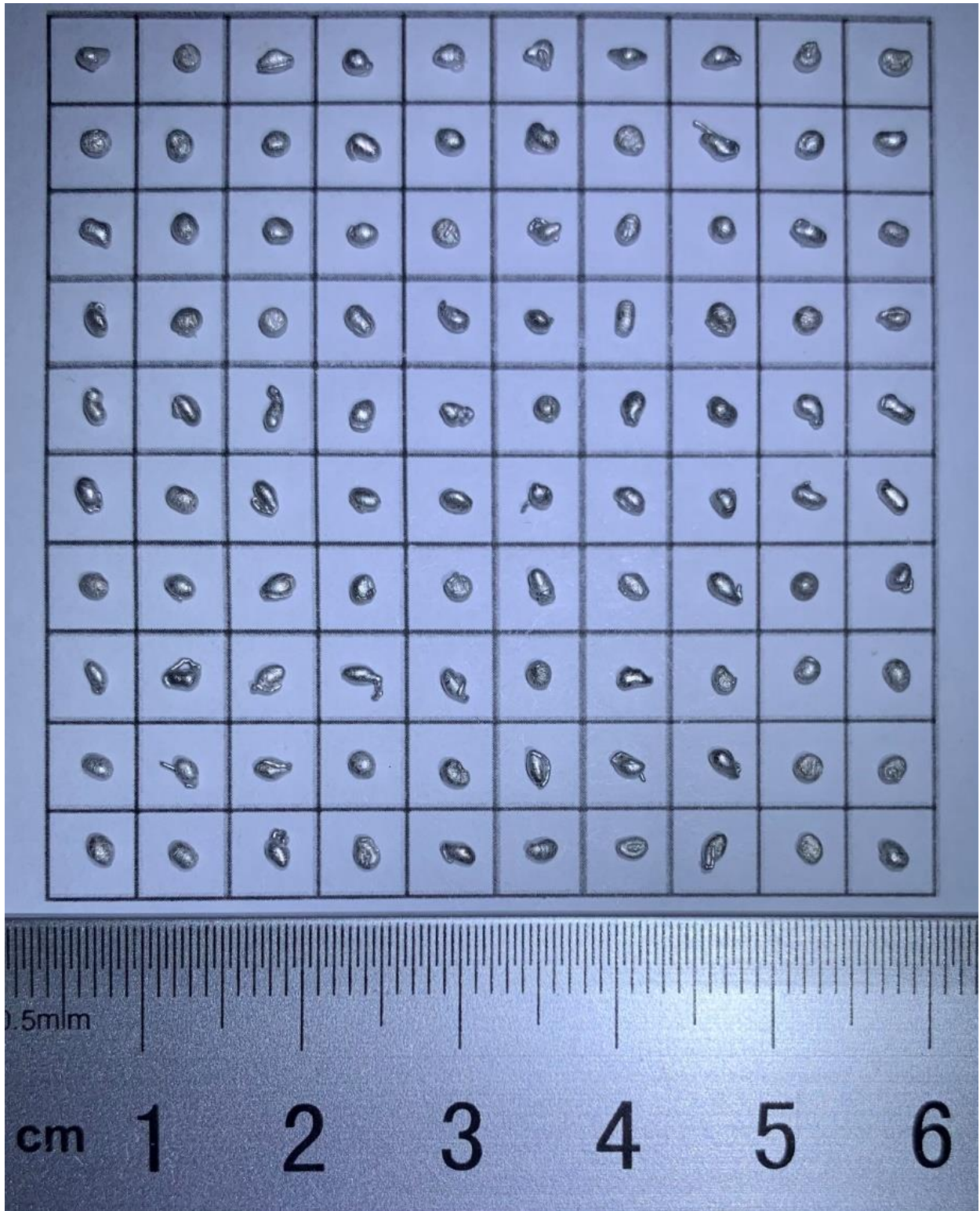


Figure 78. 100 droplets sample 1.

Using the calculated diameter, the average droplet diameter of sample 1 was 1.62mm and the standard deviation was 0.086mm.

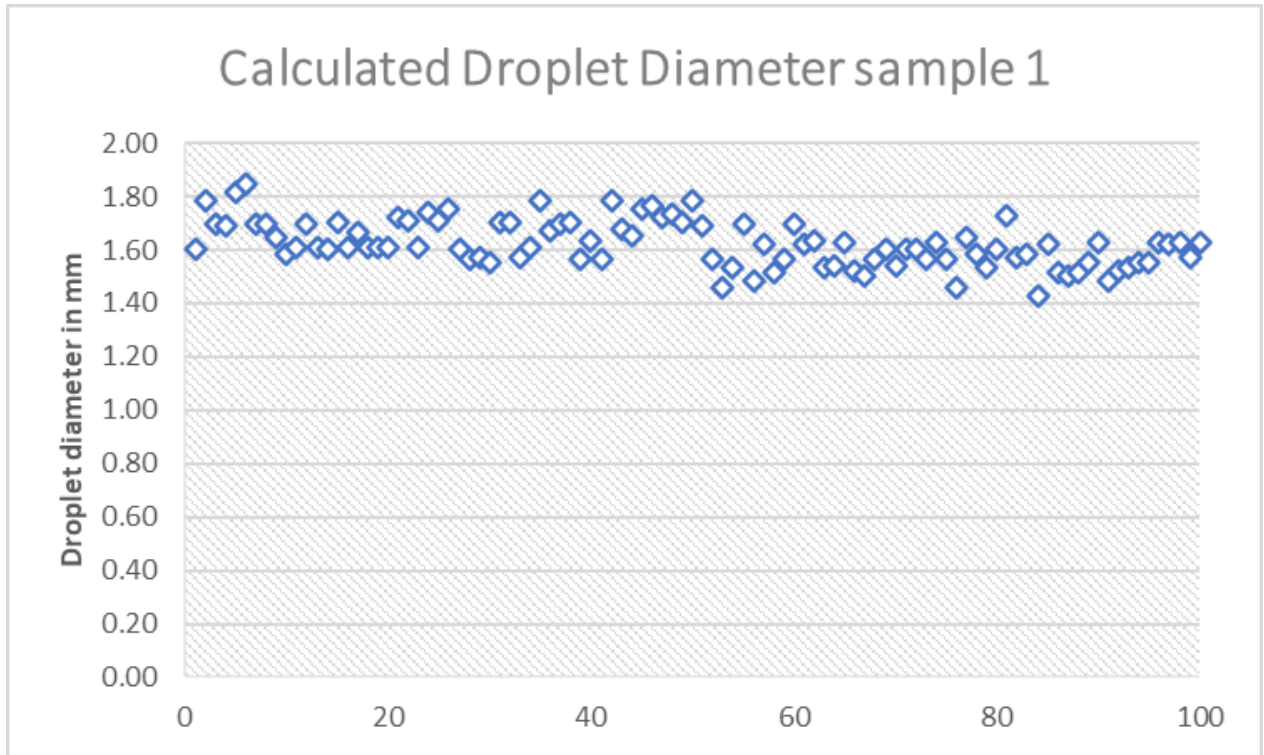


Figure 79. Calculated droplet diameter of sample 1.

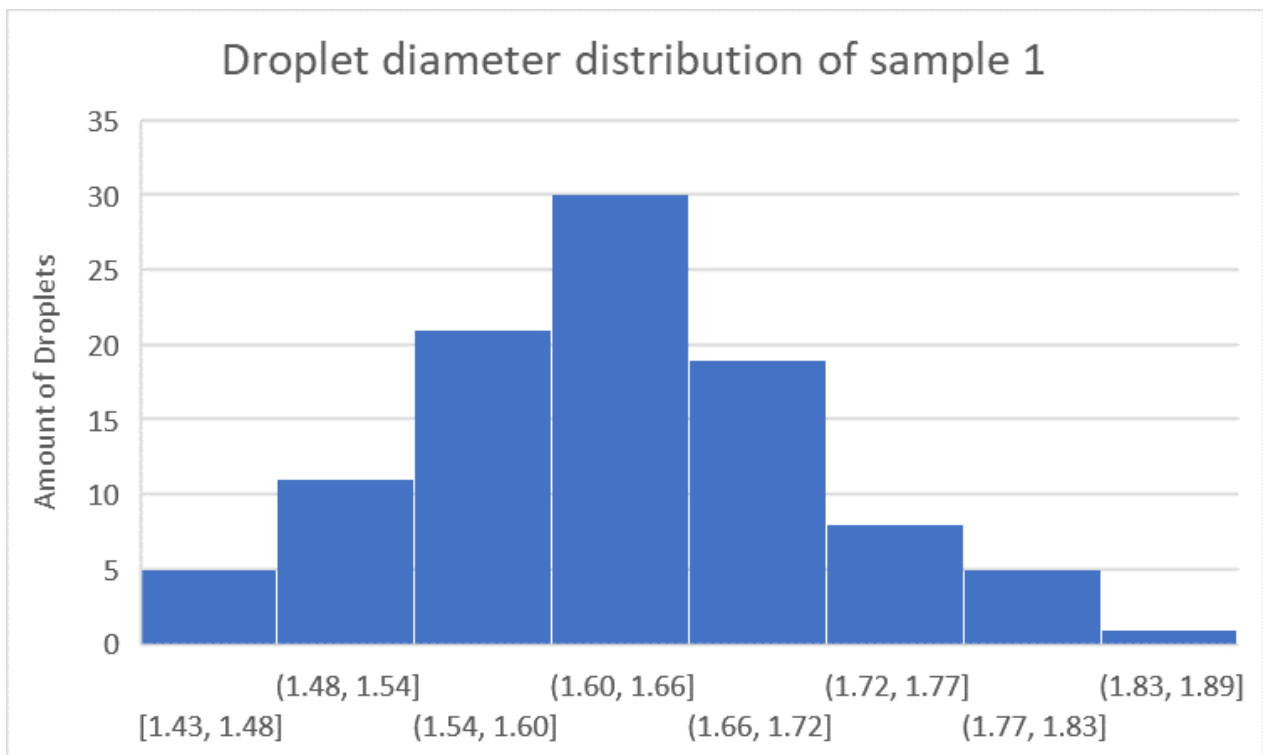


Figure 80. Calculated droplet diameter distribution of sample 1.

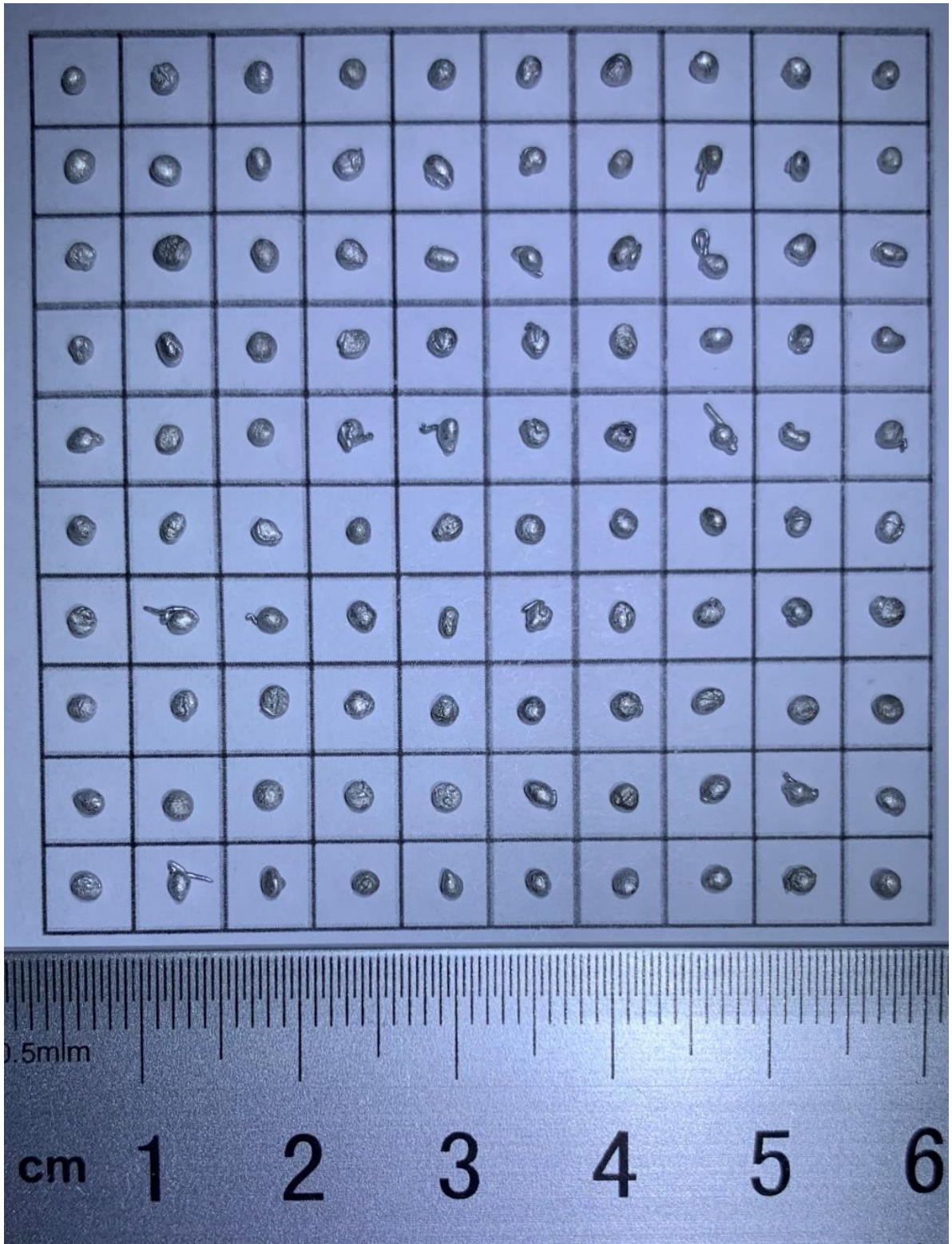


Figure 81. 100 droplets sample 2.

Using the calculated diameter, the average droplet diameter of sample 2 was 1.59mm and the standard deviation was 0.085mm.

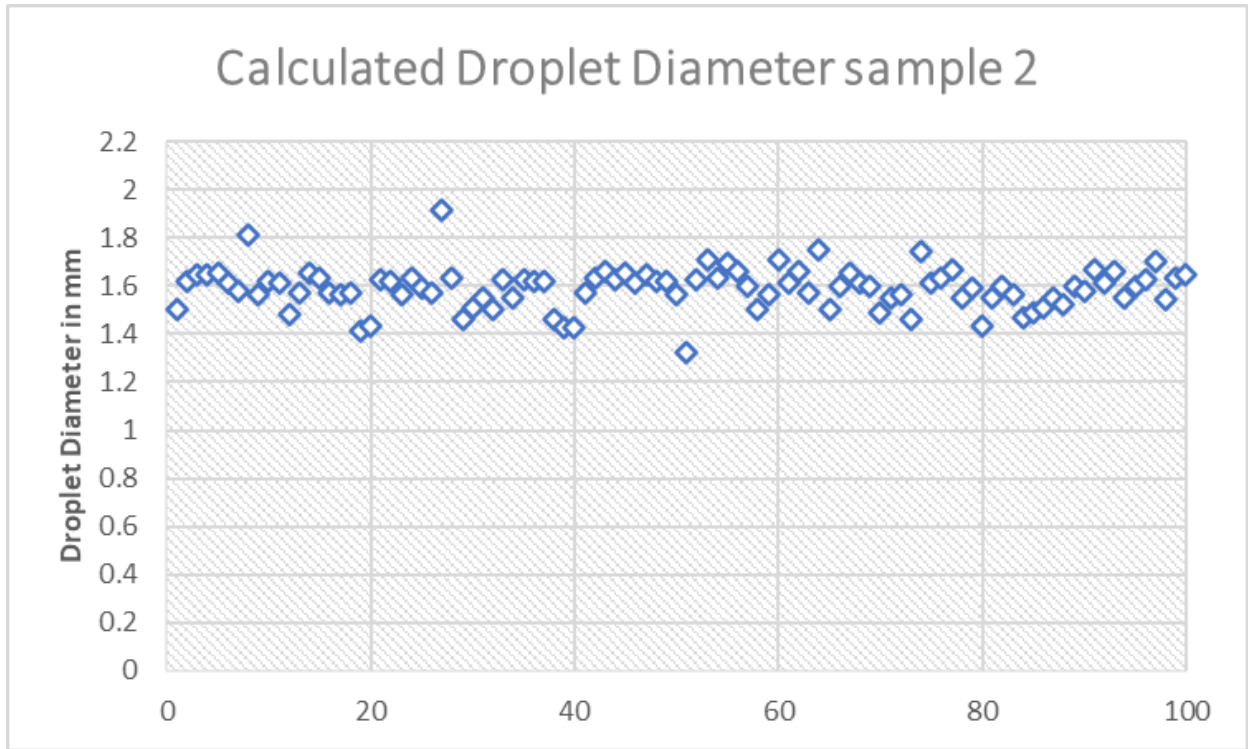


Figure 82. Calculated droplet diameter of sample 2.

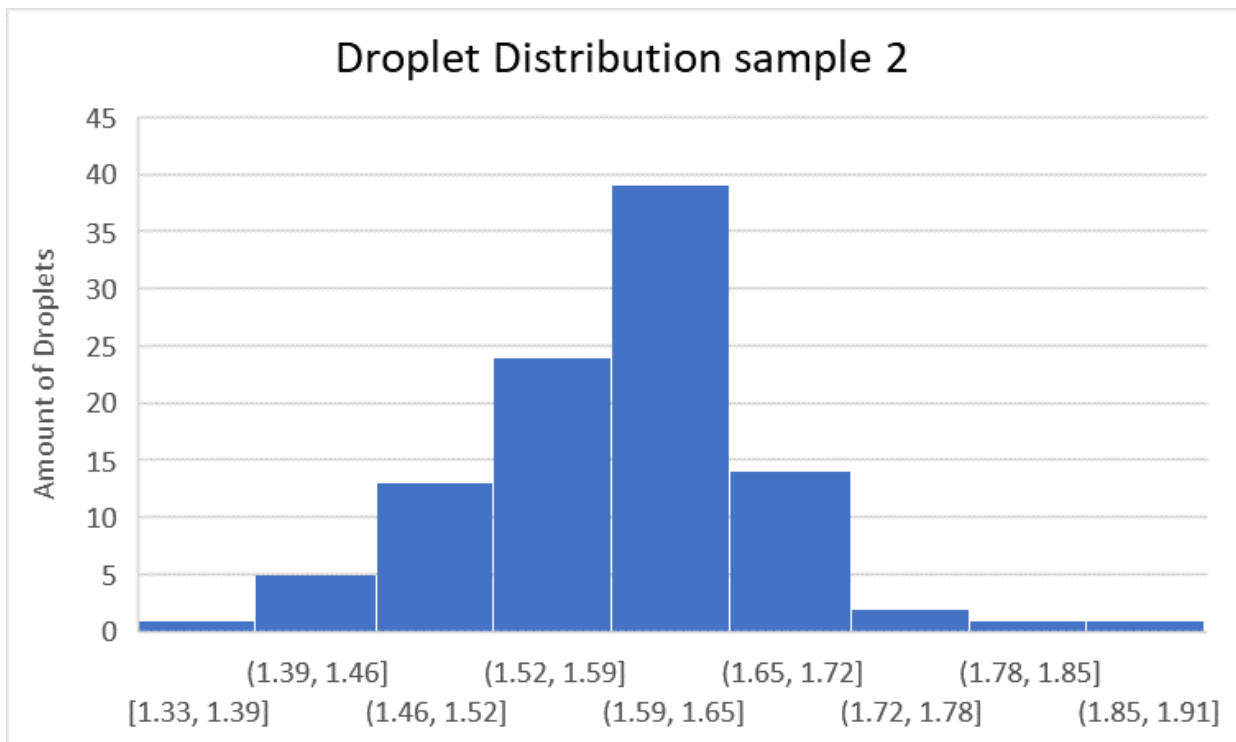


Figure 83. Calculated droplet diameter distribution of sample 2.

Using the calculated diameter, the average droplet diameter of both samples combined was 1.61mm and the standard deviation was 0.087mm.

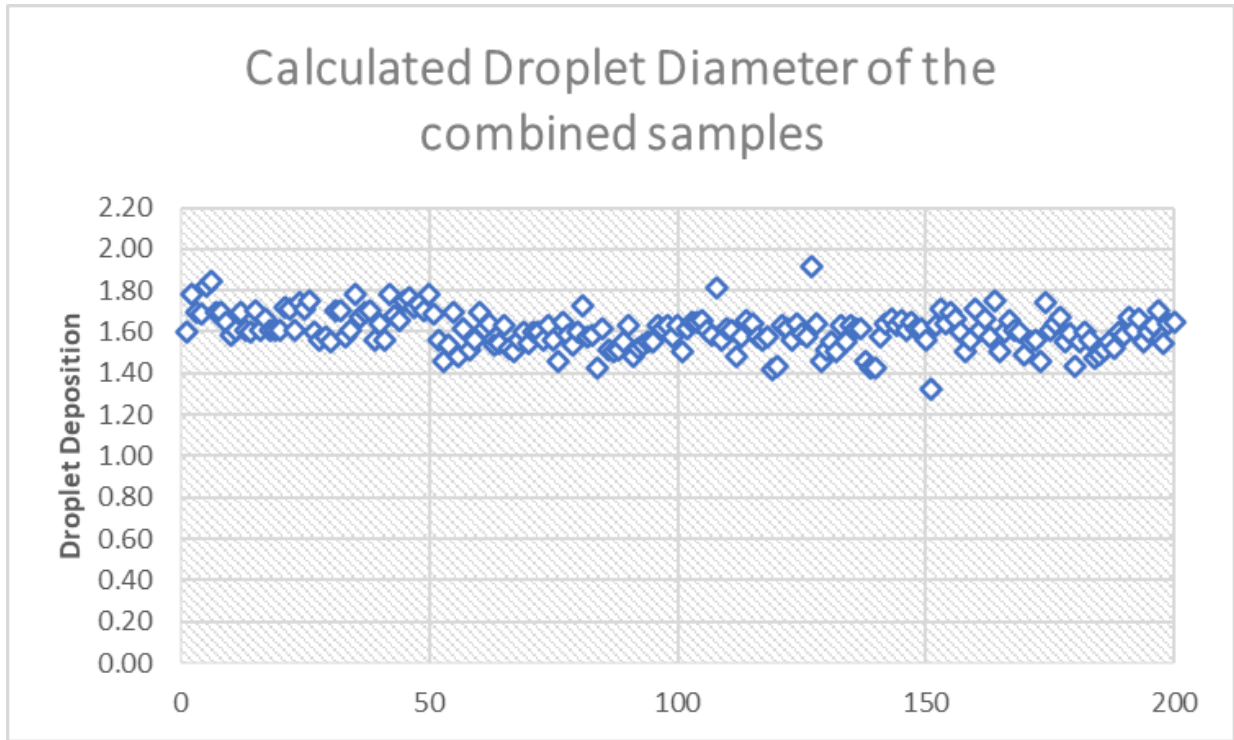


Figure 84. Calculated droplet diameter of the combined samples.

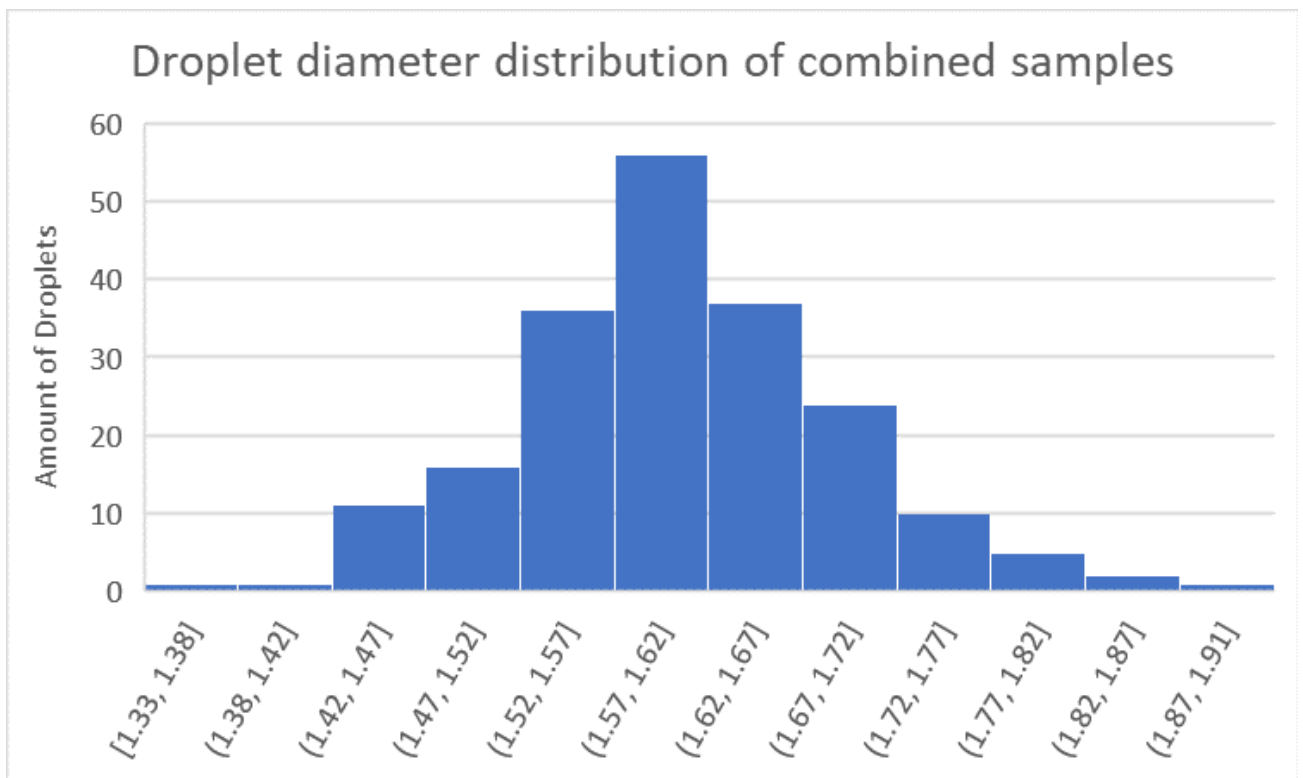


Figure 85. Calculated droplet diameter distribution of the combined samples.

The droplets of both samples show consistent droplet production both individually and combined, they also show a normal distribution. The droplet diameter size of 1.61mm is 2.7 times larger than the nozzle aperture. This most likely is due to the wetting behavior that aluminum has with the tungsten carbide nozzle, which will create a large, wetted region around the nozzle with prevents small droplets from be detach, thus the droplet size needs to be increased for it to be generated. This effect does not affect the consistency of the droplet production, but its reduction will mean smaller droplets are produced.

Table 14. Calculated steps needed to produce the obtained droplets.

Desired droplet diameter	Droplet of desired Volume	Mass of desired droplet	Volume of wire needed	Length of wire needed	Angular displacement needed	Steps needed
1.61mm	$0.11304mm^3$	0.005622g	$2.093728mm^3$	1.0418863mm	3.318035°	3.686706

As shown in table 8 the calculated steps needed to produce droplets of a size of is 3.78 steps, which can be approximated to 4 steps, since the downwards move is 7 and the upwards move is 3, the final wire movement is 4 steps, which agrees with the calculated steps needed, showing that the material is flowing from the molten pool through the nozzle and creating the droplet without any issue, thus the droplet production can achieve a consistent production. The shape of the droplets produced is not ideal, there are two problems that can be explained, the first problem is the existence of a tail in some of the droplets, this can be due to the distance between the water and the nozzle being too close and does not allow the droplet to fully form a perfect shaped droplet, the other thing is that the droplets are a little bit bigger in one direction instead of being more uniform, this is due to deformation that occurs when the droplet still in liquid form impacts against the water and it instantly solidifies. Both issues can be solved by having a longer distance between the nozzle and a heated substrate.

The standard deviation of the calculated diameter of a sphere is a good indicative of a droplet consistent production, since for the final step in the process of metal 3D printing by DoD, it involves the droplet be deposited in a substrate in which due to surface tension will form a partially spherical structure that can be directly linked to the diameter of the perfect sphere. If the standard deviation of the perfect sphere is within acceptable ranges it will mean that the deposited droplets will be a consistent distance within each other, allowing for proper remelting and formation of a fully dense part.

With the results obtained and the parameters shown in Table 13, together with the properties of aluminum at melting temperature from Sukhotskiy et al. [101]:

$$\rho = 2385 \text{ Kg} \cdot \text{m}^{-3}$$

$$D_1 = 0.0006 \text{ m}$$

$$v = 7.07 \text{ m} \cdot \text{s}^{-1}$$

$$\eta = 0.00134 \text{ Pa} \cdot \text{s}$$

$$\gamma = 0.914 \text{ N} \cdot \text{m}^{-1}$$

The dimensionless numbers can be calculated using Equations 1-4:

$$Re = 7550.13$$

$$Ca = 0.0104$$

$$We = 78.25$$

$$Oh = 0.0012$$

The relation between the Weber number and Ohnersorge number show that droplets produced by the system are in region 1 of droplets behavior (see figure 50), which indicates that the droplet generation process is driven by the impact and pressure generated by the wire feeder, also indicates that the resistance force is created by the inertia of the molten metal and not its viscosity. It also shown that the system is closest to regime 5 (see figure 51), even though the behavior is more like regime 3. This may indicate that there is some parameter affecting the droplet formation, that slows the droplet production but allows for a single droplet to form.

Comparing the results of the produced droplet's size (1.61mm) to other DoD techniques, it was found that the droplet size was bigger than all of the reviewed techniques, with the closest diameter size being the EHD technique that had a diameter of 1.6 mm, followed closely by the impact driven technique which had a diameter of up to 1.42 mm. This is due to the nozzle diameter used (0.6mm) that is also bigger than any other nozzle diameter used by the review DoD. If the relation that exist between the droplet size and the nozzle size is compared between the results obtained and other DoD methods is found that the droplet diameter obtained, which is 2.68 times bigger than the nozzle, is close to multiple DoD techniques, like one of the reviewed pneumatic techniques that had a droplet size that was 2.36 times bigger than the

nozzle, and is better than a third of the other reviewed DoD techniques, like EHD that has a droplet diameter 10 times bigger than the nozzle. Overall, even though the droplet size is bigger than other methods, due to the diameter of the nozzle used, the performance of the droplet size of the printhead seems to be at the same level than the other DoD techniques.

Comparing the results of the droplet's size standard deviation to other DoD techniques, it was found that the obtained standard deviation, 0.087mm which is 5.4% of the droplet size, is within other standards deviations reviewed. One of the reviewed piezoelectric techniques had a standard deviation of 6.23% the diameter of the droplet, while a Pneumatic technique and an electromagnetic MHD technique had a standard deviation of 2.69% and 2.29% of their droplet size respectively. This shows that the droplet production is comparable to other existing techniques, but it still has to improve to be able to achieve the same level of consistency as some DoD techniques have.

4.3 Other materials results

Tests with other materials were also carried out to see how the system will handle them. Experiments with brass, stainless steel 304, and Inconel 718 were conducted.

Inconel 718 and steel 304 were tested in the form of a wire with a diameter of 2.4mm, which made it hard to create droplets. The current of the ZVS induction heater needed to reach the temperatures needed to melt the materials (over 1400°C) was too high for the laboratory, which is not equipped with high power outlets, thus the breakers prevented the system to draw the necessary current to reach the temperatures needed. No droplets were produced with these two materials, but with a high-power outlet, the possibilities of creating droplets are very high.

For a 1.6mm diameter brass wire, with a melting point of around 900°C, experiments were carried out. And droplets were created, and the best results obtained are shown in Figure 86. The droplets produced were of a variety of sizes ranging from 0.25mm to 1.72mm, with the majority of droplets being between 0.25mm and 0.4mm. The peculiarity is that only a downward movement of 1 step was used continuously, and for each step, multiple droplets were created.

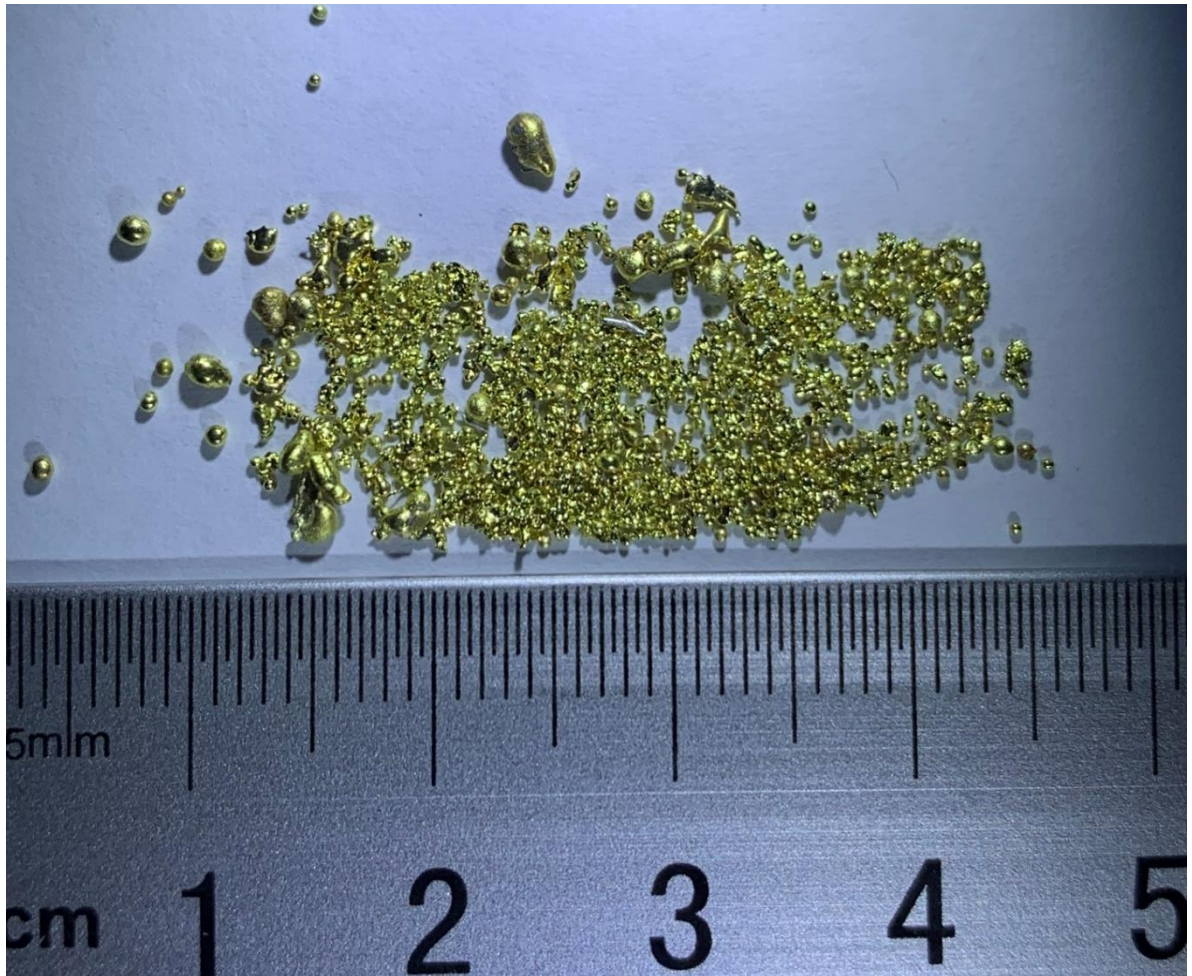


Figure 86. Brass droplet produced.

Chapter 5 Conclusion

5.1 Conclusion of the Research

Metal DoD printing has shown to be one of the metal 3D printing methods that shows the most potential to become a commercial and manufacturing method success, with multiple techniques that allows for a wide range of applications and reduce price compared to available commercial 3D printers. The literature review shows how the different DoD techniques have been advancing in the last decade and how in some years can become an influential manufacturing method for small metal parts.

This research aimed to achieve consistent droplet production for a novel 3D printer. During this research, multiple changes to the printhead systems and to the control system have been made to try to achieve a consistent droplet production. It started with the replacement of the wire feeder to accommodate different diameter wires in the machines. Then the temperature system was improved by changing the ZVS induction heater with one in which the power output can be controlled. The crucible system also sustained a number of relevant changes, like the addition of the tungsten carbide nozzle. And finally, the control system was improved by adding an infrared pyrometer and a PID temperature control box and redoing the code to allow for a more customizable control of the movement of the wire. All these changes together with the calculations and experiments that allowed to find the best input parameters for droplet production, allowed the DoD novel 3D printer to achieve consistent droplet production. The consistent droplet production was of droplets of an average diameter of 1.61 mm with a standard deviation of 0.087 mm on a sample of 200 droplets. Since these values are within the values established at the beginning of the research (Droplet diameter between 0.6 mm and 2 mm and a standard deviation of less than 0.167 mm) it is concluded that the aim of obtaining a consistent droplet production was achieved.

Objective 1, which was to research other DoD techniques to understand the droplet formation, has been shown to be completed in the literature review section of the thesis, in which the different ways of generating droplets are explained. Due to the understanding of other DoD techniques various improvements were made to the DoD printer.

Objective 2, which was to replace/optimize the printhead and improve droplet production, was achieved by changing all the systems in some form, and by achieving a

consistent droplet production. All the changes in the different systems of the DoD metal 3D printer were listed on the methods section of the thesis.

Objective 3, which was to test the droplet consistency, was completed by producing two samples of 100 droplets each, measuring them and calculating their standard deviation and average diameter, which shows that the samples are part of a consistent droplet production.

The three proposed deliverables/outcome, which are: having a better understanding of the droplet formation, optimize and test the printhead of the metal 3D printer and create a statistical analysis of the droplet's consistency, have been achieved/made. The first one was achieved while understanding how other DoD techniques work and by conducting multiple droplet production experiments which gave a better understanding of droplet production. The second one was completed while modifying the machine to achieve consistent droplet production and while creating the two samples of droplets. And finally, the third was made in the Results sections of this thesis, showing the distribution of the produce droplets.

In conclusion the novel DoD technique Metal Droplet Extrusion /Filament Droplet Extrusion has been proved to be able to have a consistent droplet production of aluminum 6061, which makes it one of the few DoD generators that is able to work with this material, even though the droplets size is not impressive at the moment, this technique still can be developed further.

5.2 Future Work and Recommendations

As mentioned before this research is just one of the first developments of this Metal Droplet Extrusion /Filament Droplet Extrusion novel technique, which has great potential due to its possible capabilities of working with high-melting point metals at a low price.

The first work that should be conducted is to carry out more experiments with other materials and find the parameters for those materials. The materials suggested are brass, stainless steel 304 and Inconel 718, all popular materials used in aerospace and other fields of engineering.

Another recommendation is to enclose the printhead in a low oxygen environment, either nitrogen or argon, which the literature review proves to be one of the main components of the DoD generators to prevent the materials to oxidize and to aid with the droplet production.

To reduce the droplet size is recommended to modify the geometry of the tungsten carbide nozzle, and maybe replace it with another material nozzle which has less wettability with the molten/liquid metals, to allow them to easily flow out of the nozzle instead of sticking at the bottom.

Overall, the research on droplet production for this technique needs to be continued, but also the other components of the printer need to be developed, like the bed/substrate system to be able to start producing metal parts with the achieved consistent droplet production, to start the analysis of the quality and physical properties of parts created by this technique.

References

- [1] C. Kavanaugh, "Wohlers Report 2022 shows double-digit growth again for additive manufacturing.," *Plastics News*, p. 23, 2 may 2022.
- [2] R. Grace, "Wohlers report says 3-D printing exploding.," *Plastics News*, p. 1, 24 June 2013.
- [3] Anonymous, "WOHLERS ASSOCIATES PUBLISHES 20TH ANNIVERSARY EDITION OF ITS INDUSTRY REPORT," *Appliance Design*, p. 10, June 2015.
- [4] T. Wohlers and N. Mostow, "Wohlers Gives State-of-the-Industry Rundown," *Manufacturing Engineering*, April 2022.
- [5] E. M. Palmero, J. Rial, J. de Vicente, J. Camarero, B. Skårman, H. Vidarsson, P.-O. Larsson and A. Bollero, "Development of permanent magnet MnAlC/polymer composites and flexible filament for bonding and 3D-printing technologies," *Science and technology of advanced materials*, vol. 19, no. 1, pp. 465-473, 2018.
- [6] Y. Wang, A. Ahmed, A. Azam, D. Bing, Z. Shan, Z. Zhang, M. K. Tariq, J. Sultana, R. T. Mushtaq, A. Mehboob, C. Xiaohu and M. Rehman, "Applications of additive manufacturing (AM) in sustainable energy generation and battle against COVID-19 pandemic: The knowledge evolution of 3D printing," *Journal of manufacturing systems*, vol. 60, pp. 709-733, 2021.
- [7] L. Jonušauskas, S. Juodkazis and M. Malinauskas, "Optical 3D printing: bridging the gaps in the mesoscale," *Journal of optics (2010)*, vol. 20, no. 5, p. 53001, 2018.
- [8] M. Sakin and Y. C. Kiroglu, "3D Printing of Buildings: Construction of the Sustainable Houses of the Future by BIM," *Energy Procedia*, vol. 134, pp. 702-711, 2017.
- [9] C. Heuer, J. Preuß, T. Habib, A. Enders and J. Bahnemann, "3D printing in biotechnology—An insight into miniaturized and microfluidic systems for

- applications from cell culture to bioanalytics," *Engineering in life sciences*, vol. 22, no. 12, pp. 744-759, 2022.
- [10] B. C. Gross, J. L. Erkal, S. Y. Lockwood, C. Chen and D. M. Spence, "Evaluation of 3D Printing and Its Potential Impact on Biotechnology and the Chemical Sciences," *Analytical Chemistry*, vol. 86, no. 7, pp. 3240-3253, 2014.
- [11] M. A. Cruz, S. Ye, M. J. Kim, C. Reyes, F. Yang, P. F. Flowers and B. J. Wiley, "Multigram Synthesis of Cu-Ag Core–Shell Nanowires Enables the Production of a Highly Conductive Polymer Filament for 3D Printing Electronics," *Particle & particle systems characterization*, vol. 35, no. 5, p. 1700385, 2018.
- [12] A. S. Ramírez, R. D'Amato, F. B. Haro, M. I. Marcos and J. A. Juanes, "Novel Technique Based on Fused Filament Fabrication (FFF) and Robocasting to Create Composite Medical Parts," *Journal of medical systems*, vol. 43, no. 5, pp. 120-129, 2019.
- [13] J. M. Jordan, 3D printing, Cambridge, Massachusetts ; London, England : The MIT Press, 2018.
- [14] C. M. Thakar, S. S. Parkhe, A. Jain, K. Phasinam, G. Murugesan and R. J. M. Ventayen, "3d Printing: Basic principles and applications," *Materials today : proceedings*, vol. 51, pp. 842-849, 2022.
- [15] M. K. Thompson, G. Moroni, T. Vaneker, G. Fadel, R. I. Campbell, I. Gibson, A. Bernard, J. Schulz, P. Graf, B. Ahuja and F. Martina, "Design for Additive Manufacturing: Trends, opportunities, considerations, and constraints," *CIRP annals*, vol. 65, no. 2, pp. 737-760, 2016.
- [16] E. Herrmann, "Metal AM Update: Growth, Processes and Barriers.," *Industrial Heating*, vol. 85, no. 12, pp. 38-40, 2017.
- [17] S. Das, D. Bourell and S. Babu, "Metallic materials for 3D printing," *MRS Bulletin*, vol. 41, no. 10, p. 729–741, 2016.
- [18] J. Huang, L. Qi, J. Luo, K. Zhang and L. Yang, "A ground-based work of droplet deposition manufacturing toward microgravity: Fine pileup of horizontally ejected

metal droplets on vertical substrates," *Journal of manufacturing processes*, vol. 66, pp. 293-301, 2021.

- [19] M. Fang, S. Chandra and C. B. Park, "Building three-dimensional objects by deposition of molten metal droplets," *Rapid prototyping journal*, vol. 14, no. 1, pp. 44-52, 2008.
- [20] T. E. Graedel, "On the Future Availability of the Energy Metals," *Annual review of materials research*, vol. 41, no. 1, pp. 323-335, 2011.
- [21] S. Mooraj, Z. Qui, C. Zhu, J. Ren, S. Peng, L. Liu, S. Zhang, S. Feng, F. Kong, Y. Liu, E. B. Duoss, S. Baker and W. Chen, "3D printing of metal-based materials for renewable energy applications," *Nano research*, vol. 14, no. 7, pp. 2105-2132, 2021.
- [22] H. Jayawardane, I. J. Davies, J. R. Gamage, M. John and W. K. Biswas, "Investigating the 'techno-eco-efficiency' performance of pump impellers: metal 3D printing vs. CNC machining," *International journal of advanced manufacturing technology*, vol. 121, no. 9-10, pp. 6811-6836, 2022.
- [23] L. E. Murr, "A Metallographic Review of 3D Printing/Additive Manufacturing of Metal and Alloy Products and Components," *Metallography, microstructure, and analysis*, vol. 7, no. 2, pp. 103-132, 2018.
- [24] J. Manriquez-Frayre and D. Bourell, "Selective Laser Sintering of Binary Metallic Powder," *Proc. 1st Solid Freeform Fabr. Symp.*, no. 1, p. 99, 1990.
- [25] V. T. Le and H. Paris, "A life cycle assessment-based approach for evaluating the influence of total build height and batch size on the environmental performance of electron beam melting," *International journal of advanced manufacturing technology*, vol. 98, no. 1-4, pp. 275-288, 2018.
- [26] M. Galatini and P. Minetola, "Analysis of Density, Roughness, and Accuracy of the Atomic Diffusion Additive Manufacturing (ADAM) Process for Metal Parts," *Materials*, vol. 12, no. 24, p. 4122, 2019.
- [27] W. E. Frazier, "Metal Additive Manufacturing: A Review," *Journal of materials engineering and performance*, vol. 23, no. 6, pp. 1927-1928, 2014.

- [28] L. Cherdo, "Metal 3D printers in 2022: a comprehensive guide," 08 June 2022. [Online]. Available: <https://www.aniwaa.com/buyers-guide/3d-printers/best-metal-3d-printer/>. [Accessed 17 August 2022].
- [29] M. Leary, *Design for additive manufacturing : tools and optimization*, Amsterdam: Elsevier, 2020.
- [30] Y. Zhang, S. Yang and Y. F. Zhao, "Manufacturability analysis of metal laser-based powder bed fusion additive manufacturing—a survey," *International journal of advanced manufacturing technology*, vol. 110, no. 1-2, pp. 57-78, 2020.
- [31] E. Louvis, P. Fox and C. J. Sutcliffe, "Selective laser melting of aluminium components," *Journal of materials processing technology*, vol. 211, no. 2, pp. 275-284, 2011.
- [32] y. Zhang, W. Jarosinski, Y.-G. Jung and J. Zhang, "Additive manufacturing processes and equipment," in *Additive Manufacturing: Materials, Processes, Quantifications and Applications*, Saint Louis, Elsevier Science & Technology, 2018, pp. 39-49.
- [33] B. Hayes, T. Hainsworth and R. MacCurdy, "Liquid–solid co-printing of multi-material 3D fluidic devices via material jetting," *Additive manufacturing*, vol. 55, p. 102785, 2022.
- [34] B. Kirchebner, C. Rehekampff, M. Tröndle, P. Lechner and W. Volk, "Analysis of salts for use as support structure in metal material jetting," *Production engineering*, vol. 15, no. 6, pp. 855-862, 2021.
- [35] M. Rombouts, J. P. Kruth, L. Froyen and P. Mercelis, "Fundamentals of Selective Laser Melting of alloyed steel powders," *CIRP annals*, vol. 55, no. 1, pp. 187-192, 2006.
- [36] M. M. Attallah, R. Jennings, X. Wang and L. N. Carter, "Additive manufacturing of Ni-based superalloys: The outstanding issues," *MRS bulletin*, vol. 41, no. 10, pp. 758-764, 2016.

- [37] W. Stopyra, K. Gruber, I. Smolina, T. Kurzynowski and B. Kuźnicka, "Laser powder bed fusion of AA7075 alloy: Influence of process parameters on porosity and hot cracking," *Additive manufacturing*, vol. 35, p. 101270, 2020.
- [38] J. H. Martin, B. D. Yahata, J. M. Hundley, J. A. Mayer, T. A. Schaedler and T. M. Pollock, "3D printing of high-strength aluminium alloys," *Nature*, vol. 549, no. 7672, pp. 375-369, 2017.
- [39] 3D Systems, Inc., "DMP Flex 100," 3D Systems, Inc., [Online]. Available: <https://www.3dsystems.com/3d-printers/dmp-flex-100>. [Accessed 18 June 2022].
- [40] EOS, "EOS M 100," EOS, [Online]. Available: <https://www.eos.info/en/additive-manufacturing/3d-printing-metal/eos-metal-systems/eos-m-100>. [Accessed 18 June 2022].
- [41] GENERAL ELECTRIC, "Arcam EBM Spectra L," GENERAL ELECTRIC, [Online]. Available: <https://www.ge.com/additive/additive-manufacturing/machines/arcam-ebm-spectra-l>. [Accessed 18 June 2022].
- [42] GENERAL ELECTRIC, "Concept Laser M2 Series 5," GENERAL ELECTRIC, [Online]. Available: <https://www.ge.com/additive/additive-manufacturing/machines/m2series5>. [Accessed 18 June 2022].
- [43] SLM SOLUTIONS, "SLM 125," SLM SOLUTIONS, [Online]. Available: <https://www.slm-solutions.com/products-and-solutions/machines/slm-125/>. [Accessed 18 June 2022].
- [44] FORMALLOY, "X & L-Series," FORMALLOY, 2021. [Online]. Available: <https://www.formalloy.com/machines>. [Accessed 19 June 2022].
- [45] Desktop Metal, "Production System™ P-1," Desktop Metal, 2020. [Online]. Available: <https://www.desktopmetal.com/uploads/SPJ-SPC-P01-201118.pdf>. [Accessed 19 June 2022].
- [46] DIGITAL METAL, "DM P2500 - 3D printing at its best," DIGITAL METAL, [Online]. Available: <https://digitalmetal.tech/printer-line/design-and-function/>. [Accessed 19 June 2022].

- [47] SPEE3D, "LightSPEE3D 3D Metal Printer," SPEE3D, [Online]. Available: <https://www.spee3d.com/product/lightspee3d/>. [Accessed 19 June 2022].
- [48] XJET, "XJET Carmel 700," XJET, [Online]. Available: <https://www.xjet3d.com/products/xjet-carmel-700/>. [Accessed 18 June 2022].
- [49] aniwaa, "MK1," aniwaa, [Online]. Available: <https://www.aniwaa.com/product/3d-printers/vader-systems-mk1/>. [Accessed 20 June 2022].
- [50] aniwaa, "Polaris," aniwaa, [Online]. Available: <https://www.aniwaa.com/product/3d-printers/vader-systems-polaris/>. [Accessed 20 June 2022].
- [51] XEROX, "3D printing resources," XEROX, [Online]. Available: <https://www.xerox.com/en-us/innovation/3d-printing-resources>. [Accessed 07 february 2022].
- [52] H. Yi, Z. Wang, H. Cao, M. Liu and J. Li, "Metal Droplet Deposition: From Foundation to Engineering Manufacturing," *Advanced Engineering Materias*, p. 2201003, 2022.
- [53] H. Wu, G. Zhao and Z. Wei, "The Additive Manufacturing Process of Electric Power Fittings," *Mechanical Engineering Science*, vol. 1, no. 1, pp. 26-31, 2019.
- [54] I. Gibson, D. W. Rosen and B. Stucker, *Additive Manufacturing Technologies: Rapid Prototyping to Direct Digital Manufacturing*, Boston: Springer-Verlag, 2010.
- [55] B. Y. Tay, J. G. Evans and M. J. Edirisinghe, "Solid freeform fabrication of ceramics," *International materials reviews*, vol. 48, no. 6, pp. 341-370, 2003.
- [56] J. Luo, L.-H. Qi, X.-S. Jiang, J.-M. Zhou and H. Huang, "Research on lateral instability of the uniform-charged droplet stream during droplet-based freeform fabrication," *International Journal of Machine Tools and Manufacture*, vol. 48, pp. 289-294, 2008.
- [57] Q. Liu and M. Orme, "High precision solder droplet printing technology and the state-of-the-art," *Journal of Material Processing Technology*, vol. 115, no. 3, pp. 271-283, 2001.

- [58] S. X. Cheng, T. Li and S. Chandra, "Producing molten metal droplets with a pneumatic droplet-on-demand generator," *Journal of materials processing technology*, vol. 159, no. 3, pp. 295-302, 2005.
- [59] L.-h. Qi, Y.-p. Chao, J. Luo, J.-m. Zhou, X.-h. Hou and H.-j. Li, "A novel selection method of scanning step for fabricating metal components based on micro-droplet deposition manufacture," *International journal of machine tools & manufacture*, vol. 56, pp. 50-58, 2012.
- [60] J. Luo, L.-h. Qi, S.-y. Zhong, J.-m. Zhou and H.-j. Li, "Printing solder droplets for micro devices packages using pneumatic drop-on-demand (DOD) technique," *Journal of materials processing technology*, vol. 212, no. 10, pp. 1066-2073, 2012.
- [61] J. Luo, L.-h. Qi, J.-m. Zhou, X.-h. Hou and H.-j. Li, "Modeling and characterization of metal droplets generation by using a pneumatic drop-on-demand generator," *Journal of materials processing technology*, vol. 212, no. 3, pp. 718-726, 2012.
- [62] H.-s. Zuo, H.-j. Li, L.-h. Qi, J. Luo, S.-y. Zhong and H.-p. Li, "Effect of wetting behavior on generation of uniform aluminum droplets obtained by pneumatic drop-on-demand technique," *Journal of materials processing technology*, vol. 214, no. 11, pp. 2566-2575, 2014.
- [63] Y. M. Shin, M. M. Hohman, M. P. Brenner and G. C. Rutledge, "Experimental characterization of electrospinning: the electrically forced jet and instabilities," *Polymer*, vol. 42, no. 25, pp. 09955-099667, 2001.
- [64] M. M. Hohman, M. Shin, G. Rutledge and M. P. Brenner, "Electrospinning and electrically forced jets. I. Stability theory," *Physics of Fluids*, vol. 13, no. 8, pp. 2201-2220, 2001.
- [65] A. Baji, Y.-W. Mai, S.-C. Wong, M. Abtahi and P. Chen, "Electrospinning of polymer nanofibers: Effects on oriented morphology," *Composites Science and Technology*, vol. 70, no. 5, pp. 703-718, 2010.

- [66] C. Wei, H. Qin, N. Ramirez-Iglesias, C.-P. Chiu, Y. Lee and J. Dong, "High-resolution ac-pulse modulated," *Journal of Micromechanics and Microengineering*, vol. 24, p. 045010, 2014.
- [67] Y. Han and J. Dong, "High-resolution direct printing of molten-metal using electrohydrodynamic jet plotting," *Manufacturing letters*, vol. 12, pp. 6-9, 2017.
- [68] Y. Han and J. Dong, "High-Resolution Electrohydrodynamic (EHD) Direct Printing of Molten Metal," *Procedia Manufacturing*, vol. 10, pp. 845-850, 2017.
- [69] S. Vader, Z. Vader, I. Karampelas and E. Furlani, "Magnetohydrodynamic liquid metal jet printing," *TechConnect Conference*, pp. 2-4, 2015.
- [70] S. Vader, Z. Vader, I. Karampelas and E. Furlani, "Advances in magnetohydrodynamic liquid metal jet printing," *TechConnect Briefs*, vol. 4, pp. 41-45, 2016.
- [71] I. Karampelas, V. Sukhotskiy, G. Garg, A. Verma, M. Tong, S. Vader, Z. Vader and E. Furlani, "Drop-on-demand 3D metal printing," *TechConnect Briefs*, vol. 4, pp. 213-215, 2017.
- [72] V. Sukhotskiy, I. Karampelas, G. Garg, A. Verma, M. Tong, S. Vader, Z. Vader and E. Furlani, "Magnetohydrodynamic drop-on-demand liquid metal 3D printing," *Solid Freeform Fabrication 2017: Proceedings of the 28th Annual International*, pp. 1806-1811, 2017.
- [73] V. Sukhotskiy, P. Vishnoi, I. Karampelas, S. Vader, Z. Vader and E. Furlani, "Magnetohydrodynamic drop-on-demand liquid metal additive manufacturing: System overview and modelling," *Proceedings of the 5th International Conference of Fluid Flow, Heat and Mass Transfer (FFHMT'18)*, pp. 7-9, 2018.
- [74] M. Meda, P. Mehta, C. Mahajan, B. Kahn and D. Cormier, "Magnetohydrodynamic liquid metal droplet jetting of highly," *Flexible and Printed Electronics*, vol. 6, p. 035002, 2021.
- [75] Z. Luo, X. Wang, L. Wang, D. Sun and Z. Li, "Drop-on-demand electromagnetic printing of metallic droplets," *Materials letters*, vol. 188, pp. 184-187, 2017.

- [76] M. Suter, E. Weingärtner and K. Wegener, "MHD printhead for additive manufacturing of metals," *Procedia CIRP*, vol. 2, no. 1, pp. 102-106, 2012.
- [77] M. Simonelli, N. Aboulkhair, M. Rasa, M. East, C. Tuck, R. Wildman, O. Salomons and R. Hague, "Towards digital metal additive manufacturing via high-temperature drop-on-demand jetting," *Additive manufacturing*, vol. 30, p. 100930, 2019.
- [78] J. Luo, L. Qi, Y. Tao, Q. Ma and C. W. Visser, "Impact-driven ejection of micro metal droplets on-demand," *International Journal of Machine Tools and Manufacture*, vol. 106, pp. 67-74, 2016.
- [79] H. Sohn and D. Yang, "Drop-on-demand deposition of superheated metal droplets for selective infiltration manufacturing," *Materials science & engineering. A, Structural materials : properties, microstructure and processing*, vol. 392, no. 1, pp. 415-421, 2005.
- [80] V. Korkut and H. Yavuz, "In-Space Additive Manufacturing Based on Metal Droplet Generation Using Drop-on-Demand Technique," *Journal of materials engineering and performance*, vol. 31, no. 8, pp. 6101-6111, 2022.
- [81] K. Li, J.-k. Liu, W.-s. Chen and L. Zhang, "Controllable printing droplets on demand by piezoelectric inkjet: applications and methods," *Microsystem technologies : sensors, actuators, systems integration*, vol. 24, no. 2, pp. 879-889, 2018.
- [82] R. E. Marusak, "Picoliter Solder Droplet Dispensing," *Proceedings of the Solid Freeform Fabrication Symposium*, pp. 81-85, 1993.
- [83] D. Rumschoettel, F. Künzel, F. Irlinger and T. C. Lueth, "A Novel Piezoelectric printhead for high melting point liquid metals," *Pan Pacific Microelectronics Symposium*, pp. 1-8, 2016.
- [84] Y. Yokoyama, K. Endo, T. Iwasaki and H. Fukumoto, "Variable-Size Solder Droplets by a Molten-Solder Ejection Method," *Journal of microelectromechanical systems*, vol. 18, no. 2, pp. 316-321, 2009.

- [85] K. Li, R. Wang, J. Liu, Y. Feng and Y. Liu, "On-demand direct printing of tin microdots by a piezoelectric microjet: design, simulation, and experimental evaluation," *Smart materials and structures*, vol. 31, no. 4, p. 45017, 2022.
- [86] D. Zhang, L. Qi, J. Luo, H. Yi, X. Hou and H. Li, "Geometry control of closed contour forming in uniform micro metal droplet deposition manufacturing," *Journal of materials processing technology*, vol. 243, pp. 474-480, 2017.
- [87] M. Ma, X. Wei, X. Shu and H. Zhang, "Producing solder droplets using piezoelectric membrane-piston-based jetting technology," *Journal of materials processing technology*, vol. 263, pp. 233-240, 2019.
- [88] T.-M. Lee, T. G. Kang, J.-S. Yang, J. Jo, K.-Y. Kim, B.-O. Choi and D.-S. Kim, "Drop-on-Demand Solder Droplet Jetting System for Fabricating Microstructure," *IEEE transactions on electronics packaging manufacturing*, vol. 31, no. 3, pp. 202-210, 2008.
- [89] Y. Yang, S. Gu, J. Liu, H. Tian and Q. Lv, "Research and development of a 3D jet printer for high-viscosity molten liquids," *Micromachines (Basel)*, vol. 9, no. 11, p. 554, 2018.
- [90] D. A. Willis and V. Grosu, "Microdroplet deposition by laser-induced forward transfer," *Applied physics letters*, vol. 86, no. 24, pp. 244103-244103-3, 2005.
- [91] L. Yang, C.-y. Wang, X.-c. Ni, Z.-j. Wang, W. Jia and L. Chai, "Microdroplet deposition of copper film by femtosecond laser-induced forward transfer," *Applied physics letters*, vol. 89, no. 16, pp. 161110-161110-3, 2006.
- [92] P. Serra, M. Duocastella, J. Fernández-Pradas and J. Morenza, "Liquids microprinting through laser-induced forward transfer," *Applied surface science*, vol. 255, no. 10, pp. 5342-4345, 2009.
- [93] E. Govekar, A. Kuznetsov and A. Jerič, "Drop on demand generation from a metal wire by means of an annular laser beam," *Journal of materials processing technology*, vol. 227, pp. 59-70, 2016.

- [94] A. Kuznetsov, A. Jeromen and E. Govekar, "Droplet detachment regimes in annular laser beam droplet generation from a metal wire," *CIRP annals*, vol. 63, no. 1, pp. 225-228, 2014.
- [95] A. Da Silva, J. Frostevarg, J. Volpp and A. F. Kaplan, "Additive Manufacturing by laser-assisted drop deposition from a metal wire," *Materials & design*, vol. 209, p. 109987, 2021.
- [96] R. Sun, Y. Shi, Z. Bing, Q. Li and R. Wang, "Metal transfer and thermal characteristics in drop-on-demand deposition using ultra-high frequency induction heating technology," *Applied thermal engineering*, vol. 149, pp. 731-744, 2019.
- [97] E. J. Vega, M. G. Cabezas, B. N. Muñoz-Sánchez, J. M. Montanero and A. M. Gañán-Calvo, "A novel technique to produce metallic microdrops for additive manufacturing," *International journal of advanced manufacturing technology*, vol. 70, no. 5-8, pp. 1395-1402, 2014.
- [98] M. Orme and R. F. Smith, "Enhanced Aluminum Properties by Means of Precise Droplet Deposition," *Journal of Manufacturing Science and Engineering*, vol. 122, pp. 484-493, 2000.
- [99] H. Zuo, H. Li, L. Qi and S. Zhong, "Influence of Interfacial Bonding between Metal Droplets on Tensile Properties of 7075 Aluminum Billets by Additive Manufacturing Technique," *Journal of materials science & technology*, vol. 32, no. 5, pp. 485-488, 2016.
- [100] Y. Idell, N. Watkins, A. Pascall, J. Jeffries and K. Blobaum, "Microstructural Characterization of Pure Tin Produced by the Drop-on-Demand Technique of Liquid Metal Jetting," *Metallurgical and materials transactions. A, Physical metallurgy and materials science*, vol. 50, no. 9, pp. 4000-4005, 2019.
- [101] V. Sukhotskiy, K. Tawil and E. Einarsson, "Printability regimes of pure metals using contactless magnetohydrodynamic drop-on-demand actuation," *Physics of Fluids*, vol. 5, no. 33, p. 053303, 2021.

- [102] C.-H. Wang, H.-L. Tsai, Y.-C. Wu and W.-S. Hwang, "Investigation of molten metal droplet deposition and solidification for 3D printing techniques," *Journal of Micromechanics and Microengineering*, vol. 26, p. 095012, 2016.
- [103] S. Schiaffino^a and A. A. Sonin^b, "Molten droplet deposition and solidification at low Weber numbers," *Physics of fluids*, vol. 9, pp. 3172-3187, 1997.
- [104] A. Rushworth, Y. Li, R. D. Castro and H. Chen, "Metal Droplet Extrusion: A Novel, Low-cost Approach to Droplet-on-Demand for High-melting-point Metal Additive Manufacturing," *Unpublished*.
- [105] National Instruments, "USER GUIDE AND SPECIFICATIONS MyRIO-1900," 2016. [Online]. Available: <https://www.ni.com/pdf/manuals/376047c.pdf>. [Accessed 13 11 2021].
- [106] H. Seli, M. Awang, A. I. Ismail, E. Rachman and Z. A. Ahmad, "Evaluation of properties and FEM model of the friction welded mild steel-AL6061-alumina," *Materials Research*, pp. 453-467, 2012.

Appendix

Old control code

The old LabVIEW code for the control of the temperature and the wire moment consisted of 2 VIs, one executed in real time processor, and one executed in the FPGA processor. The VI executed in real-time acts the UI and sends the input parameters to the VI executed in the FPGA processor, together these VIs achieve the control of the temperature and the movement of the wire.

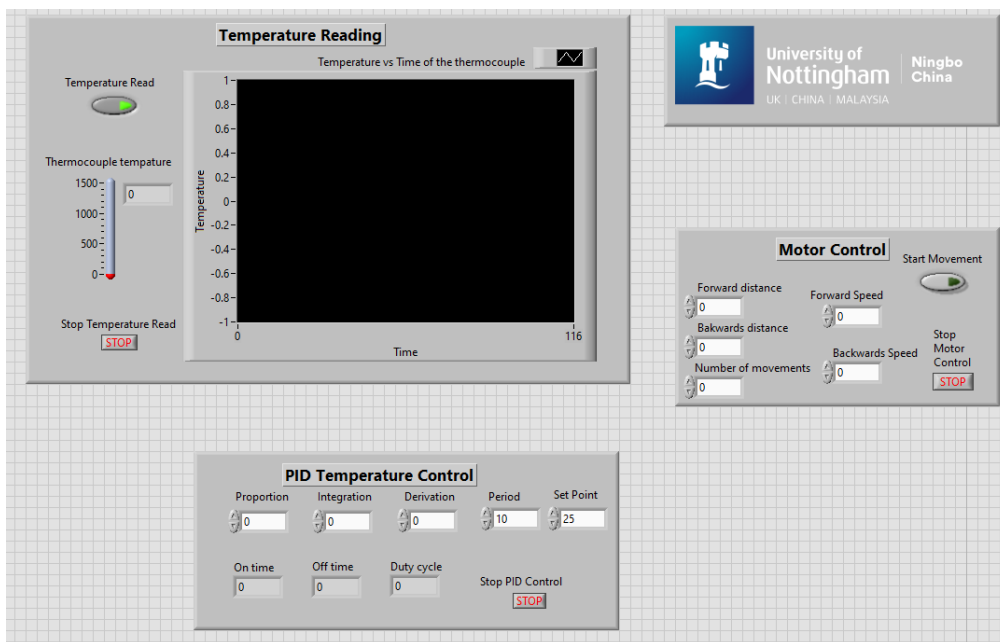


Figure 87. UI of the VI executed in real-time.

The VI executed in the real-time processor is divided into three segments, the motor control, the PID temperature control and the temperature reading, as shown in Figure 87. The user needs to input the values of the desired PID temperature parameters, and it will show the On and OFF times generated with the input values, which will control the temperature of the ZVS induction heater. The motor control segment allows the user the input the forwards and backwards distance and the speed of each of them, also they need to input the number of times the droplet producing movements needs to be repeated.

The code of the VI executed in the real-time processor can be seen separated into three figures, Figure 88,

Figure 89 and Figure 90.

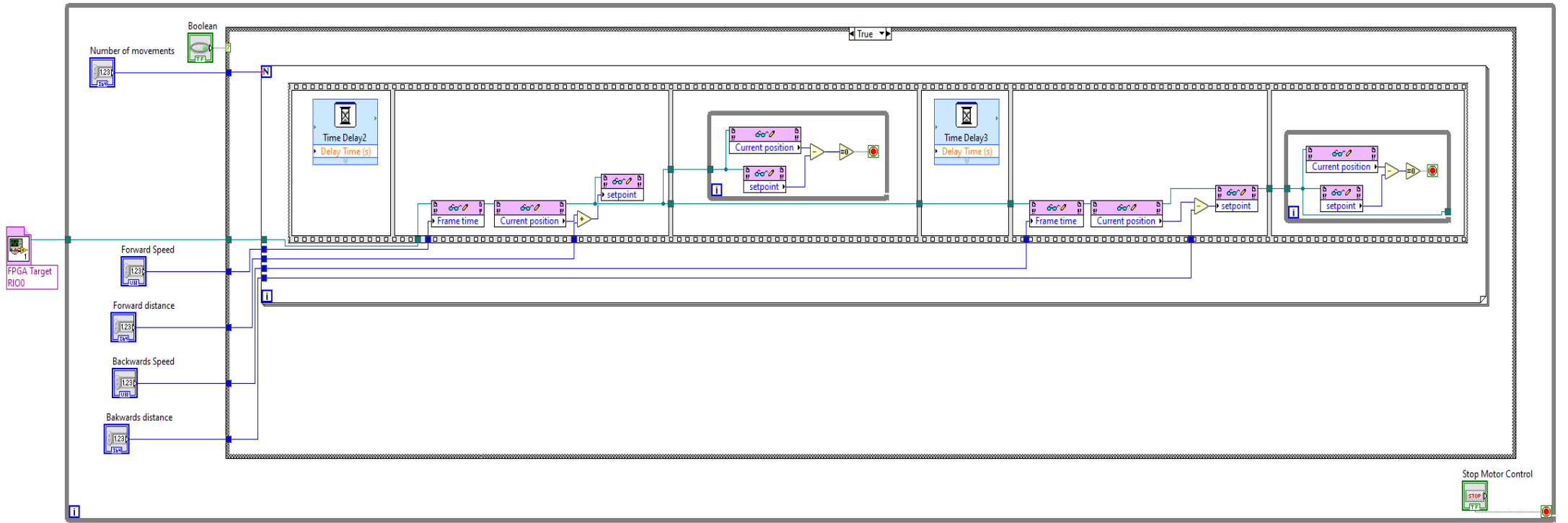


Figure 88. Block diagram of the motor control section of the VI.

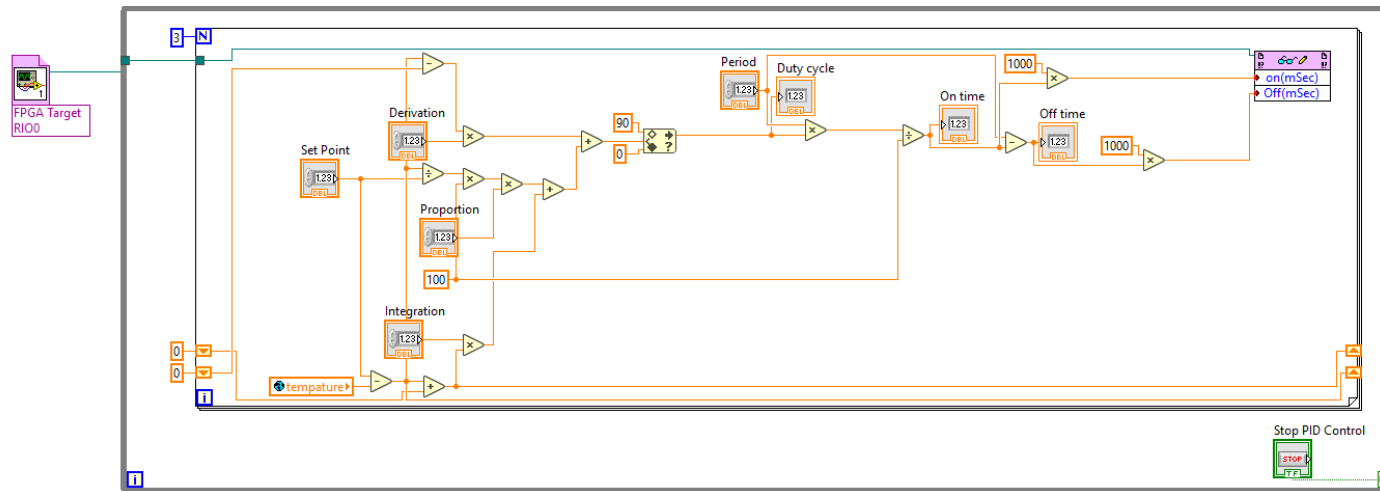


Figure 89. Block diagram of the PID control section of the VI.

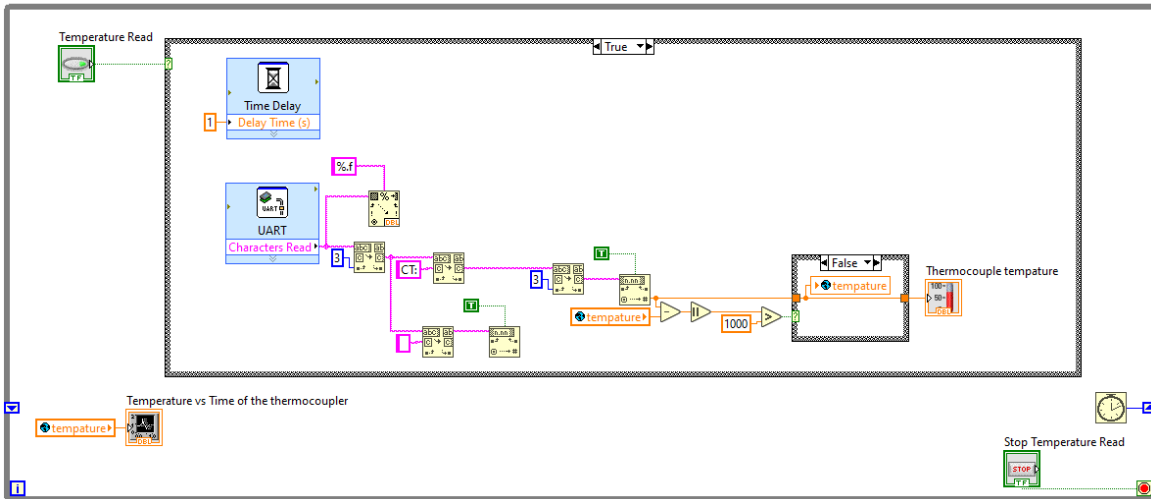


Figure 90. Block diagram of the temperature reading section of the VI.

On the other hand, the VI executed in the FPGA processor is divided into two sections, the top section which receives the input for the motor control of the previous VI and then send the outputs needed to move the wire in the desire movement to the motor driver, and the bottom section which controls the on and off of a relay with the timings receive from the previous VI, this allows it to control the temperature of the graphite nozzle by controlling the on and off timings of the ZVS induction heater, the code is shown in Figure 91.

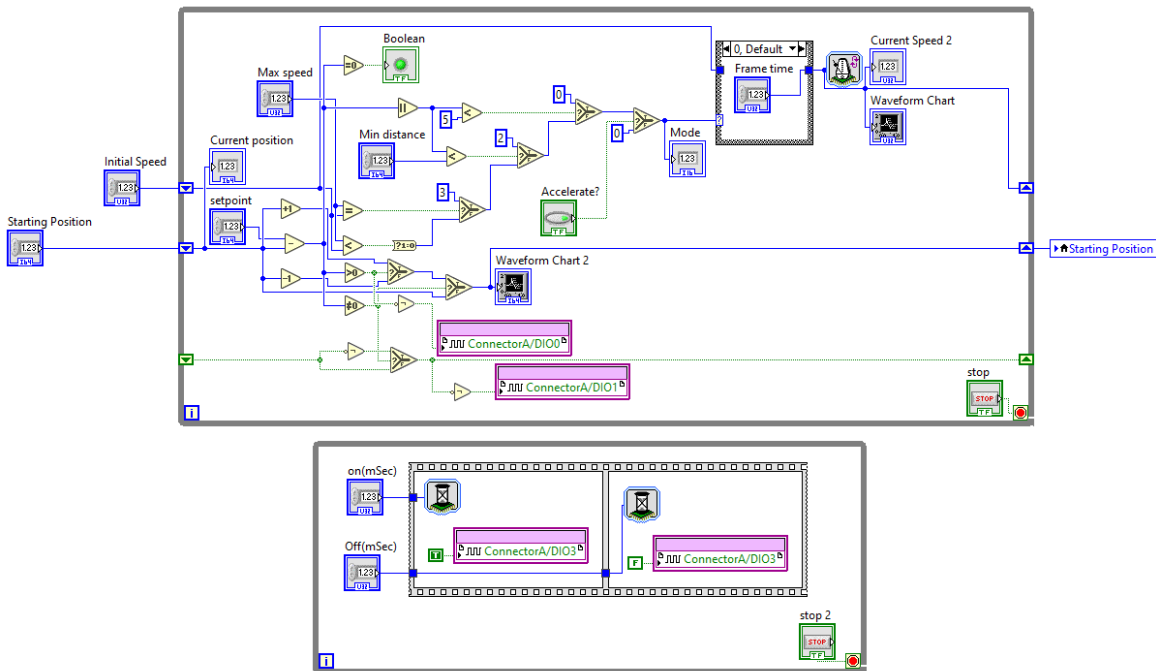
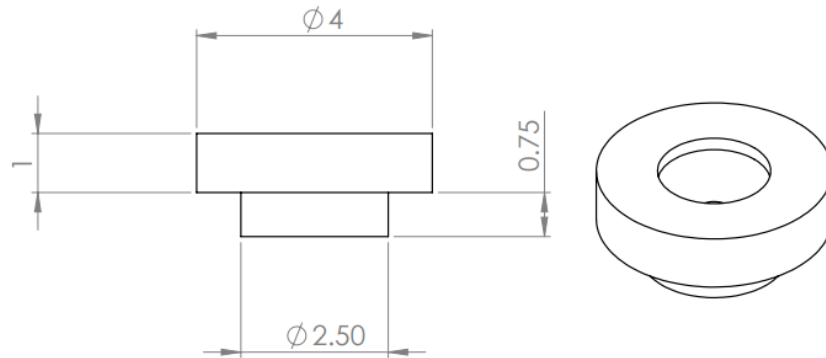
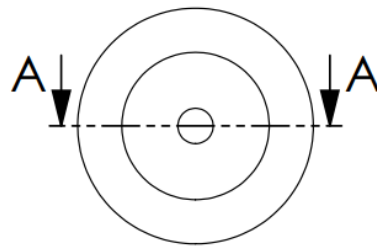


Figure 91. Block diagram code of the VI execute in the FPGA processor.

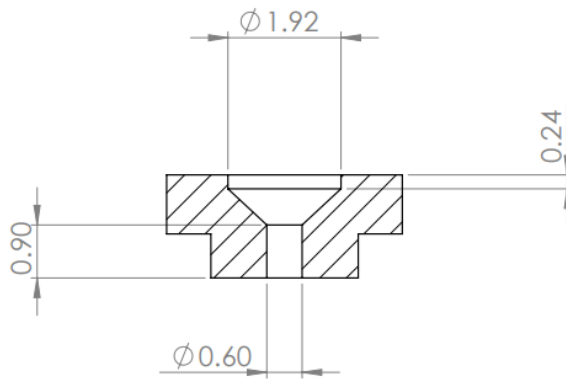
Engineering Drawings





Front View

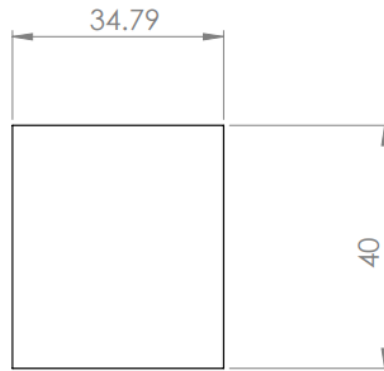
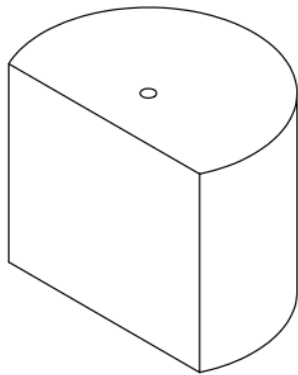


Bottom View

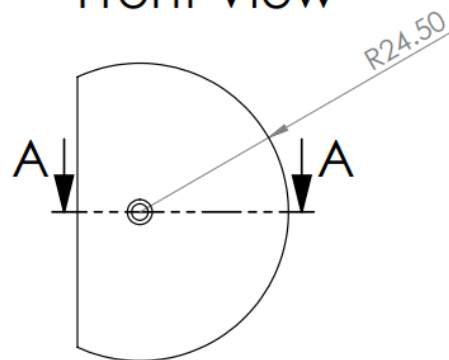


Section View A-A

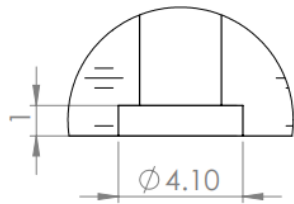
	 University of Nottingham <small>UK CHINA MALAYSIA</small>					
	<h2>Tungsten Carbide Nozzle</h2>					
TOLERANCE LINEAR: ± 0.5 ANGULAR: ± 1	MATERIAL Tungsten Carbide	ISS. DATE 11/15/2021	REV 1a	DRN BY R.D.C.B	DWG NO. 1	
ALL DIMENSIONS IN MILLIMETRES DRAFTING STANDARD 8888			SCALE 10:1	SIZE A4	SHEET 1 of 1	



Front View

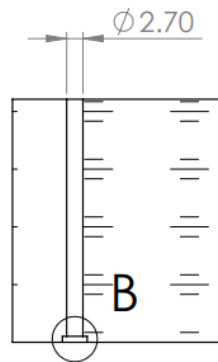


Bottom View



Detail View B

SCALE 5 : 1



Section View A-A



University of
Nottingham
UK | CHINA | MALAYSIA

TOLERANCE
LINEAR: ± 0.5
ANGULAR: ± 1

Quartz Insert

ALL DIMENSIONS IN
MILLIMETRES

MATERIAL
Fused Silica

ISS. DATE
03/17/2021

REV
1a

DRN BY
R.D.C.B

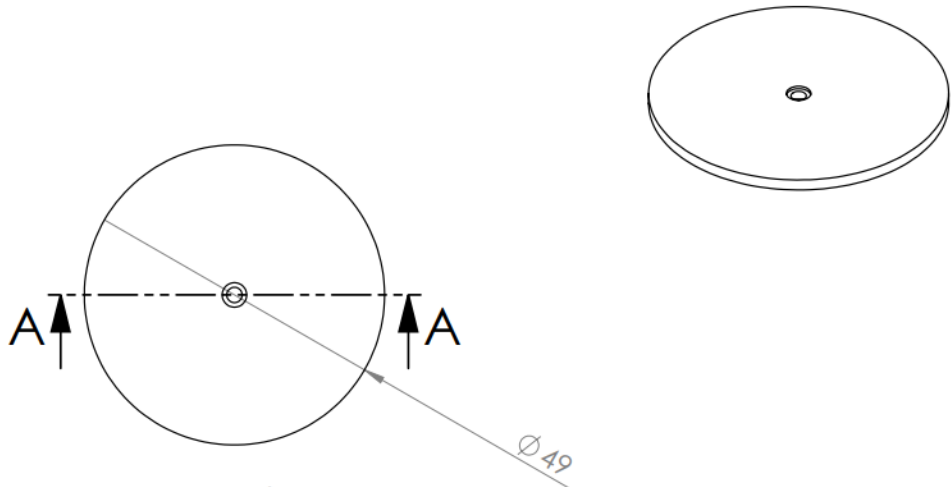
DWG NO.
2

DRAFTING STANDARD
8888

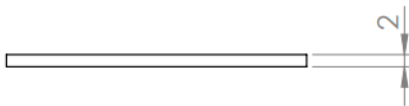
SCALE
1:1

SIZE
A4

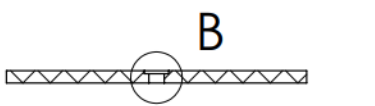
SHEET
1 of 1



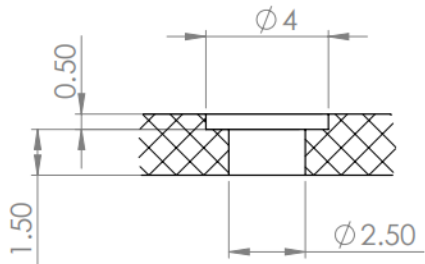
Top View



Front View



Section View A-A



Detail View B

SCALE 5 : 1

				University of Nottingham <small>UK CHINA MALAYSIA</small>	
TOLERANCE LINEAR: ±0.5 ANGULAR: ±1		Graphite Disk			
ALL DIMENSIONS IN MILLIMETRES	MATERIAL Graphite	ISS. DATE 03/17/22	REV 1a	DRN BY R.D.C.B.	DWG NO. 3
DRAFTING STANDARD 8888			SCALE 1:1	SIZE A4	SHEET 1 of 1

M

Droplet production sample measurements

Table 15. 100 droplets sample 1 measurements.

Droplet	Length	Width	Thickness	Mass	Calculated Diameter
1	2.49 mm	1.52 mm	1.40 mm	0.0058 g	1.60 mm
2	2.04 mm	1.54 mm	1.28 mm	0.0080 g	1.78 mm
3	2.98 mm	1.14 mm	0.82 mm	0.0069 g	1.70 mm
4	2.34 mm	1.54 mm	1.10 mm	0.0068 g	1.69 mm
5	2.08 mm	1.78 mm	1.14 mm	0.0085 g	1.82 mm
6	2.60 mm	1.55 mm	1.23 mm	0.0089 g	1.85 mm
7	2.15 mm	1.64 mm	1.48 mm	0.0069 g	1.70 mm
8	1.85 mm	1.69 mm	1.33 mm	0.0069 g	1.70 mm
9	1.86 mm	1.67 mm	1.36 mm	0.0063 g	1.65 mm
10	1.71 mm	1.64 mm	1.43 mm	0.0056 g	1.58 mm
11	2.11 mm	1.64 mm	1.25 mm	0.0059 g	1.61 mm
12	1.96 mm	1.65 mm	1.20 mm	0.0069 g	1.70 mm
13	1.93 mm	1.52 mm	1.43 mm	0.0059 g	1.61 mm
14	2.31 mm	1.53 mm	1.26 mm	0.0058 g	1.60 mm
15	2.13 mm	1.54 mm	1.27 mm	0.0070 g	1.70 mm
16	1.81 mm	1.63 mm	1.35 mm	0.0059 g	1.61 mm
17	2.11 mm	1.63 mm	1.43 mm	0.0065 g	1.66 mm
18	1.89 mm	1.81 mm	1.08 mm	0.0059 g	1.61 mm
19	2.07 mm	1.65 mm	1.31 mm	0.0059 g	1.61 mm
20	2.15 mm	1.53 mm	1.25 mm	0.0059 g	1.61 mm
21	1.91 mm	1.72 mm	1.24 mm	0.0072 g	1.72 mm
22	2.26 mm	1.63 mm	1.28 mm	0.0071 g	1.71 mm
23	2.03 mm	1.50 mm	1.16 mm	0.0059 g	1.61 mm
24	2.00 mm	1.73 mm	1.39 mm	0.0075 g	1.74 mm
25	1.80 mm	1.70 mm	1.19 mm	0.0071 g	1.71 mm
26	2.33 mm	1.85 mm	1.27 mm	0.0076 g	1.75 mm
27	1.86 mm	1.79 mm	1.38 mm	0.0058 g	1.60 mm
28	2.11 mm	1.55 mm	1.24 mm	0.0054 g	1.56 mm
29	1.92 mm	1.60 mm	1.23 mm	0.0055 g	1.57 mm
30	2.32 mm	1.43 mm	1.21 mm	0.0053 g	1.55 mm
31	1.92 mm	1.85 mm	1.43 mm	0.0070 g	1.70 mm
32	2.11 mm	1.63 mm	1.37 mm	0.0070g	1.70 mm
33	2.52 mm	1.51 mm	1.27 mm	0.0055 g	1.57 mm
34	2.21 mm	1.60 mm	1.37 mm	0.0059 g	1.61 mm
35	2.46 mm	1.53 mm	1.37 mm	0.0080 g	1.78 mm
36	2.59 mm	1.51 mm	1.23 mm	0.0066 g	1.67 mm

37	2.14 mm	1.59 mm	1.25 mm	0.0069 g	1.70 mm
38	2.19 mm	1.48 mm	1.31 mm	0.0070 g	1.70 mm
39	1.91 mm	1.60 mm	1.25 mm	0.0054 g	1.56 mm
40	1.94 mm	1.88 mm	1.68 mm	0.0062 g	1.64 mm
41	1.82 mm	1.61 mm	1.27 mm	0.0054 g	1.56 mm
42	2.18 mm	1.71 mm	1.35 mm	0.0080 g	1.78 mm
43	1.82 mm	1.77 mm	1.30 mm	0.0067 g	1.68 mm
44	1.74 mm	1.69 mm	1.15 mm	0.0064 g	1.65 mm
45	2.11 mm	1.50 mm	1.16 mm	0.0076 g	1.75 mm
46	2.46 mm	1.38 mm	1.35 mm	0.0078 g	1.77 mm
47	2.07 mm	1.66 mm	1.40 mm	0.0072 g	1.72 mm
48	2.29 mm	1.35 mm	1.20 mm	0.0074 g	1.74 mm
49	2.18 mm	1.54 mm	1.15 mm	0.0070 g	1.70 mm
50	2.09 mm	1.62 mm	1.18 mm	0.0080 g	1.78 mm
51	2.63 mm	1.55 mm	1.19 mm	0.0068 g	1.69 mm
52	2.43 mm	1.71 mm	1.20 mm	0.0054 g	1.56 mm
53	1.89 mm	1.47 mm	1.07 mm	0.0044 g	1.46 mm
54	2.24 mm	1.46 mm	1.20 mm	0.0051 g	1.53 mm
55	2.46 mm	1.66 mm	1.30 mm	0.0069 g	1.70 mm
56	2.17 mm	1.46 mm	1.23 mm	0.0046 g	1.48 mm
57	1.88 mm	1.72 mm	1.27 mm	0.0060 g	1.62 mm
58	2.12 mm	1.52 mm	1.21 mm	0.0049 g	1.51 mm
59	1.97 mm	1.76 mm	1.59 mm	0.0054 g	1.56 mm
60	2.38 mm	1.73 mm	1.36 mm	0.0069 g	1.70 mm
61	1.75 mm	1.57 mm	1.40 mm	0.0060 g	1.62 mm
62	2.26 mm	1.36 mm	1.12 mm	0.0062 g	1.64 mm
63	2.15 mm	1.48 mm	1.34 mm	0.0051 g	1.53 mm
64	1.86 mm	1.57 mm	1.40 mm	0.0052 g	1.54 mm
65	2.58 mm	1.33 mm	1.23 mm	0.0061 g	1.63 mm
66	2.18 mm	1.70 mm	1.11 mm	0.0050 g	1.52 mm
67	2.26 mm	1.65 mm	1.21 mm	0.0048 g	1.50 mm
68	1.87 mm	1.70 mm	1.06 mm	0.0054 g	1.56 mm
69	2.06 mm	1.59 mm	1.25 mm	0.0058 g	1.60 mm
70	2.24 mm	1.26 mm	1.20 mm	0.0052 g	1.54 mm
71	1.86 mm	1.63 mm	1.24 mm	0.0058 g	1.60 mm
72	2.35 mm	1.47 mm	1.36 mm	0.0058 g	1.60 mm
73	2.37 mm	1.49 mm	1.19 mm	0.0054 g	1.56 mm
74	1.91 mm	1.71 mm	1.35 mm	0.0061 g	1.63 mm
75	2.55 mm	1.40 mm	1.27 mm	0.0054 g	1.56 mm
76	2.02 mm	1.65 mm	1.03 mm	0.0044 g	1.46 mm
77	1.79 mm	1.73 mm	1.31 mm	0.0063 g	1.65 mm
78	2.67 mm	1.33 mm	1.23 mm	0.0056 g	1.58 mm
79	18.4 mm	1.67 mm	1.20 mm	0.0051 g	1.53 mm

80	2 mm	1.66 mm	1.39 mm	0.0058 g	1.60 mm
81	2.71 mm	1.46 mm	1.27 mm	0.0073 g	1.73 mm
82	2.02 mm	1.65 mm	1.26 mm	0.0055 g	1.57 mm
83	2.38 mm	1.48 mm	1.25 mm	0.0056 g	1.58 mm
84	2.02 mm	1.45 mm	1.32 mm	0.0041 g	1.43 mm
85	2.39 mm	2.10 mm	1.28 mm	0.0060 g	1.62 mm
86	2.17 mm	1.66 mm	1.33 mm	0.0049 g	1.51 mm
87	2.03 mm	1.65 mm	1.21 mm	0.0048 g	1.50 mm
88	1.96 mm	1.36 mm	1.33 mm	0.0049 g	1.51 mm
89	2.34 mm	1.67 mm	1.11 mm	0.0053 g	1.55 mm
90	1.82 mm	1.76 mm	1.30 mm	0.0061 g	1.63 mm
91	2.16 mm	1.40 mm	1.16 mm	0.0046 g	1.48 mm
92	2.27 mm	1.36 mm	1.23 mm	0.0050 g	1.52 mm
93	1.83 mm	1.71 mm	1.20 mm	0.0051 g	1.53 mm
94	2.09 mm	1.42 mm	1.26 mm	0.0053 g	1.55 mm
95	2.16 mm	1.56 mm	1.44 mm	0.0053 g	1.55 mm
96	1.98 mm	1.72 mm	1.35 mm	0.0061 g	1.63 mm
97	2.55 mm	1.28 mm	1.02 mm	0.0060 g	1.62 mm
98	2.61 mm	1.39 mm	1.31 mm	0.0061 g	1.63 mm
99	2.09 mm	1.48 mm	1.20 mm	0.0055 g	1.57 mm
100	2.26 mm	1.81 mm	1.18 mm	0.0061 g	1.63 mm

Table 16. 100 droplets sample 2 measurements.

Droplet	Length	width	thickness	Mass	Calculated Diameter
1	1.91 mm	1.55 mm	1.41 mm	0.0048 g	1.50 mm
2	1.71 mm	1.68 mm	1.49 mm	0.0060 g	1.62 mm
3	2.00 mm	1.67 mm	1.09 mm	0.0063 g	1.65 mm
4	1.88 mm	1.72 mm	1.35 mm	0.0063 g	1.65 mm
5	1.90 mm	1.85 mm	1.26 mm	0.0064 g	1.65 mm
6	1.76 mm	1.65 mm	1.23 mm	0.0059 g	1.61 mm
7	1.96 mm	1.62 mm	1.11 mm	0.0056 g	1.58 mm
8	2.17 mm	1.80 mm	1.36 mm	0.0084 g	1.81 mm
9	1.84 mm	1.61 mm	1.30 mm	0.0054 g	1.56 mm
10	1.93 mm	1.85 mm	1.16 mm	0.0060 g	1.62 mm
11	1.82 mm	1.70 mm	1.41 mm	0.0059 g	1.61 mm
12	1.51 mm	1.44 mm	1.33 mm	0.0046 g	1.48 mm
13	1.95 mm	1.69 mm	1.16 mm	0.0055 g	1.57 mm
14	1.93 mm	1.60 mm	1.18 mm	0.0064 g	1.65 mm
15	2.70 mm	1.56 mm	1.41 mm	0.0062 g	1.64 mm
16	2.02 mm	1.63 mm	1.14 mm	0.0055 g	1.57 mm
17	1.91 mm	1.76 mm	1.22 mm	0.0054 g	1.56 mm

18	1.86 mm	1.74 mm	1.35 mm	0.0055 g	1.57 mm
19	1.93 mm	1.47 mm	1.28 mm	0.0040 g	1.41 mm
20	1.49 mm	1.43 mm	1.20 mm	0.0042 g	1.44 mm
21	1.91 mm	1.79 mm	1.50 mm	0.0061 g	1.63 mm
22	2.01 mm	1.83 mm	1.36 mm	0.0060 g	1.62 mm
23	1.85 mm	1.61 mm	1.32 mm	0.0054 g	1.56 mm
24	1.88 mm	1.78 mm	1.25 mm	0.0062 g	1.64 mm
25	2.09 mm	1.70 mm	1.30 mm	0.0057 g	1.59 mm
26	1.86 mm	1.71 mm	1.49 mm	0.0055 g	1.57 mm
27	2.46 mm	2.10 mm	1.36 mm	0.0099 g	1.91 mm
28	1.86 mm	1.76 mm	1.24 mm	0.0062 g	1.64 mm
29	1.91 mm	1.43 mm	1.38 mm	0.0044 g	1.46 mm
30	2.00 mm	1.84 mm	1.21 mm	0.0049 g	1.51 mm
31	1.94 mm	1.60 mm	1.45 mm	0.0053 g	1.55 mm
32	1.68 mm	1.59 mm	1.27 mm	0.0048 g	1.50 mm
33	2.15 mm	1.80 mm	1.47 mm	0.0061 g	1.63 mm
34	1.75 mm	1.65 mm	1.57 mm	0.0053 g	1.55 mm
35	1.77 mm	1.72 mm	1.23 mm	0.0061 g	1.63 mm
36	2.05 mm	1.76 mm	1.19 mm	0.0060 g	1.62 mm
37	1.92 mm	1.75 mm	1.34 mm	0.0060 g	1.62 mm
38	1.69 mm	1.55 mm	1.48 mm	0.0044 g	1.46 mm
39	2.05 mm	1.27 mm	1.19 mm	0.0041 g	1.43 mm
40	1.90 mm	1.51 mm	1.26 mm	0.0041 g	1.43 mm
41	1.82 mm	1.67 mm	1.45 mm	0.0055 g	1.57 mm
42	1.91 mm	1.85 mm	1.17 mm	0.0062 g	1.64 mm
43	1.96 mm	1.79 mm	1.43 mm	0.0065 g	1.66 mm
44	1.72 mm	1.63 mm	1.47 mm	0.0061 g	1.63 mm
45	1.98 mm	1.62 mm	1.36 mm	0.0064 g	1.65 mm
46	2.79 mm	1.75 mm	1.29 mm	0.0059 g	1.61 mm
47	1.83 mm	1.69 mm	1.42 mm	0.0063 g	1.65 mm
48	1.96 mm	1.64 mm	1.20 mm	0.0060 g	1.62 mm
49	1.88 mm	1.61 mm	1.31 mm	0.0060 g	1.62 mm
50	2.02 mm	1.66 mm	1.22 mm	0.0054 g	1.56 mm
51	1.91 mm	1.17 mm	1.00 mm	0.0033 g	1.33 mm
52	1.75 mm	1.71 mm	1.15 mm	0.0061 g	1.63 mm
53	1.82 mm	1.70 mm	1.65 mm	0.0071 g	1.71 mm
54	2.31 mm	1.53 mm	1.12 mm	0.0062 g	1.64 mm
55	1.87 mm	1.76 mm	1.39 mm	0.0069 g	1.70 mm
56	1.96 mm	1.61 mm	1.24 mm	0.0065 g	1.66 mm
57	1.77 mm	1.62 mm	1.47 mm	0.0058 g	1.60 mm
58	1.63 mm	1.56 mm	1.25 mm	0.0048 g	1.50 mm
59	1.85 mm	1.64 mm	1.11 mm	0.0054 g	1.56 mm
60	1.93 mm	1.87 mm	1.07 mm	0.0071 g	1.71 mm

61	2.00 mm	1.60 mm	1.32 mm	0.0059 g	1.61 mm
62	1.91 mm	1.73 mm	1.44 mm	0.0065 g	1.66 mm
63	2.06 mm	1.56 mm	1.27 mm	0.0055 g	1.57 mm
64	2.17 mm	1.83 mm	1.34 mm	0.0076 g	1.75 mm
65	1.96 mm	1.58 mm	1.53 mm	0.0048 g	1.50 mm
66	3.28 mm	1.50 mm	1.28 mm	0.0058 g	1.60 mm
67	1.90 mm	1.70 mm	1.44 mm	0.0064 g	1.65 mm
68	1.94 mm	1.82 mm	1.41 mm	0.0059 g	1.61 mm
69	2.49 mm	1.49 mm	1.33 mm	0.0058 g	1.60 mm
70	1.65 mm	1.59 mm	1.29 mm	0.0047 g	1.49 mm
71	1.84 mm	1.52 mm	1.20 mm	0.0053 g	1.55 mm
72	1.87 mm	1.62 mm	1.30 mm	0.0054 g	1.56 mm
73	1.91 mm	1.64 mm	1.45 mm	0.0044 g	1.46 mm
74	1.91 mm	1.71 mm	1.35 mm	0.0075 g	1.74 mm
75	2.24 mm	1.69 mm	1.29 mm	0.0059 g	1.61 mm
76	1.92 mm	1.71 mm	1.24 mm	0.0062 g	1.64 mm
77	1.99 mm	1.68 mm	1.32 mm	0.0066 g	1.67 mm
78	1.99 mm	1.50 mm	1.19 mm	0.0053 g	1.55 mm
79	1.97 mm	1.87 mm	1.22 mm	0.0057 g	1.59 mm
80	1.63 mm	1.52 mm	1.21 mm	0.0042 g	1.44 mm
81	1.85 mm	1.75 mm	1.24 mm	0.0053 g	1.55 mm
82	2.07 mm	1.61 mm	1.46 mm	0.0058 g	1.60 mm
83	2.33 mm	1.72 mm	1.22 mm	0.0054 g	1.56 mm
84	1.95 mm	1.28 mm	1.14 mm	0.0045 g	1.47 mm
85	1.86 mm	1.75 mm	1.14 mm	0.0047 g	1.49 mm
86	1.90 mm	1.61 mm	1.16 mm	0.0049 g	1.51 mm
87	1.91 mm	1.46 mm	1.39 mm	0.0053 g	1.55 mm
88	2.27 mm	1.48 mm	1.30 mm	0.0050 g	1.52 mm
89	1.89 mm	1.62 mm	1.16 mm	0.0058 g	1.60 mm
90	2.15 mm	1.53 mm	1.30 mm	0.0056 g	1.58 mm
91	2.02 mm	1.54 mm	1.27 mm	0.0066 g	1.67 mm
92	2.31 mm	1.49 mm	1.21 mm	0.0059 g	1.61 mm
93	2.04 mm	1.76 mm	1.32 mm	0.0065 g	1.66 mm
94	1.97 mm	1.47 mm	1.37 mm	0.0053 g	1.55 mm
95	2.09 mm	1.31 mm	1.20 mm	0.0058 g	1.60 mm
96	2.42 mm	1.47 mm	1.44 mm	0.0061 g	1.63 mm
97	1.98 mm	1.53 mm	1.33 mm	0.0070 g	1.70 mm
98	1.60 mm	1.55 mm	1.35 mm	0.0052 g	1.54 mm
99	2.37 mm	1.48 mm	1.20 mm	0.0062 g	1.64 mm
100	2.33 mm	1.44 mm	1.28 mm	0.0063 g	1.65 mm